nature catalysis

Supplementary information

https://doi.org/10.1038/s41929-026-01574-z

Copper-catalysed carbon monoxide electrolysis under dynamic operation

In the format provided by the authors and unedited

Table of Contents

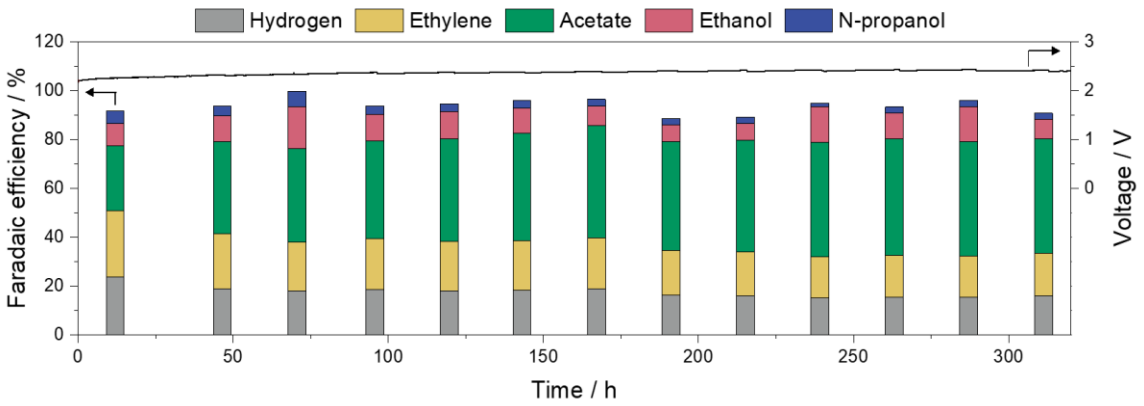

Supplementary Fig. 1 | Faradaic efficiency (FE) and voltage over time under steady state operation. Measurements were performed in a 5 cm^2 zero-gap CO electrolyzer at 200 mA cm^{-2} in 1 M KOH. The system demonstrated stable performance for 325 hours, maintaining a C_{2+} FE of approximately 75% and a voltage of 2.4 V. The hydrogen FE and voltage up to 175 h are depicted in Fig. 2.

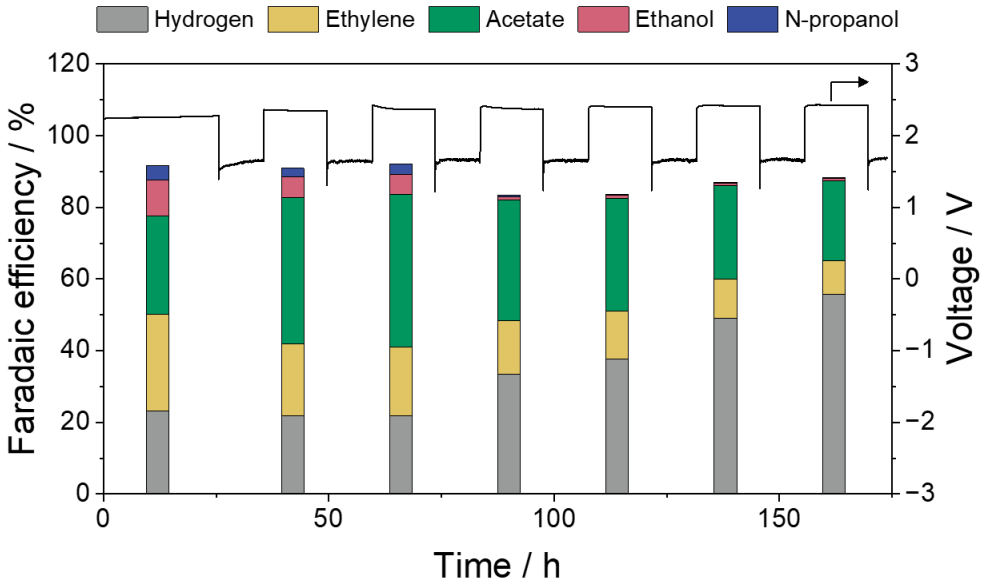

Supplementary Fig. 2 | Faradaic efficiency and voltage over time during dynamic operation with power-off/power-on operation. Measurements were performed in a 5 cm^2 zero-gap CO electrolyzer in 1 M KOH, alternating between 200 mA cm^{-2} and open-circuit voltage (OCV) conditions. The system degraded within 175 hours, with a sudden rise in hydrogen FE after three power-off/power-on cycles that eventually surpassed 60%.

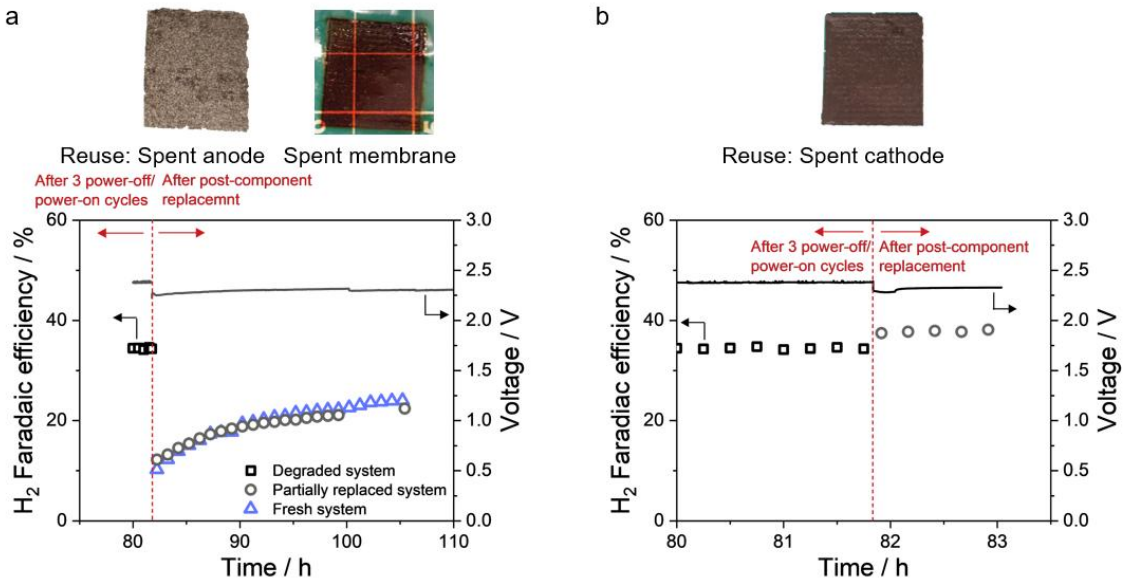

Supplementary Fig. 3 | Identifying the degradation source in the CO electrolyzer. Components were replaced from a degraded CO electrolyzer that underwent power-off/power-on dynamic operation for three times (~ 80 hours), following the same procedure as in Fig. 2, to identify the failure components. **a** | The spent anode and membrane from the degraded CO electrolyzer were reused, while the cathode was replaced with a fresh one. The hydrogen FE followed the same trend as that of a fresh CO electrolyzer, indicating that degradation is not attributed to the anode or membrane. **b** | The spent cathode from the degraded CO electrolyzer was reused, while the anode and membrane were replaced with fresh components. The hydrogen FE remained around 40%, similar to that of the degraded CO electrolyzer, suggesting that the cathode is the primary source of degradation.

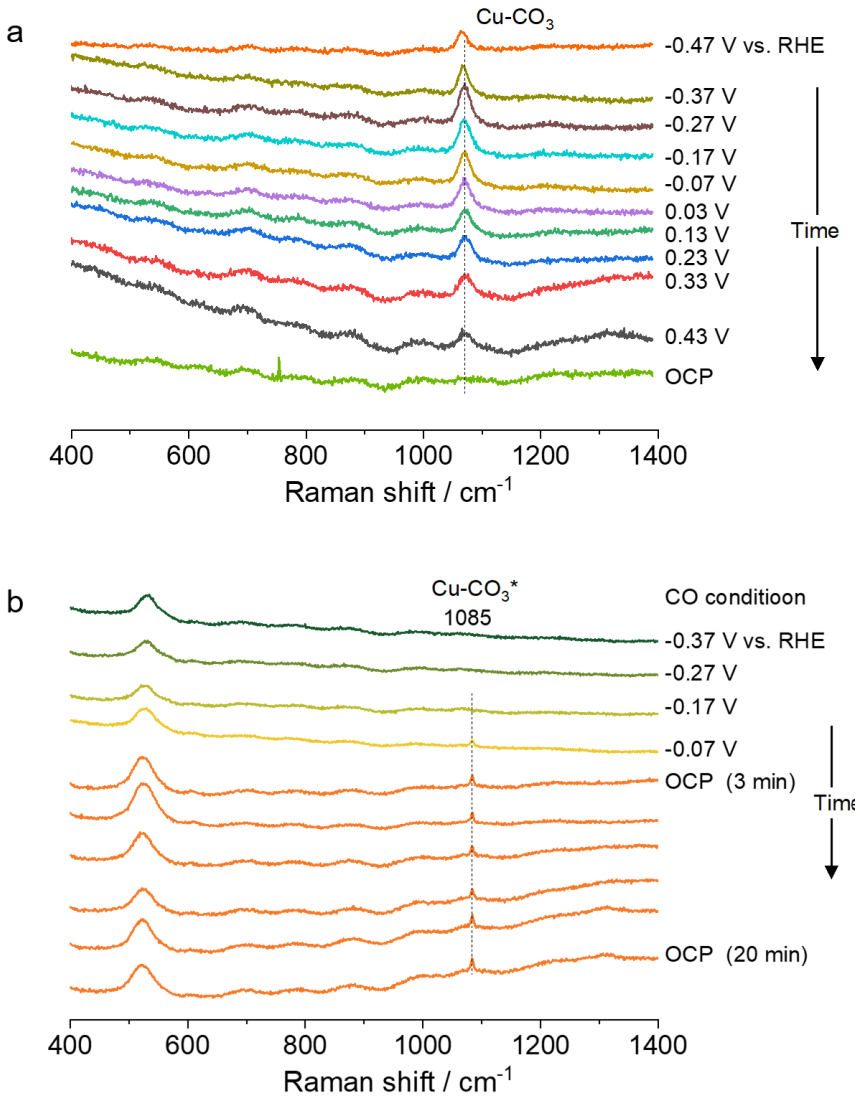

Supplementary Fig. 4 | In-situ surface-enhanced Raman spectra. a | Raman spectra were measured from –0.47 V vs. RHE to open-circuit potential (OCP) in an 0.5 M K_2CO_3 electrolyte under Ar atmosphere. This experiment confirms that the peak at 1085 cm^{-1} originates from carbonate species. **b** | Raman spectra were measured from –0.37 V vs. RHE to OCP, and then held at OCP for 20 minutes in a CO-saturated 1 M KOH electrolyte under CO atmosphere. The peak at 1085 cm^{-1},[1-3] indicative of carbonate formation, gradually increases over time under OCP conditions.

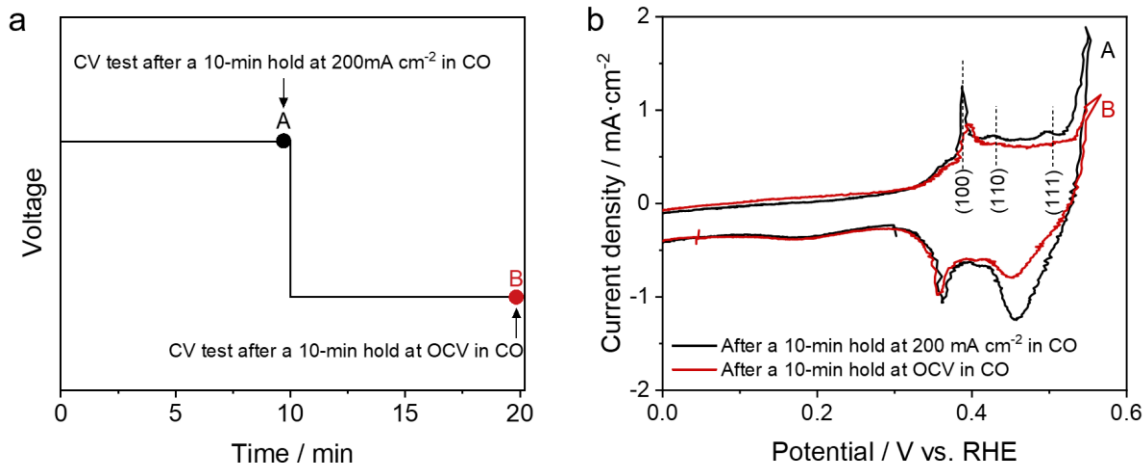

Supplementary Fig. 5 | Cyclic voltammetry (CV) test of the Cu catalyst before and after OCV for 10 minutes in CO. a | Schematic of the test procedure. The initial CV was measured at point A after activating the Cu catalyst during CO reduction for 10 minutes to establish a stable CV baseline. After collecting the CV at point A, the CO electrolyzer was completely power-off and held at OCV for 10 minutes, followed by a CV measurement at point B. **b** | Comparison of CVs at points A and B. All Cu facet-related features, including (100), (110), and (111),[4,5] decreased significantly after 10 minutes of OCV operation, indicating substantial changes in the catalyst state. All experimental details are provided in the Methods section. The CVs were measured under Ar conditions at a scan rate of 20 mV s^{-1}.

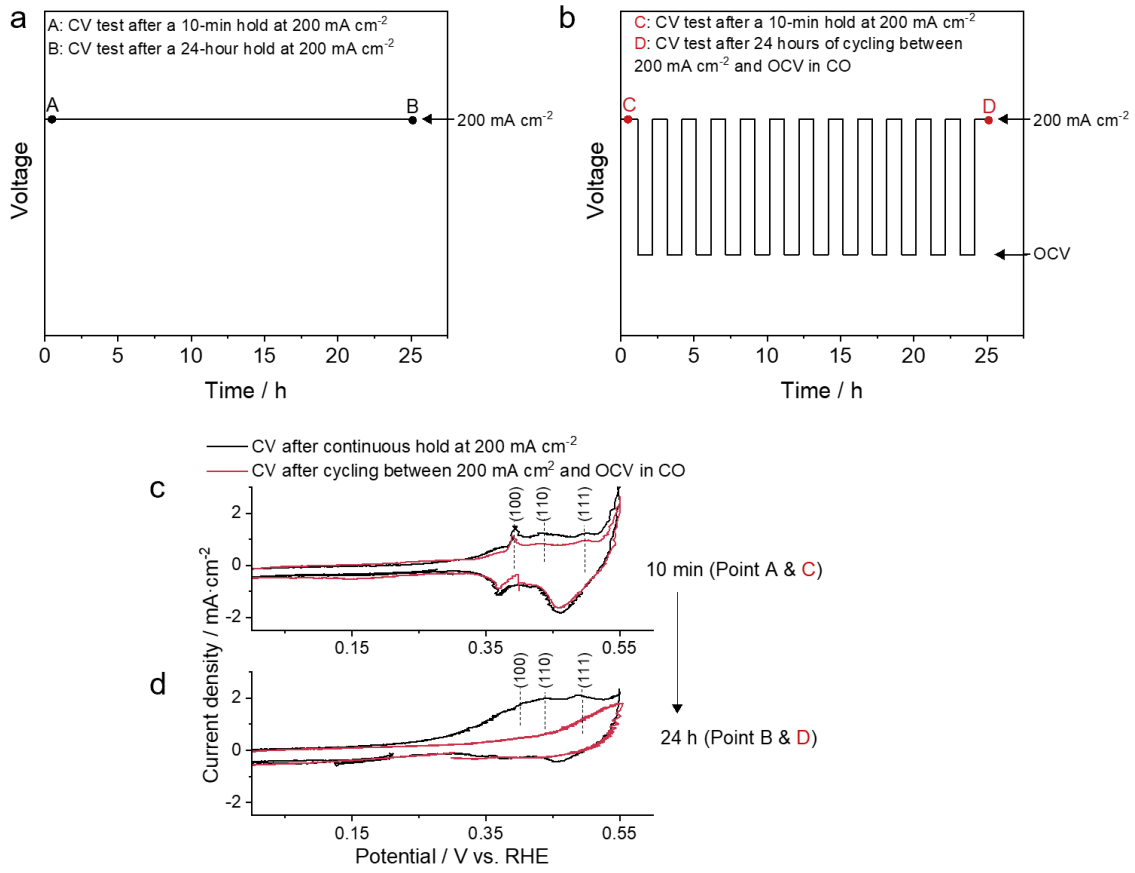

Supplementary Fig. 6 | CV test of the Cu catalyst after 24 hours of steady state operation versus power-off/power-on dynamic operation in CO. a, **b** | Schematic of the test procedure. The initial CV was measured at points A and C after activating the Cu catalyst during CO reduction for 10 minutes at 200 mA cm^{-2} to establish a stable CV baseline. After collecting the CVs at point A and C, the CO electrolyzer was either operated continuously at 200 mA cm^{-2} or subjected to dynamic operation cycling between 200 mA cm^{-2} for one hour and OCV in CO for one hour over a 24-hour period, followed by CV measurements at points B and D, respectively. **c** | Comparison of CVs at points A and C. The initial Cu CV profiles for both experiments exhibit similar Cu facet structures, eliminating potential baseline effects from different experimental setups. **d** | Comparison of CVs at points B and D. All Cu facet-related features, including (100), (110), and (111),[4,5] show a more pronounced decrease compared to the 10-minute OCV power-off result (Supplementary Fig. 5), indicating significant changes in the catalyst state after 24 hours of dynamic operation with complete power-off operation. All experimental details can be found in the Methods section. The CVs were measured under Ar conditions at a scan rate of 20 mV s^{-1}.

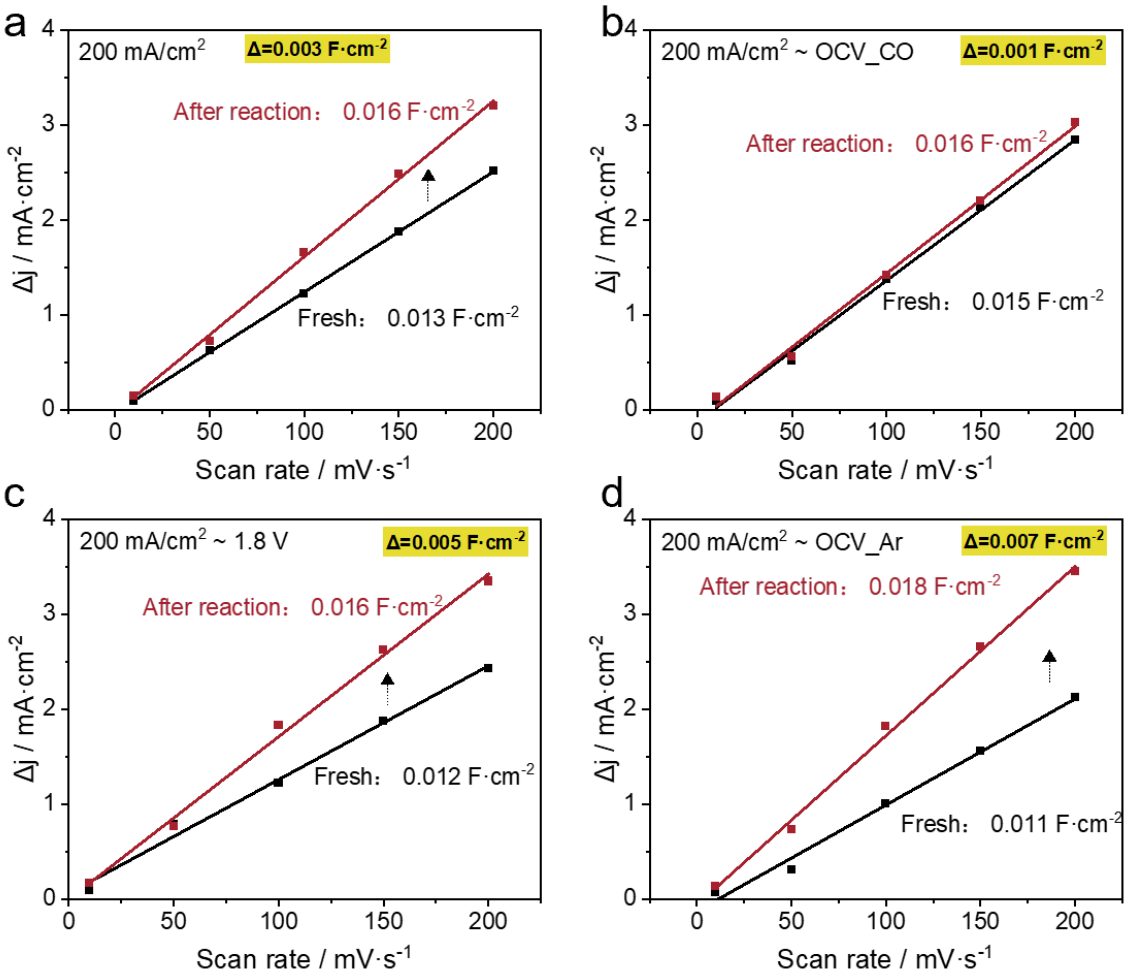

Supplementary Fig. 7 | Electrochemical active surface area (ECSA) of the Cu catalyst. The fresh Cu cathode was measured after 10 minutes of activation under CO electroreduction in four different experiments. Post-reaction ECSA measurements were conducted under the following conditions: **a** | Steady state operation at 200 mA cm^{-2} for 24 hours (measured at point B in Supplementary Fig. 6a). **b** | Power-off/power-on dynamic operation in CO for 24 hours (measured at point D in Supplementary Fig. 6b). **c** | Dynamic operation cycling between 200 mA cm^{-2} and 1.8 V in CO for 24 hours (measured at point D in Supplementary Fig. 37b). **d** | Power-off/power-on dynamic operation in Ar during power-off operation for 24 hours (measured at point D in Supplementary Fig. 26b).

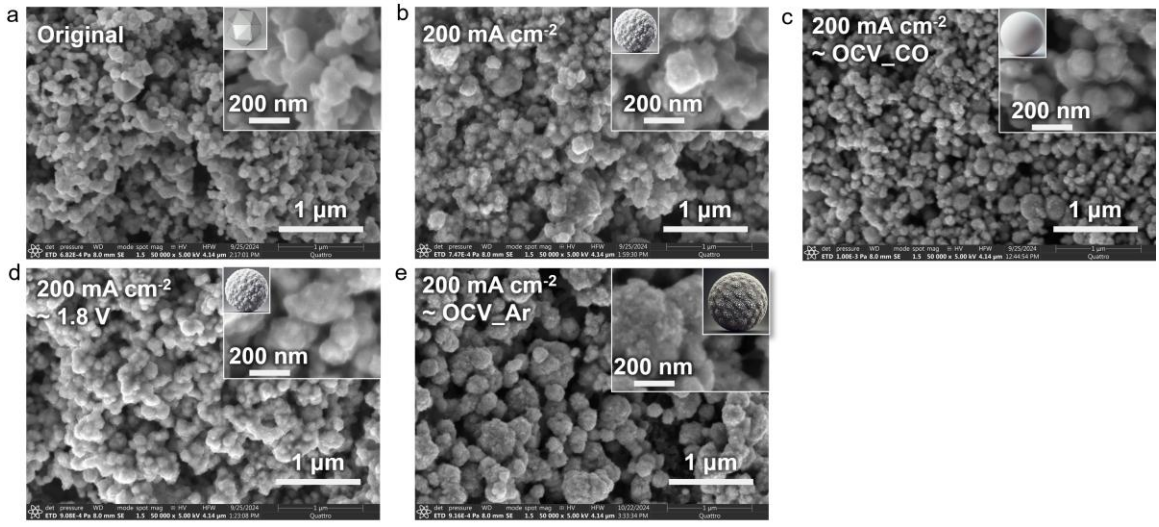

Supplementary Fig. 8 | Scanning electron microscopy (SEM) analysis of the Cu catalyst morphology. a | SEM image of the pristine Cu cathode before the reaction. The post-reaction SEM images were taken after the following operational conditions: **b** | Steady state operation at 200 mA cm^{-2} for 24 hours (measured at point B in Supplementary Fig. 6a). **c** | Power-off/power-on dynamic operation in CO for 24 hours (measured at point D in Supplementary Fig. 6b). **d** | Dynamic operation cycling between 200 mA cm^{-2} and 1.8 V in CO for 24 hours (measured at point D in Supplementary Fig. 37b). **e** | Power-off/power-on dynamic operation in Ar during power-off operation for 24 hours (measured at point D in Supplementary Fig. 26b). To minimize the effect of oxygen exposure on the Cu structure, all samples were prepared and stored in an Ar-filled glovebox immediately after cell disassembly and cathode washing with Milli-Q water. Samples were transferred from the glovebox to the SEM equipment using an argon-purged plastic bag, keeping total air exposure under 30 seconds during the entire preparation time. More experimental detail can be found in the Methods section.

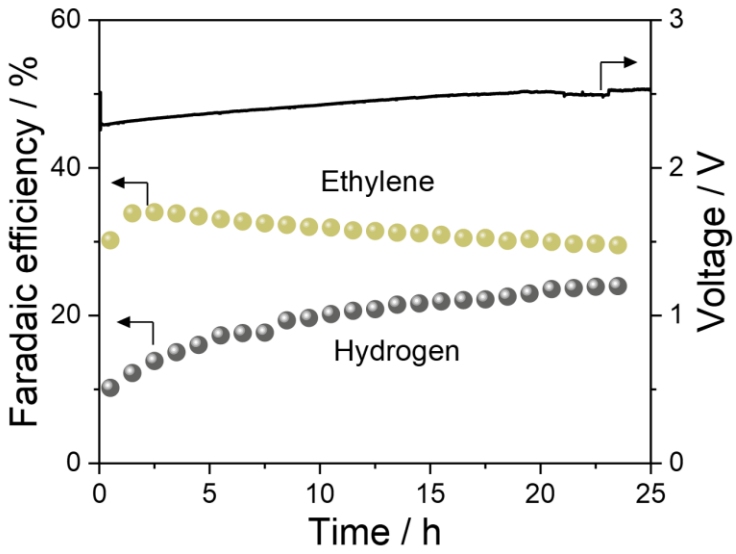

Supplementary Fig. 9 | Performance of a zero-gap CO electrolyzer during the first 24 hours. After 24 hours of steady state operation at 200 mA cm^{-2}, the electrolyzer was used to explore dynamic operation strategies, ensuring consistent initial performance in later experiments. The electrolyzer demonstrated a stable performance after this period.

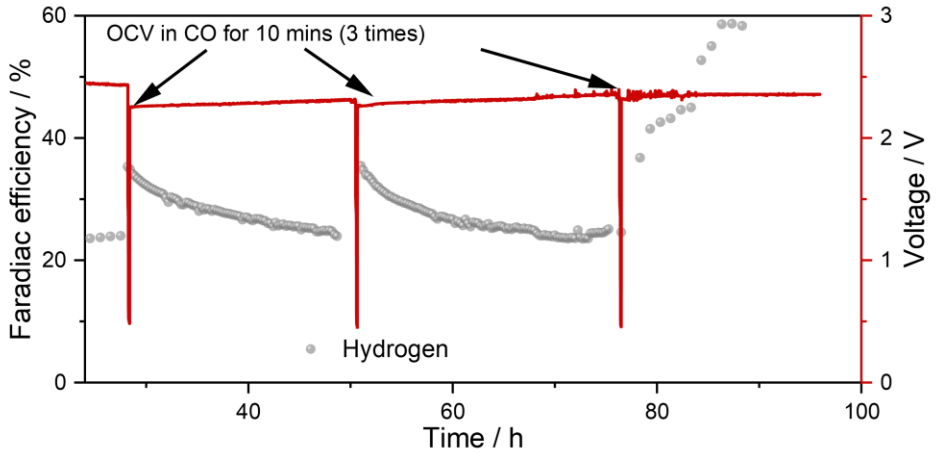

Supplementary Fig. 10 | Activity decay upon repeated OCP interruptions under CO atmosphere. Three consecutive 10-minute OCP periods cause progressive loss of Faradaic efficiency, confirming partial irreversibility of carbonate accumulation.

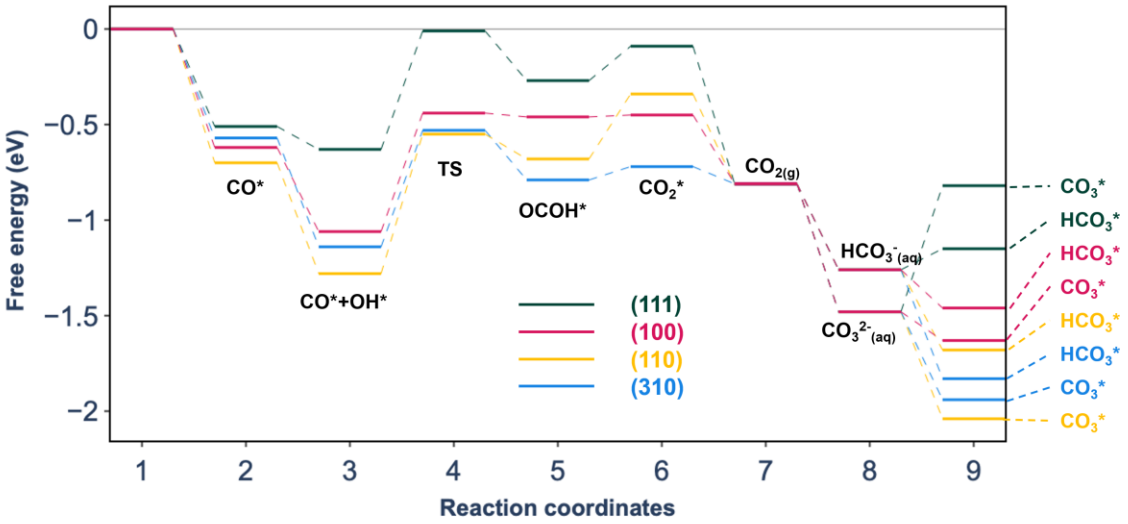

Supplementary Fig. 11 | Free energy landscape at -0.07 V vs. RHE at pH 14 on different facets of Cu.

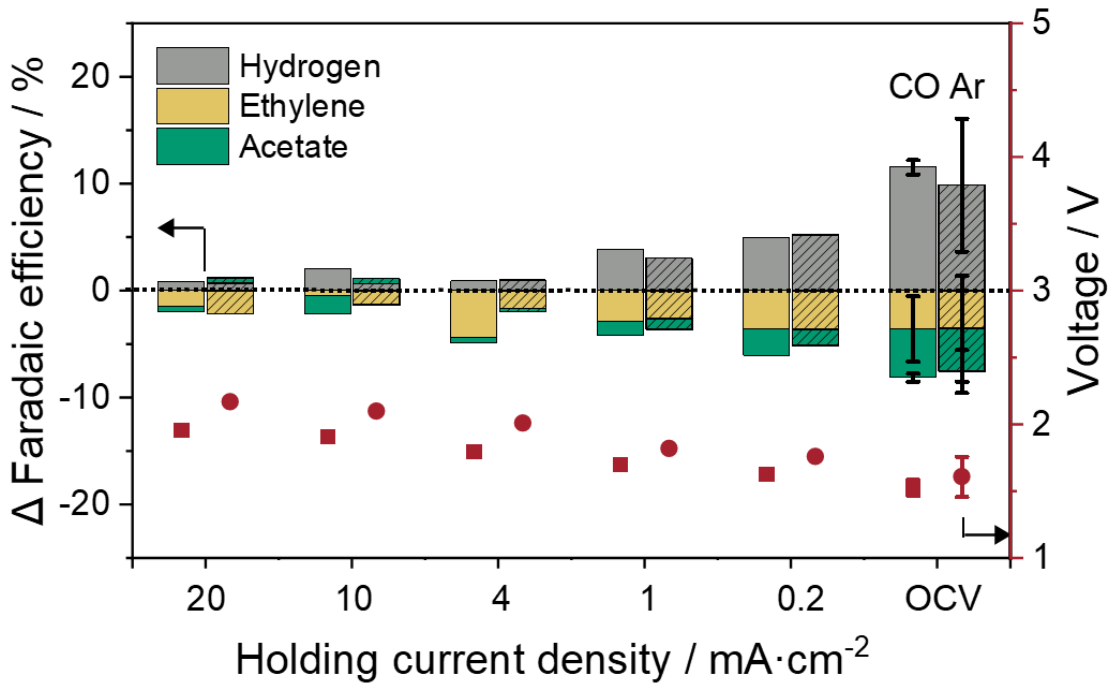

Supplementary Fig. 12 | Effects of different holding current densities on the change in Faradaic efficiency (ΔFE) and the corresponding voltage under Argon (Ar) conditions. Data are presented as mean ± standard deviation (SD) from three independent experiments.

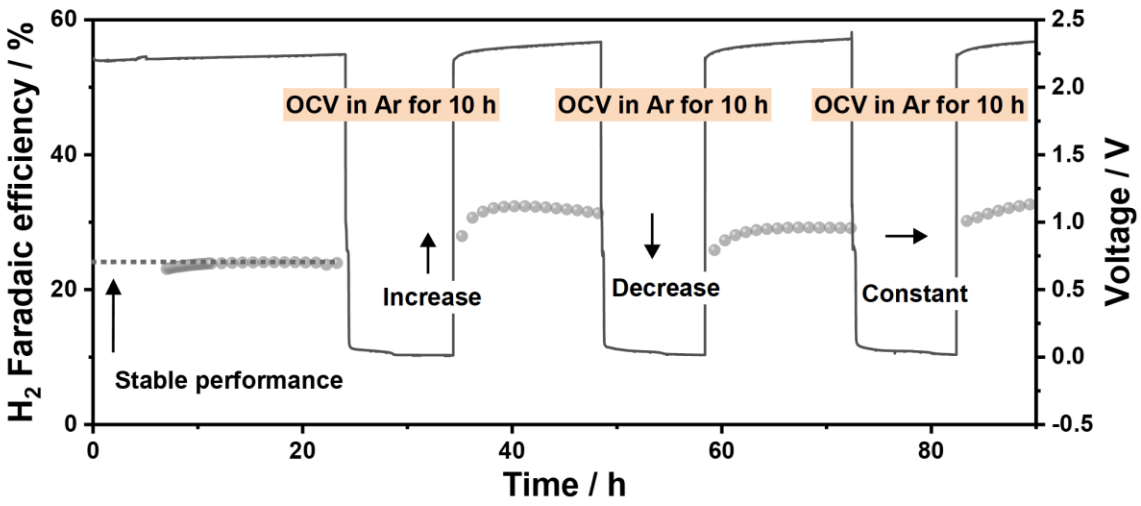

Supplementary Fig. 13 | Hydrogen Faradaic efficiency and voltage over time during dynamic operation between 200 mA cm-2 and OCV in Ar. Measurements were performed in a 5 cm^2 zero-gap CO electrolyzer in 1 M KOH, alternating between 200 mA cm^{-2} and OCV in Ar for three cycles after stabilizing at 200 mA cm^{-2} for 24 hours. The hydrogen FE exhibited varying trends across the three cycles after the electrolyzer was turned on. In the first cycle, hydrogen FE increased by approximately 4.0%. In the second, it decreased by around 5.4%. In the third cycle, hydrogen FE remained relatively stable, with only a slight increase of 0.9%.

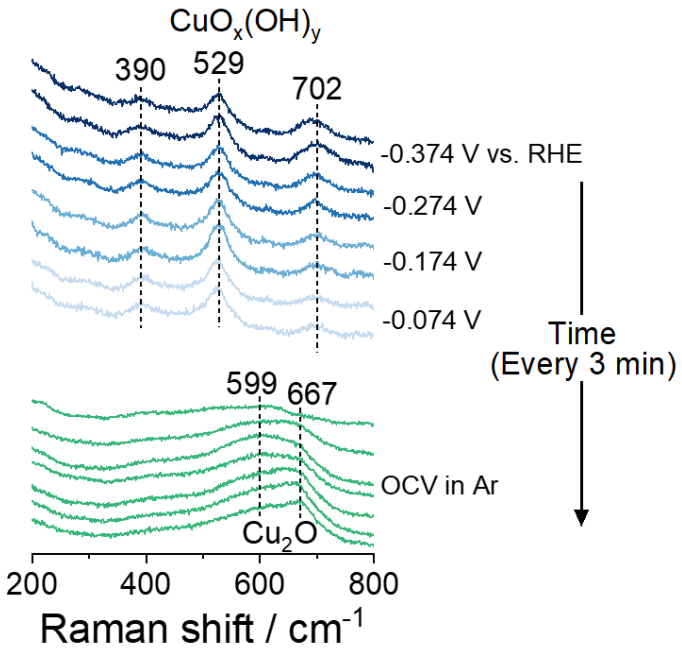

Supplementary Fig. 14 | *In-situ* surface-enhanced Raman spectra collected during CO electrolysis and at OCV in Ar, showing Cu_2O formation[6,7].

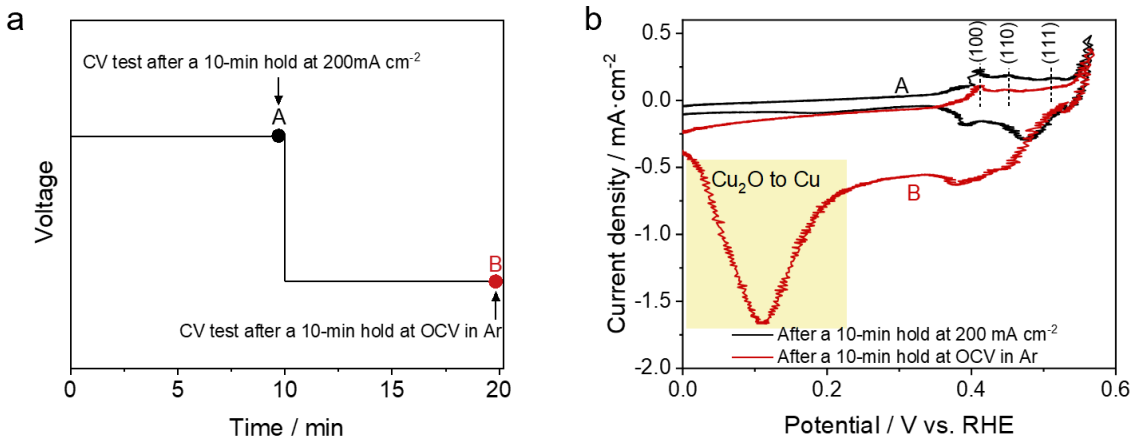

Supplementary Fig. 15 | CV test of the Cu catalyst before and after OCV in Ar for 10 mins. **a** | Schematic of the test procedure. The initial CV was measured at points A after activating the Cu catalyst during CO reduction for 10 minutes to establish a stable CV baseline. After collecting the CV at point A, the CO electrolyzer was power-off at OCV in Ar for 10 mins, followed by CV measurement at point B. **b** | Comparison of CVs at points A and B. Under OCV in Ar, the Cu surface underwent significant oxidation, forming Cu_2O.[6,8] The CVs were measured in Ar condition at a scan rate of 20 mV s^{-1}. More experimental detail can be found in the Methods section.

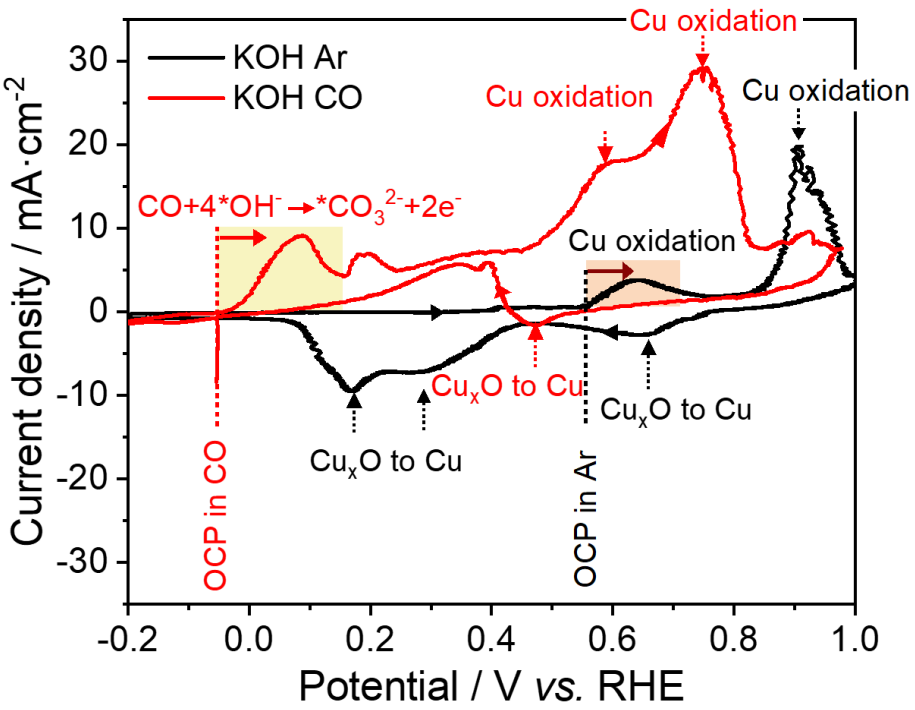

Supplementary Fig. 16 | CV test of the Cu catalyst in Ar and CO. This experiment was conducted in both Ar and CO condition after activating the Cu catalyst for 10 minutes under CO reduction at 200 mA cm^{-2}, at a scan rate of 20 mV s^{-1}. The OCP in CO and Ar environments is approximately –0.07 V and 0.55 V *vs.* RHE, respectively. Notably, the potential required for Cu oxidation in a CO environment is around 0.59 V vs. RHE, which exceeds the OCP. This suggests that under power-off operation, Cu oxidation is thermodynamically unfavorable in a CO-rich environment, potentially leading to carbonate formation instead.

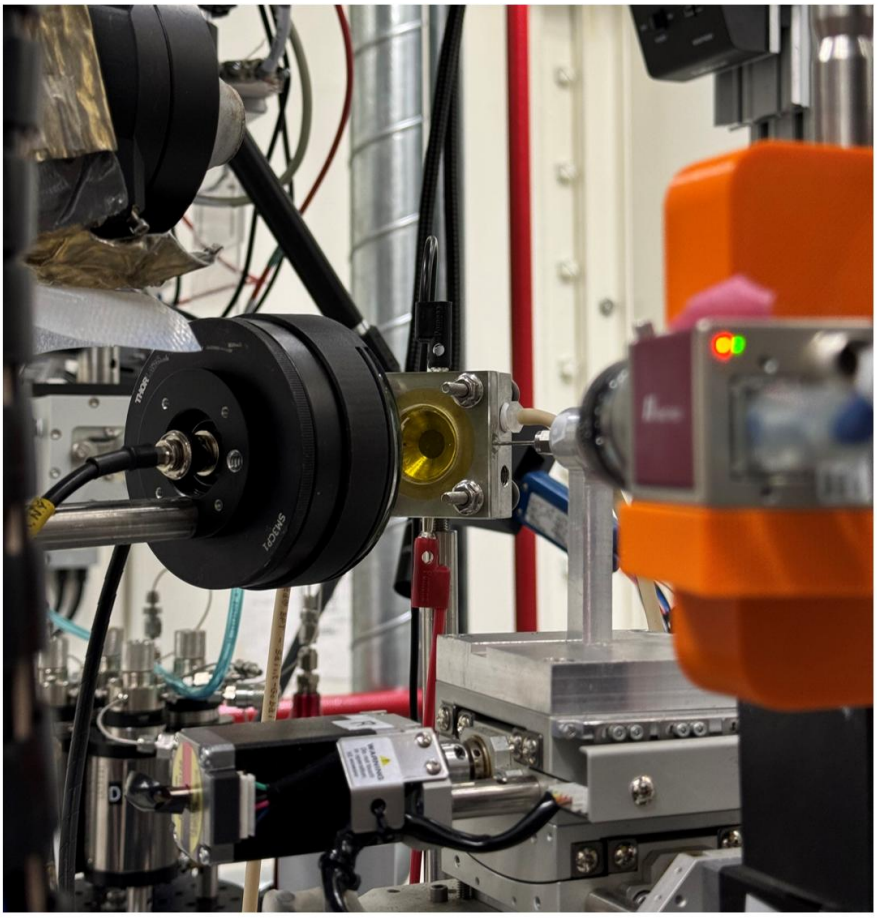

Supplementary Fig. 17 | In-situ XAS cell in the beamline setup. *In-situ* XAS was measured at the 8-ID Inner Shell Spectroscopy beamline of the National Synchrotron Light Source II at Brookhaven National Laboratory. The cathode compartment has an open window with two different diameters: the smaller inner hole is 1 cm in diameter (active area 0.785 cm^2), and the larger outer hole is 2.5 cm in diameter, covered by Kapton film. CO gas was introduced through the cathode compartment through stainless steel tubing. The anode compartment is the same 5 cm^2 zero-gap electrolyzer used in the other experiments. The gasket size was adjusted to 1.5 × 1.5 cm^2.

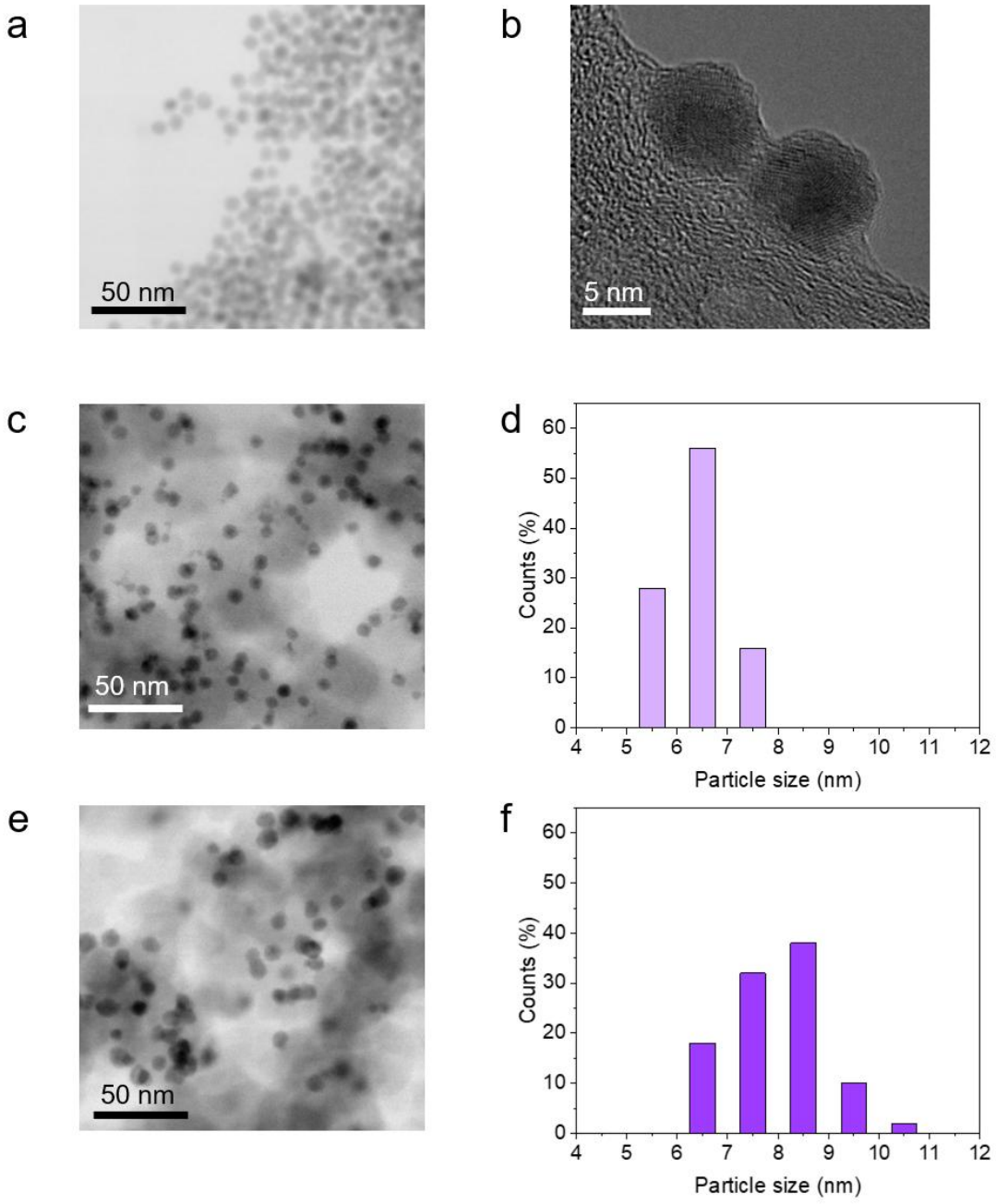

Supplementary Fig. 18 | TEM images of homemade Cu nanoparticles and carbon-supported Cu nanoparticles. a | As-synthesized Cu nanoparticles before the addition of the carbon support, and **b** | a magnified view. **c** | Cu nanoparticles supported on Vulcan XC-72R carbon, and **d** | the corresponding particle size distribution, around 6.4 ± 0.6 nm. **d** | CuO-Cu on Vulcan XC-72R carbon after heat treatment (CuO-Cu/C), and **f** | its particle size distribution, around 8.0 ± 0.9 nm.

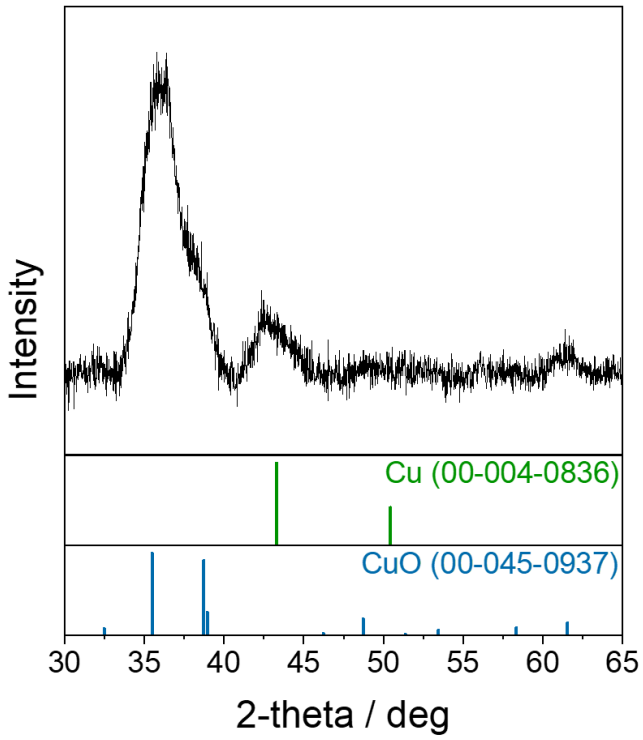

Supplementary Fig. 19 | X-ray diffraction (XRD) pattern of CuO-Cu/C catalyst. The XRD results confirmed a mixed-phase composition of Cu and CuO.

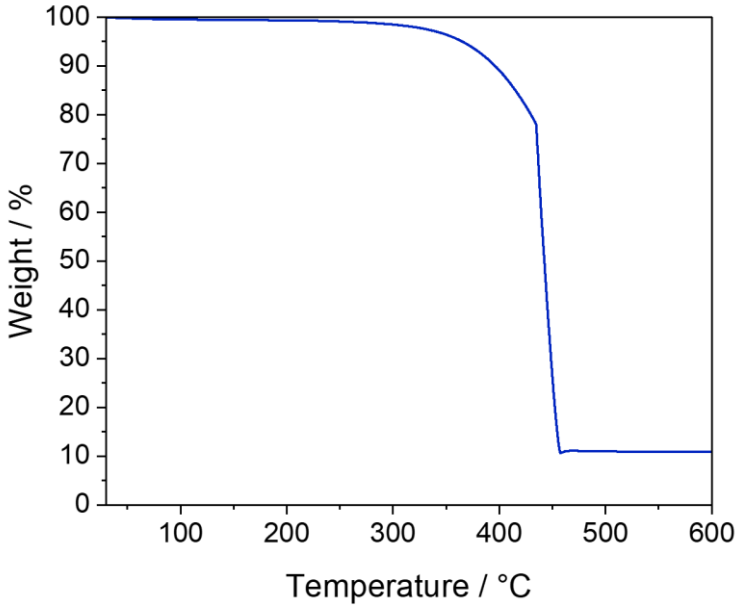

Supplementary Fig. 20 | Thermogravimetric analysis (TGA) of heat-treated CuO-Cu/C catalyst. The TGA results indicated a CuO-Cu loading of 10 wt%,

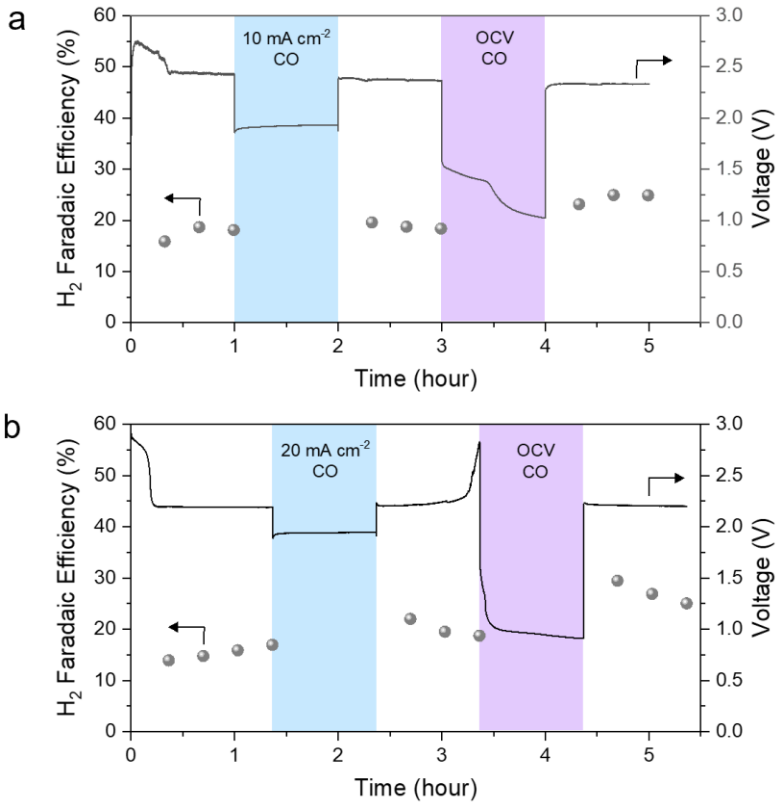

Supplementary Fig. 21 | Dynamic operation experiments using an in-situ X-ray absorption spectroscopy (XAS) cell. a | Dynamic operation cycling between 200 mA cm^{-2} and 10 mA cm^{-2}, as well as between 200 mA cm^{-2} and OCV, under CO conditions using a commercial 40–60 nm copper catalyst. **b** | Dynamic operation cycling between 200 mA cm^{-2}, 20 mA cm^{-2}, and 200 mA cm^{-2} and OCV under CO conditions using a homemade CuO-Cu/C catalyst. The current density was set at 20 mA cm^{-2} in **b** | because 90% of the catalyst is carbon, which has a higher double-layer capacity. No detectable carbon product was observed at 20 mA cm^{-2}.

To validate our in-situ XAS setup, we tested the Cu catalyst used in the other experiments (Cu, 40–60 nm, Sigma-Aldrich) under dynamic conditions. Hydrogen FE recovered after holding at 10 mA cm^{-2} for an hour, but did not recover after holding at OCV for an hour, consistent with trends observed in our 5 cm^2 zero-gap electrolyzer (Supplementary Fig. 12). Similarly, the CuO-Cu/C catalysts exhibited increased hydrogen FE after OCV exposure, while the hydrogen FE recovered after holding at 20 mA cm^{-2} for an hour.

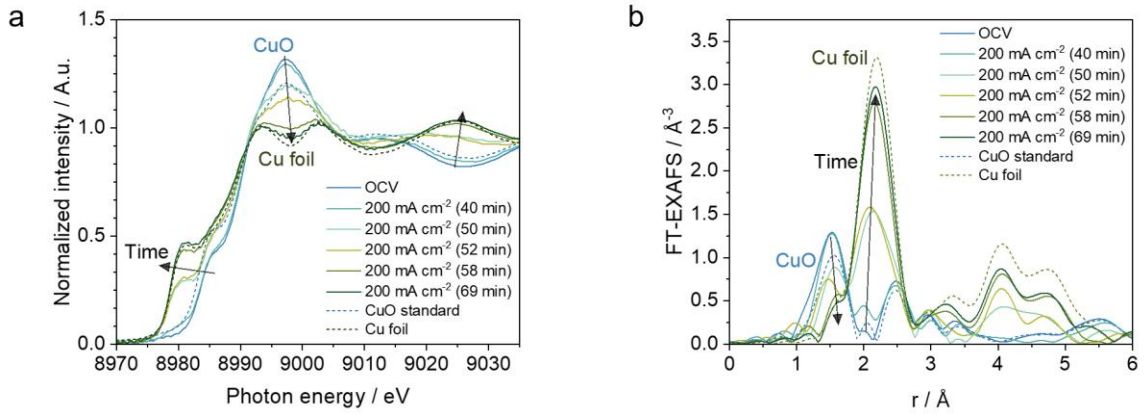

Supplementary Fig. 22 | In-situ XAS of CuO-Cu/C catalysts for CO electrolysis. a | XANES and **b** | EXAFS spectra measured before applying current (OCV) and during CO electrolysis at 200 mA cm^{-2}. In-situ XAS revealed that CuO-Cu/C was gradually reduced from CuO to Cu over time during CO electrolysis at 200 mA cm^{-2}.

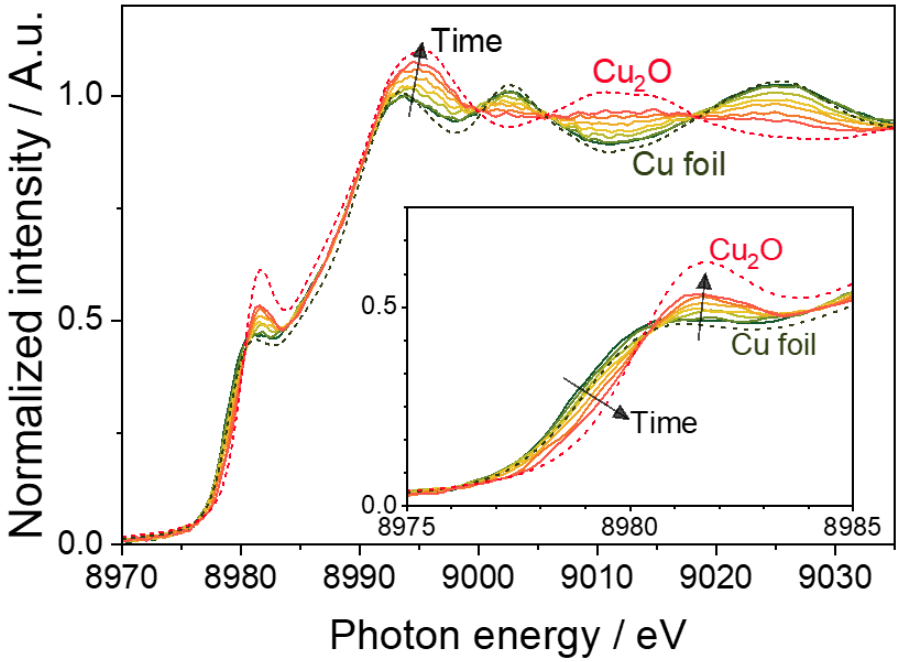

Supplementary Fig. 23 | In-situ X-ray absorption near-edge structure (XANES) spectra under OCV in Ar following CO reduction at 200 mA cm-2. The catalyst was gradually oxidized from metallic Cu to Cu_2O over time under these conditions.

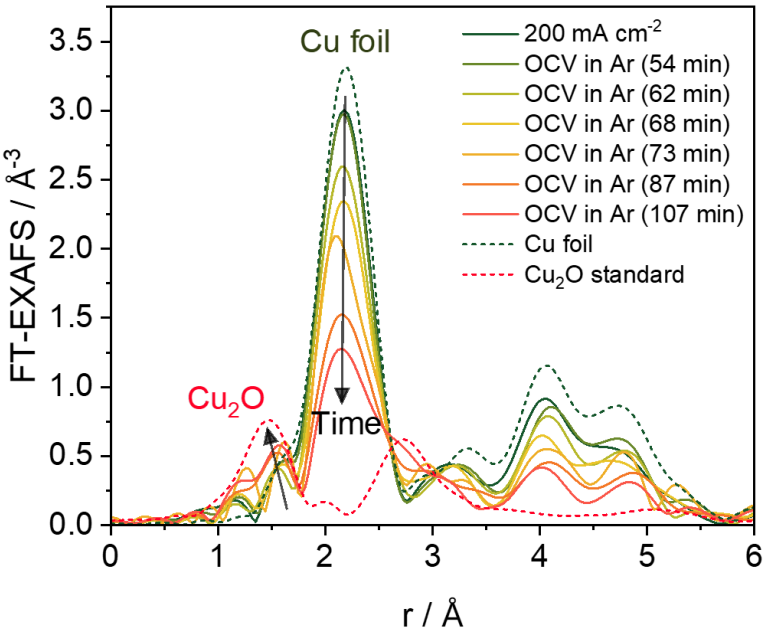

Supplementary Fig. 24 | In-situ EXAFS spectra of CuO-Cu/C catalysts during CO electrolysis at 200 mA cm-2 and after stop applying current (OCV) in Ar. Once fully reduced, the catalyst was held at OCV under Ar conditions. The EXAFS spectra indicated that Cu gradually oxidized into Cu_2O, as also shown in Supplementary Fig. 23 and 25.

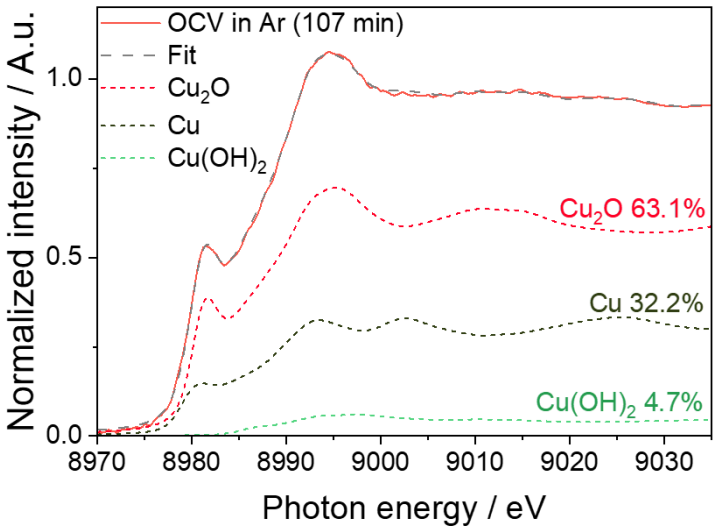

Supplementary Fig. 25 | Linear combination analysis of XANES spectra under OCV in Ar after CO reduction at 200 mA cm-2. The Cu speciation was quantified as 63.1% Cu_2O, 32.2% Cu, and 4.7% $Cu(OH)_2$ (Reduced χ^2 = 0.00010).

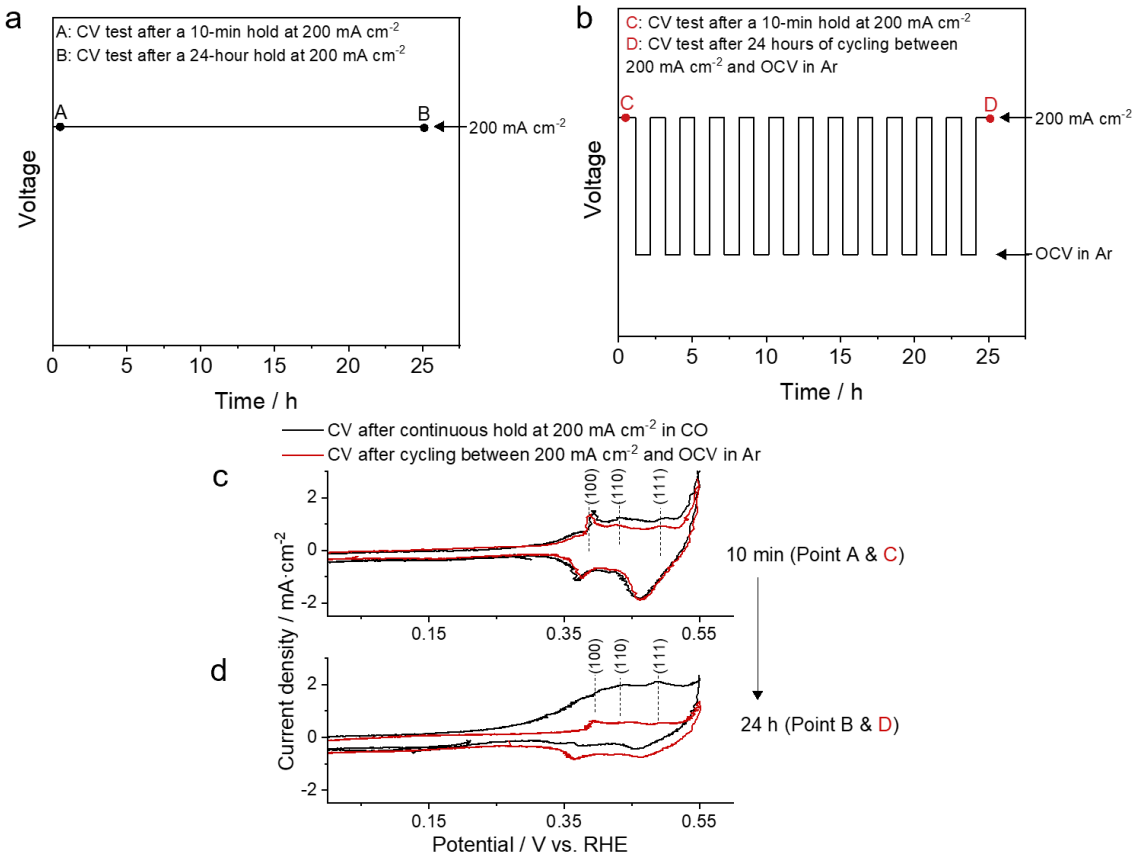

Supplementary Fig. 26 | CV test of the Cu catalyst before and after dynamic operation at OCV in Ar for 24 hours. a, **b** | Schematic of the test procedure. The initial CV was measured at points A and C after activating the Cu catalyst during CO reduction for 10 minutes to establish a stable baseline. After collecting the CVs at point A and C, the CO electrolyzer was either operated continuously at 200 mA cm^{-2} or subjected to a dynamic operation—cycling between 200 mA cm^{-2} for one hour and OCV in Ar for one hour—over a 24-hour period, followed by CV measurements at points B and D, respectively. **c** | Comparison of CVs at points A and C. The initial Cu CV profiles for both experiments exhibit similar Cu facet structures, eliminating potential baseline effects from different experimental setups. **d** | Comparison of CVs at points B and D. All Cu facet-related features, including (100), (110), and (111), exhibit structural differences, indicating that the reconstruction pathway differs between steady state operation and dynamic operation at OCV in Ar. The CVs were measured under Ar conditions at a scan rate of 20 mV s^{-1}.

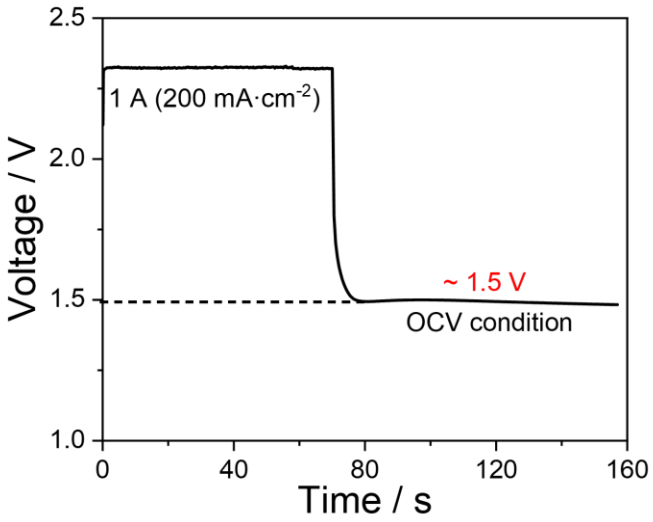

Supplementary Fig. 27 | Voltage of the zero-gap CO electrolyzer at 200 mA cm-2 and OCV in CO. The electrolyzer's OCV in CO is approximately 1.5 V.

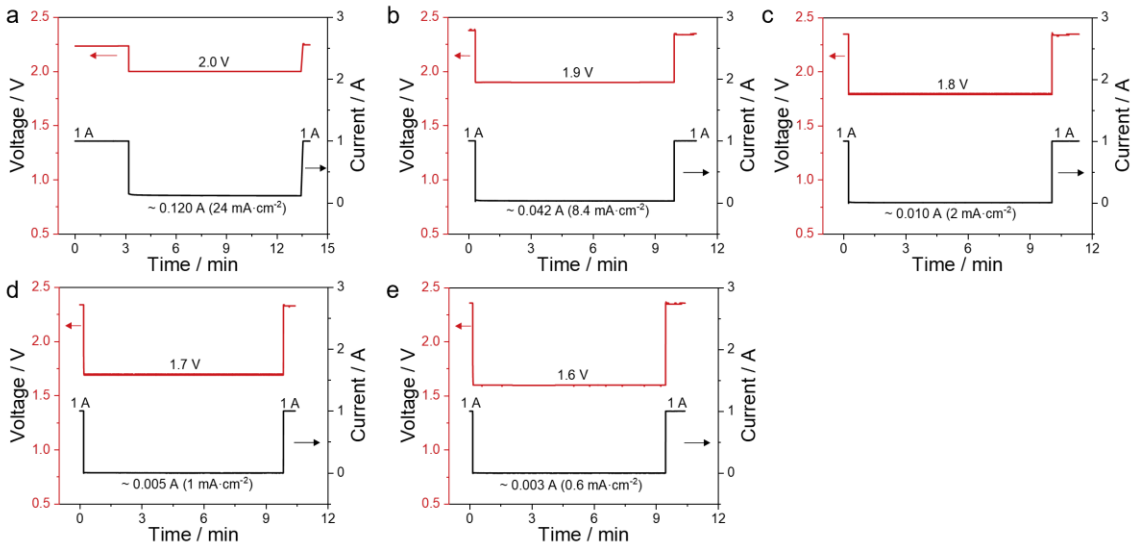

Supplementary Fig. 28 | Exploration of dynamic operation voltage conditions from 2.0 V to 1.6 V. a–e, Voltage and current profiles during power-down operation at holding voltages of **2.0 V (a), 1.9 V (b), 1.8 V (c), 1.7 V (d), and 1.6 V (e)**. The left y-axis shows the voltage, and the right y-axis shows the current. In each experiment, the cell was first operated at a constant current density of 200 mA cm^{-2} (1 A), then powered down at the specified constant voltage for 10 min, before switching back to 200 mA cm^{-2}. The entire experiment was conducted under CO gas conditions. More detailed experimental procedures are provided in the Methods section.

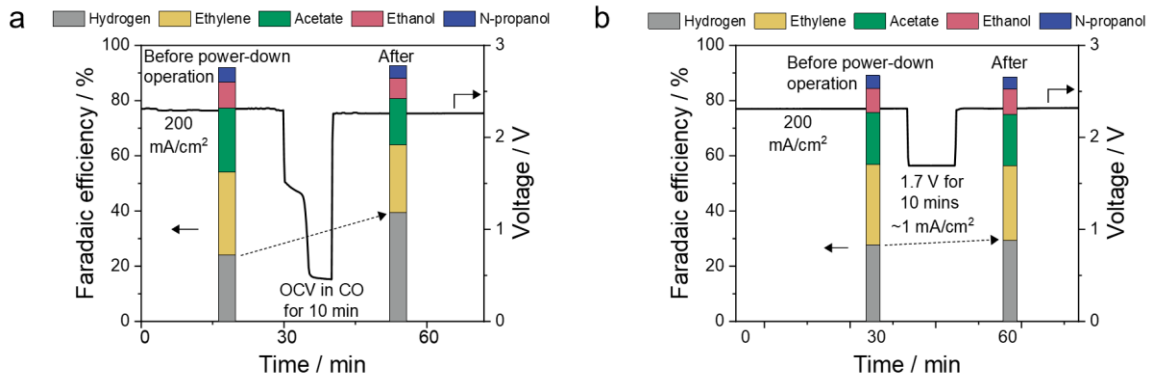

Supplementary Fig. 29 | Performance of a zero-gap CO electrolyzer during dynamic operation at (a) OCV in CO and (b) 1.7 V in CO for 10 minutes. The left y-axis shows FE, and the right y-axis shows the voltage, where the electrolyzer was operated at 200 mA cm^{-2}. These data were selected as an example to illustrate the data collection and calculation method used for Fig. 4b.

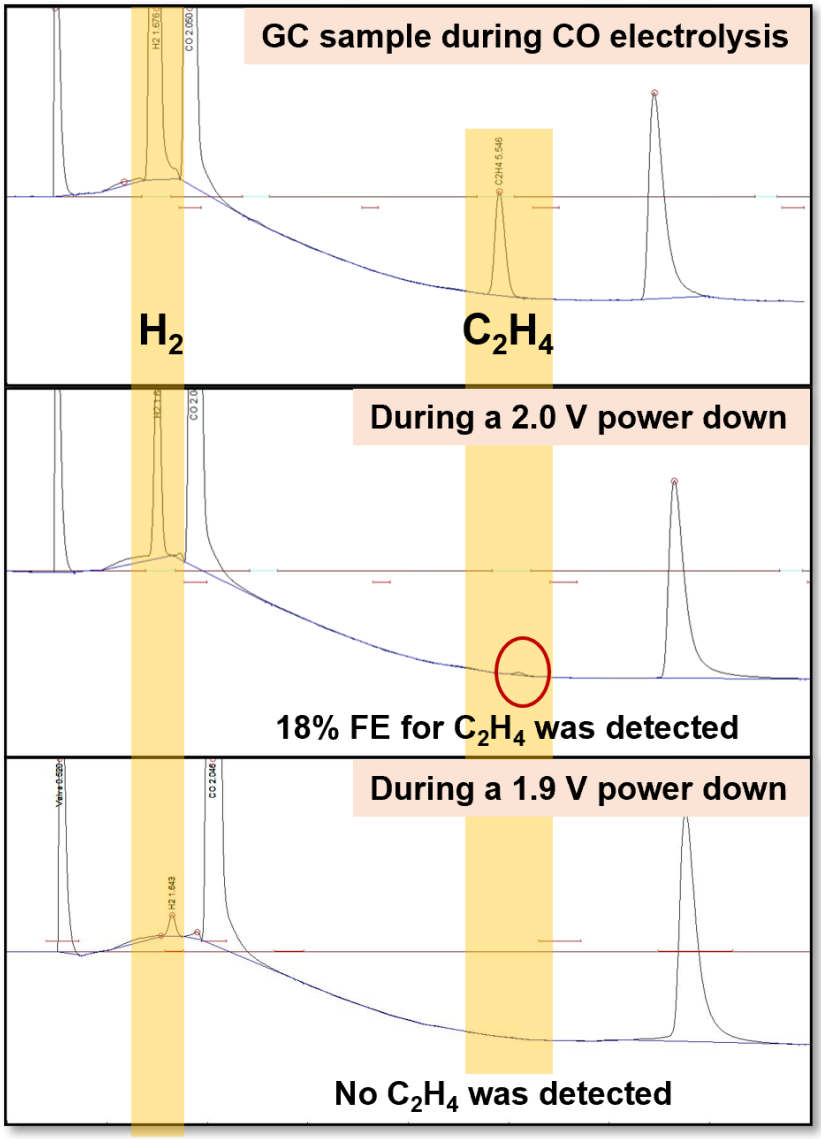

Supplementary Fig. 30 | Raw GC data during CO electrolysis at 200 mA cm-2, 2.0 V, and 1.9 V. At 1.9 V, no detectable CO reduction products (e.g., C_2H_4) were observed, while a small amount of hydrogen evolution reaction (HER) activity was present. At 2.0 V, 18% FE of C_2H_4 (~3.2 mA cm^{-2}) was observed in addition to hydrogen.

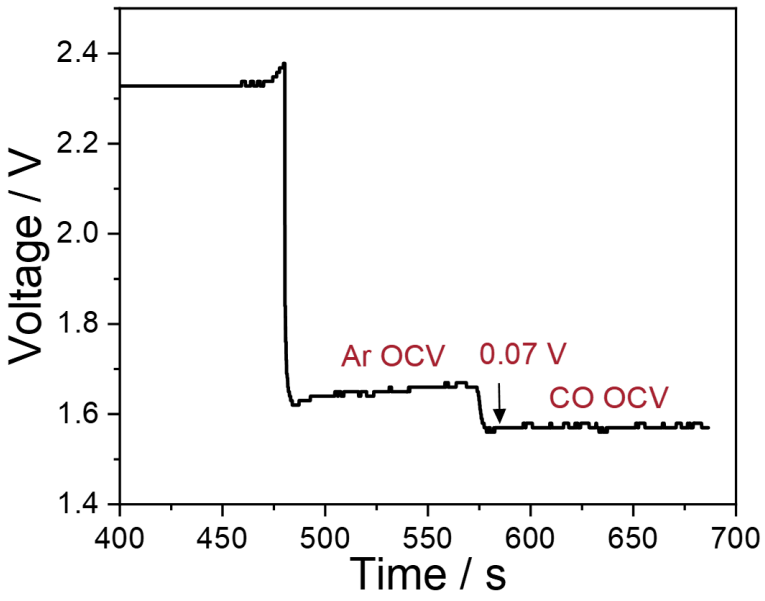

Supplementary Fig. 31 | Voltage of the zero-gap CO electrolyzer at 200 mA cm^{-2} and OCV under Ar and CO conditions. The OCV in Ar is approximately 0.07 V higher than under CO conditions.

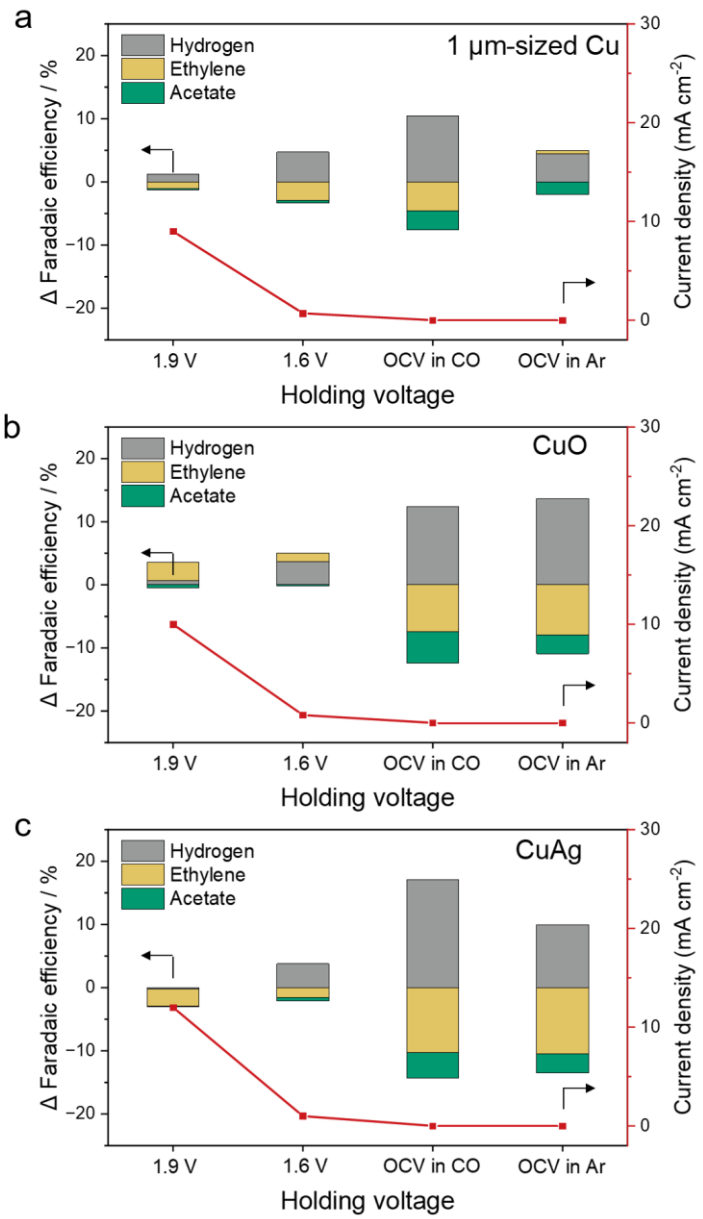

Supplementary Fig. 32 | Evaluation of the applicability of the dynamic operation strategy on other Cu based catalyst including micron-sized sized Cu, CuO, and CuAg. The same cathode preparation method was used (Copper powder, –625 mesh, APS 0.50–1.5 micron, 99%, Thermo Scientific Chemicals; Copper(II) oxide, nanopowder <50 nm, Sigma-Aldrich; Silver-copper alloy, nanopowder <100 nm particle, Sigma-Aldrich). The left y-axis shows ΔFE, and the right y-axis shows the current density at the specific holding voltage.

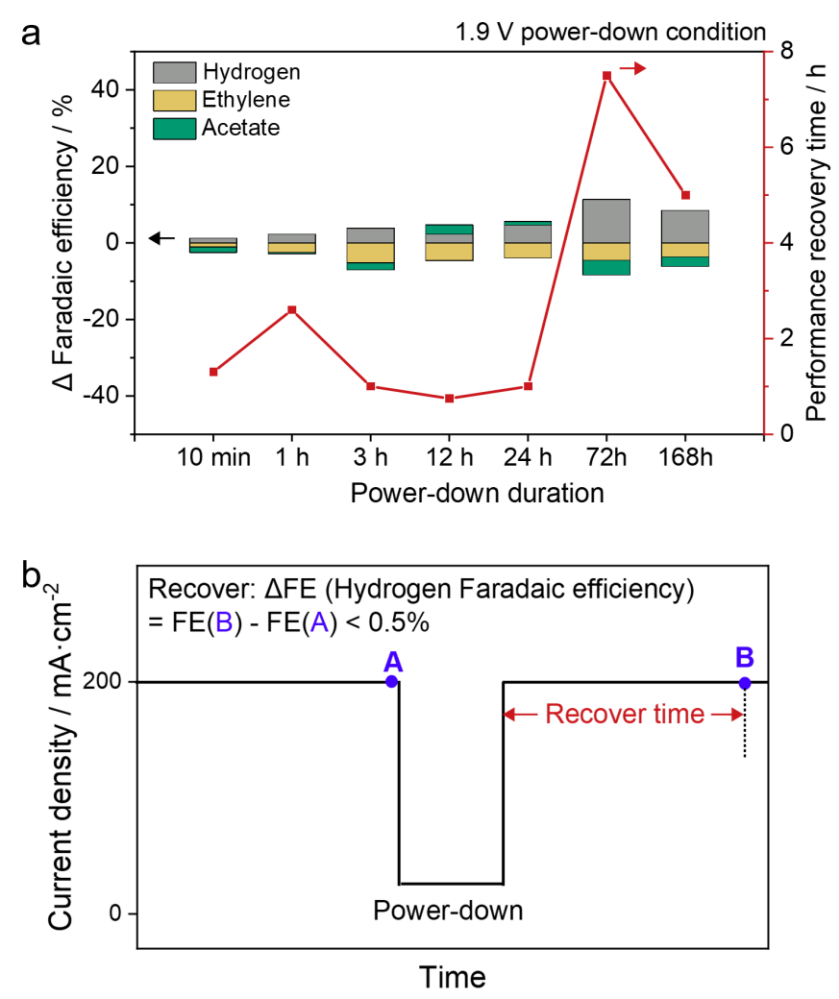

Supplementary Fig. 33 | Exploration of power-down duration in dynamic operation. a | Power-down operation at 1.9 V in CO**.** The left y-axis shows ΔFE, and the right y-axis shows the performance recovery time. **b |** Performance recovery time was defined as the duration required for the ΔFE of hydrogen (calculated as $FE_{after\ power\text{-}down} - FE_{before\ power\text{-}down}$) to fall below 0.5%.

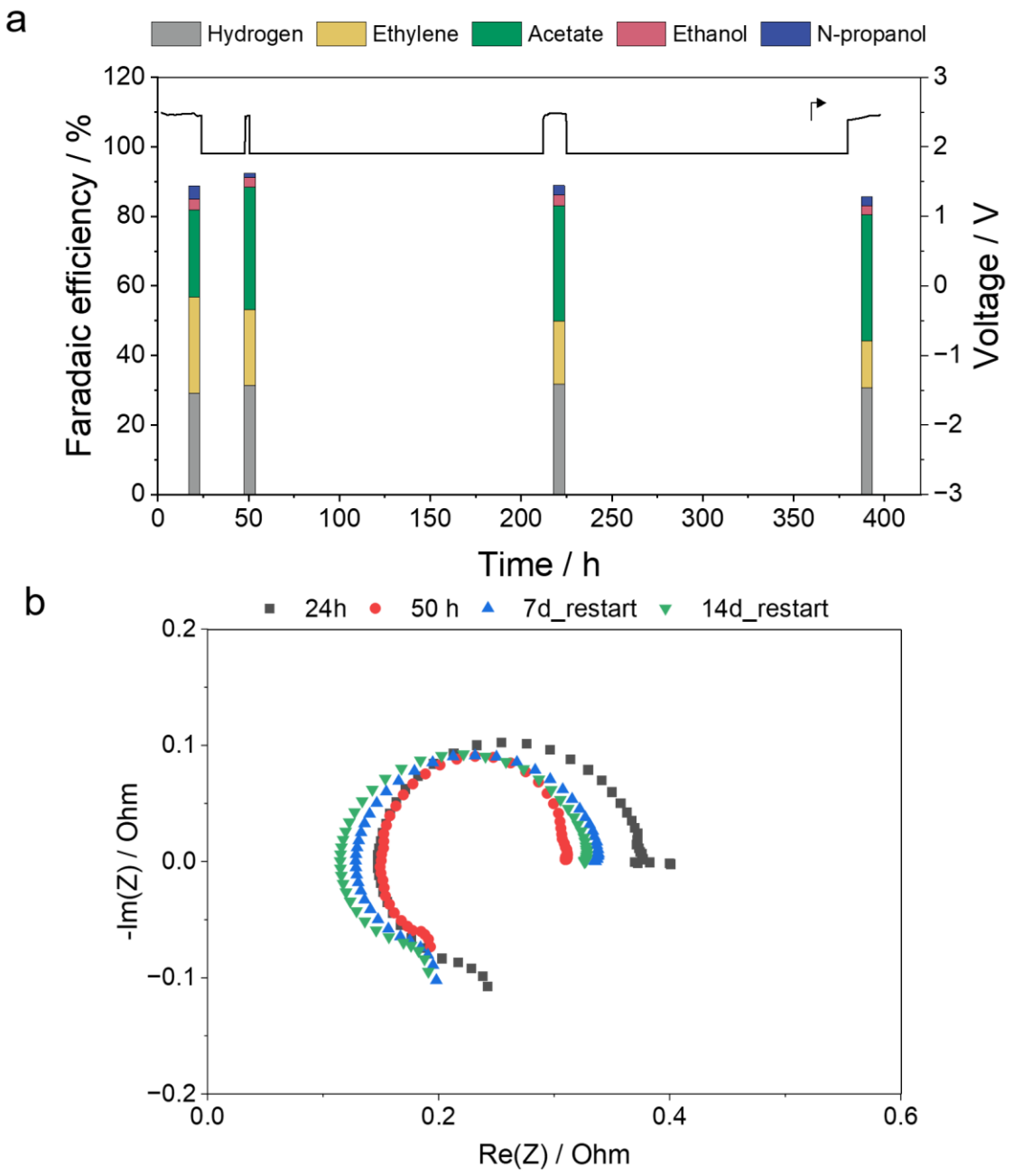

Supplementary Fig. 34 | Electrochemical impedance spectra of the CO electrolyzer at different stages of dynamic operation. a | Power-down operation at 1.9 V in CO for 7days two times**. b |** Nyquist plots collected after 24 h of initial stabilization (black), 50 h of operation (red), after the first 7-day power-down cycle (green), and after the second 7-day power-down cycle (purple) in Panel a.

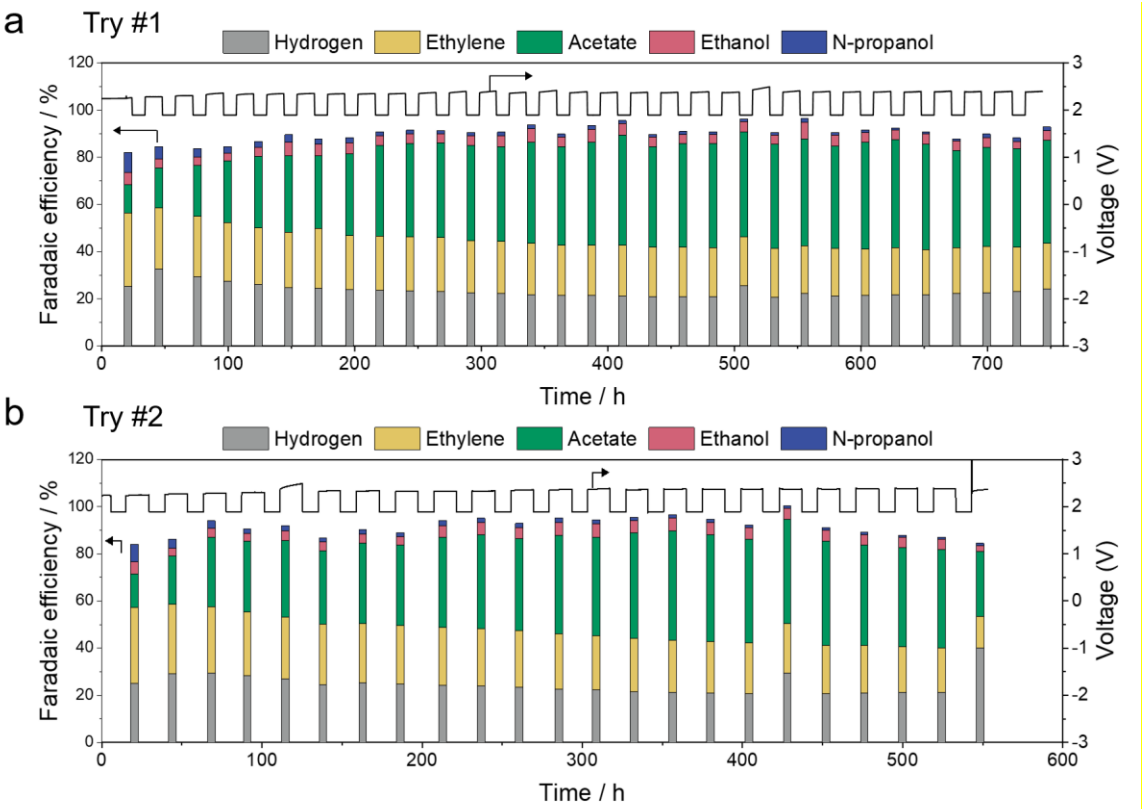

Supplementary Fig. 35 | Faradaic efficiency and voltage over time during dynamic operation between 200 mA cm-2 and 1.9 V in CO. a, b, Two independent dynamic operation tests, denoted as **Try #1 (a)** and **Try #2 (b)**. Measurements were performed in a 5 cm^2 zero-gap CO electrolyzer in 1 M KOH for two times**.** The system demonstrated stable performance for 750 hours, maintaining a C_{2+} Faradaic efficiency of approximately 75% and a voltage of 2.35 V. For “Try #2” in panel **b**, the experiment was compromised due to accidental drying of the cell during anolyte replacement.

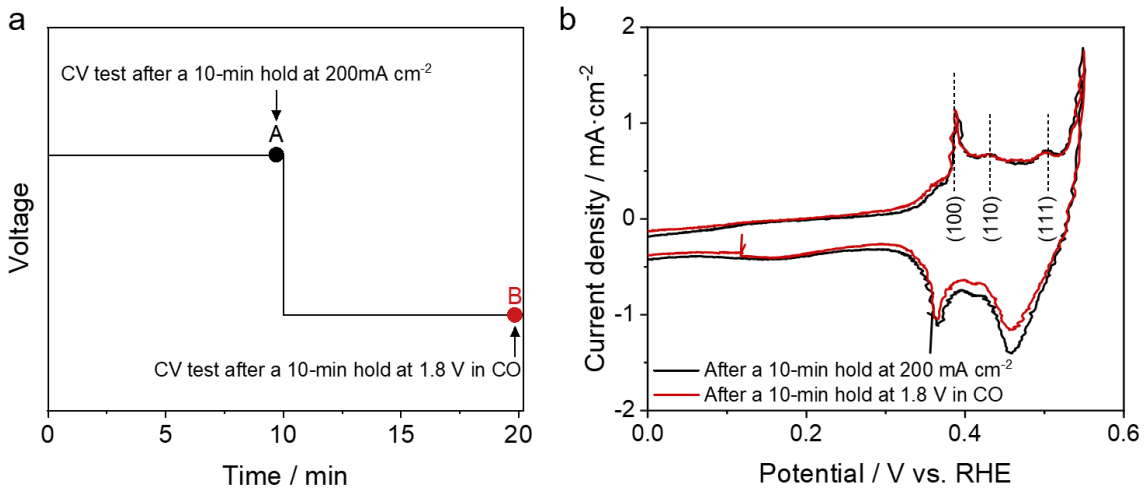

Supplementary Fig. 36 | CV test of the Cu catalyst before and after a 1.8 V power-down operation in CO for 10 minutes. a | Schematic of the test procedure. The initial CV was measured at point A after activating the Cu catalyst during CO reduction for 10 minutes to establish a stable CV baseline. After collecting the CV at point A, the CO electrolyzer was power down at 1.8 V for 10 minutes, followed by a CV measurement at point B. **b** | Comparison of CVs at points A and B. All Cu facet-related features, including (100), (110), and (111), were retained, indicating that the Cu catalyst remained stable during power-down operation at 1.8 V. All experimental details can be found in the Methods section. The CVs were measured under Ar conditions at a scan rate of 20 mV s^{-1}.

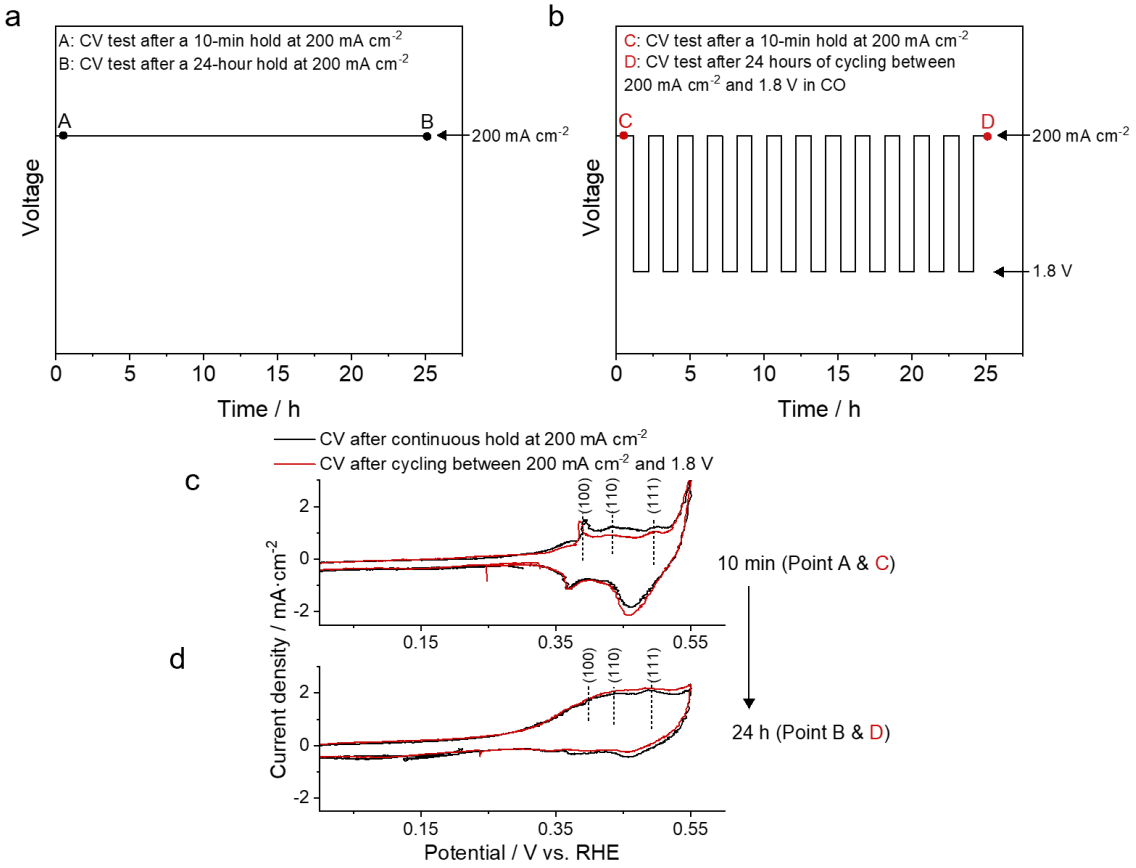

Supplementary Fig. 37 | CV test of the Cu catalyst before and after a 1.8 V power-down dynamic operation for 24 hours. a, **b** | Schematic of the test procedure. The initial CV was measured at points A and C after activating the Cu catalyst during CO reduction for 10 minutes to establish a stable CV baseline. After collecting the CVs at point A and C, the CO electrolyzer was either operated continuously at 200 mA cm^{-2} or subjected to dynamic operation—cycling between 200 mA cm^{-2} for one hour and 1.8 V for one hour—over a 24-hour period, followed by CV measurements at points B and D, respectively. **c** | Comparison of CVs at points A and C. The initial Cu CV profiles for both experiments exhibit similar Cu facet structures, eliminating potential baseline effects from different experimental setups. **d** | Comparison of CVs at points B and D. All Cu facet-related features, including (100), (110), and (111), remained similar despite exhibiting differences compared to the 10-minute result. These variations are attributed to Cu reconstruction during the CO reduction reaction. All experimental details can be found in the Methods section. The CVs were measured under Ar conditions at a scan rate of 20 mV s^{-1}.

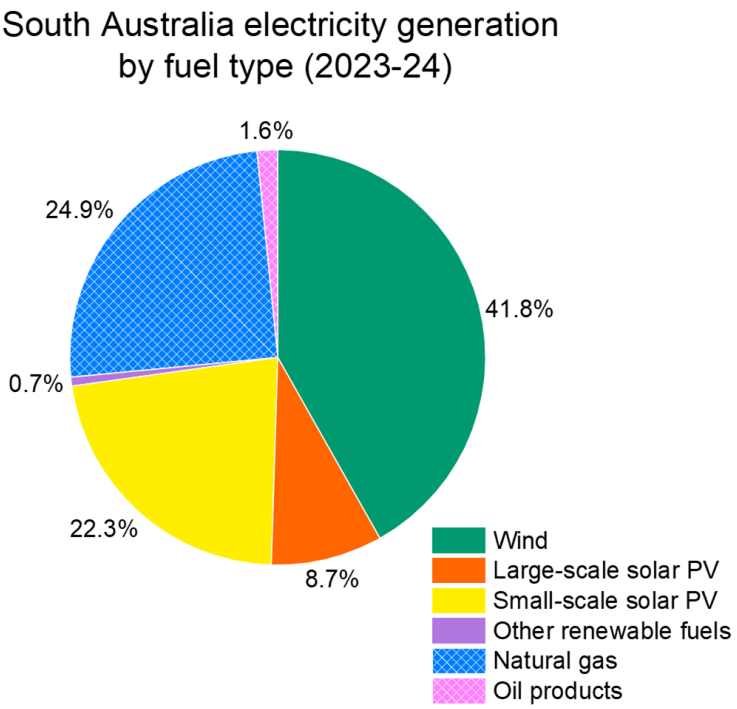

Supplementary Fig. 38 | Electricity generation by fuel type (2023–24) in South Australia. More than 70% of South Australia's electricity generation comes from renewable sources. "Other renewable fuels" include biogas and hydropower.[9]

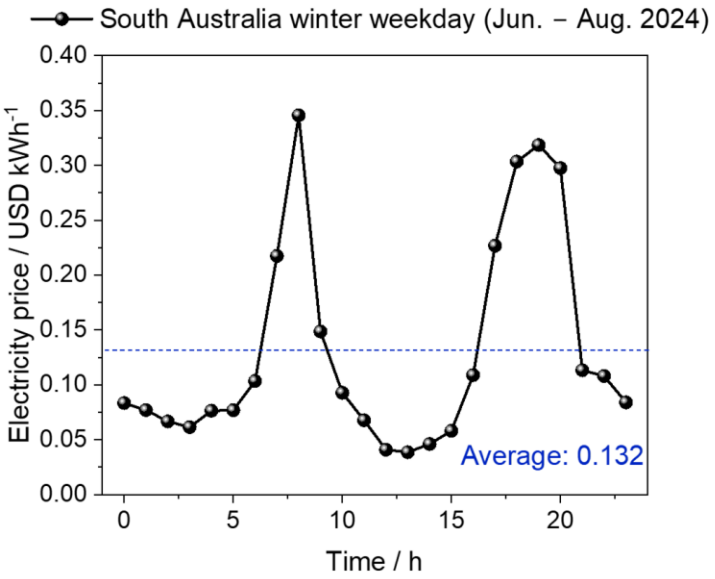

Supplementary Fig. 39 | Hourly averaged weekday electricity prices in South Australia from June to August 2024. The average electricity price is 0.132 USD kWh^{-1}, with a standard deviation of 0.097 USD kWh^{-1}.[10]

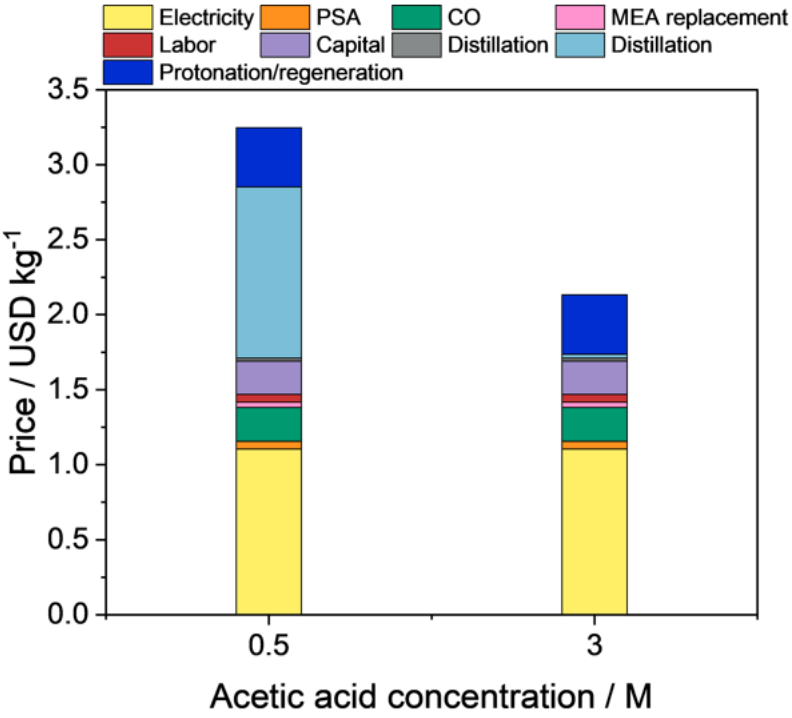

Supplementary Fig. 40 | Cost breakdown for acetic acid production from CO electrolyzers, comparing final product concentrations of 0.5 M and 3 M at full capacity (50,000 kg day-1). The analysis assumes an average weekday electricity price of 0.132 USD kWh^{-1} in South Australia from June to August 2024.[10] The "Other" category includes cell compartment replacements, maintenance, and water for the oxygen evolution reaction at the anode. Base-case capital expenses were used in this analysis.

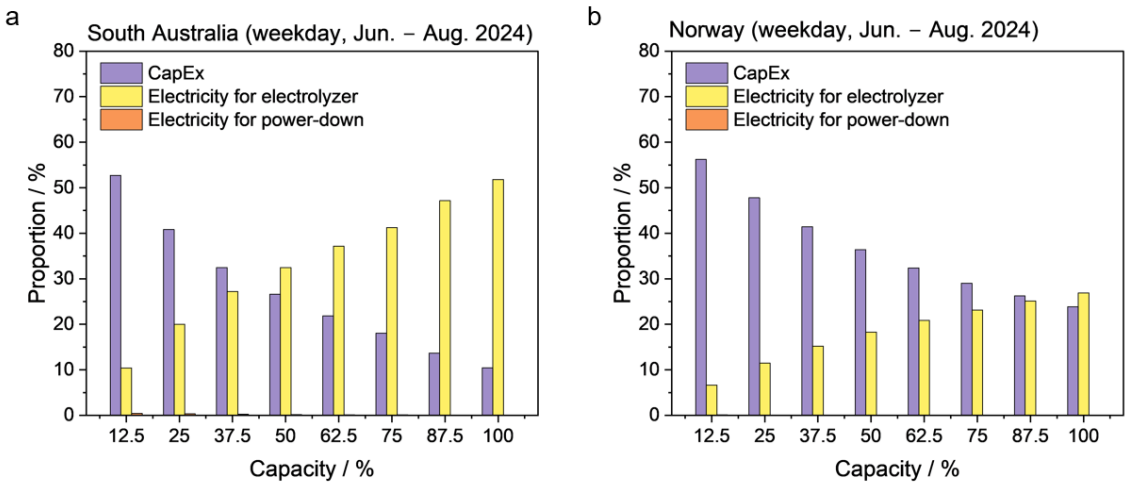

Supplementary Fig. 41 | Proportional contributions of CapEx, electrolyzer electricity, and power-down electricity to the total production cost of acetic acid from CO electrolyzers in South Australia (a) and Norway (b) from June to August 2024. The acetic acid production cost saving relative to operation at 100% capacity is shown in Fig. 5a. Base-case capital expenses were used in this analysis.

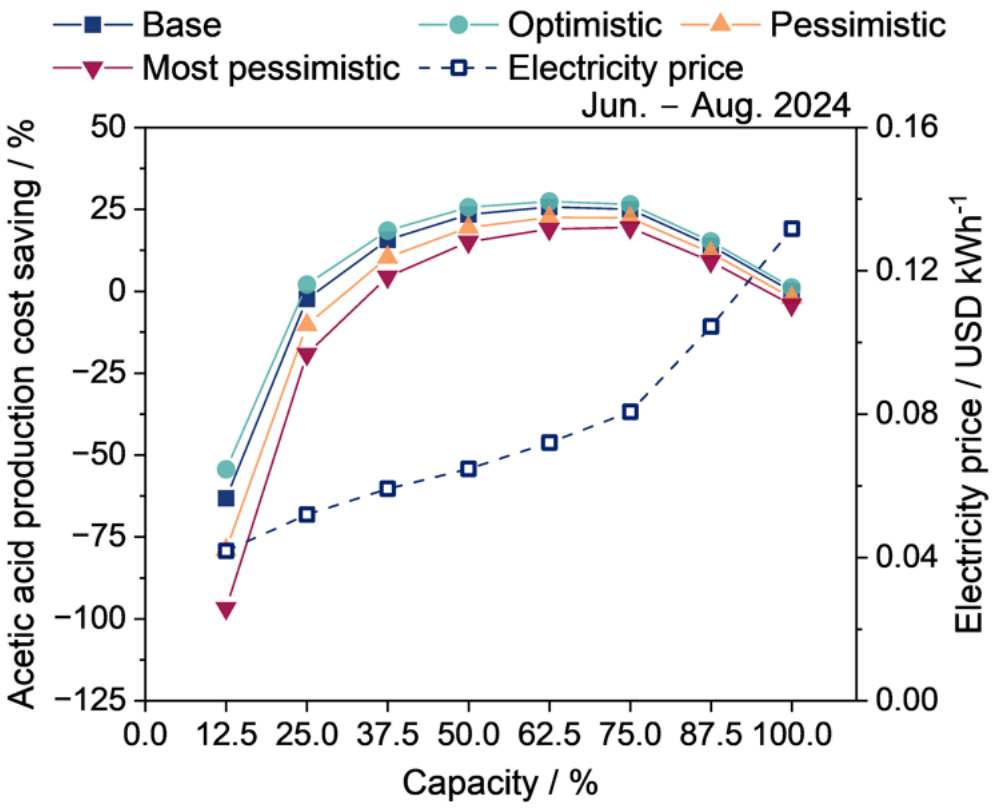

Supplementary Fig. 42 | Sensitivity analysis of capital expenditure (CapEx) for the South Australia case. The corresponding sensitivity parameters are listed in Supplementary Table 14.

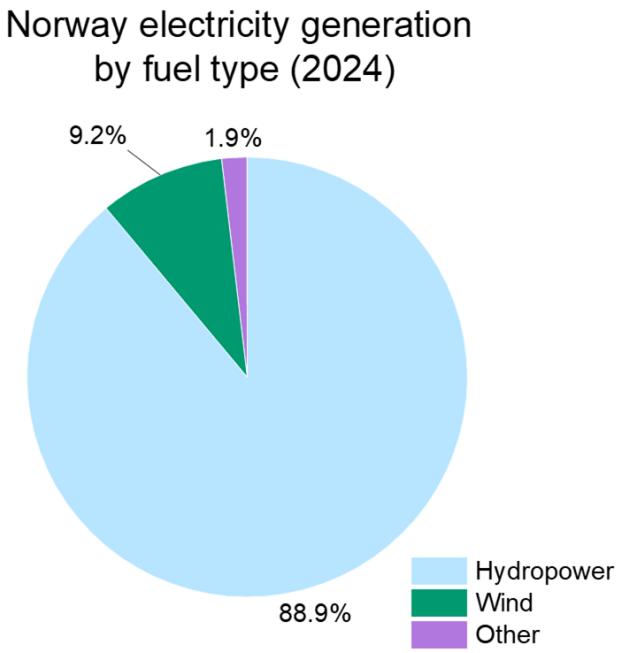

Supplementary Fig. 43 | Electricity generation by fuel type (2024) in Norway. More than 98% of Norway's electricity generation comes from renewable sources, with hydropower accounting for 89% and wind energy for 9%. "Other" includes coal, oil, natural gas, biofuels, waste, and solar PV[11].

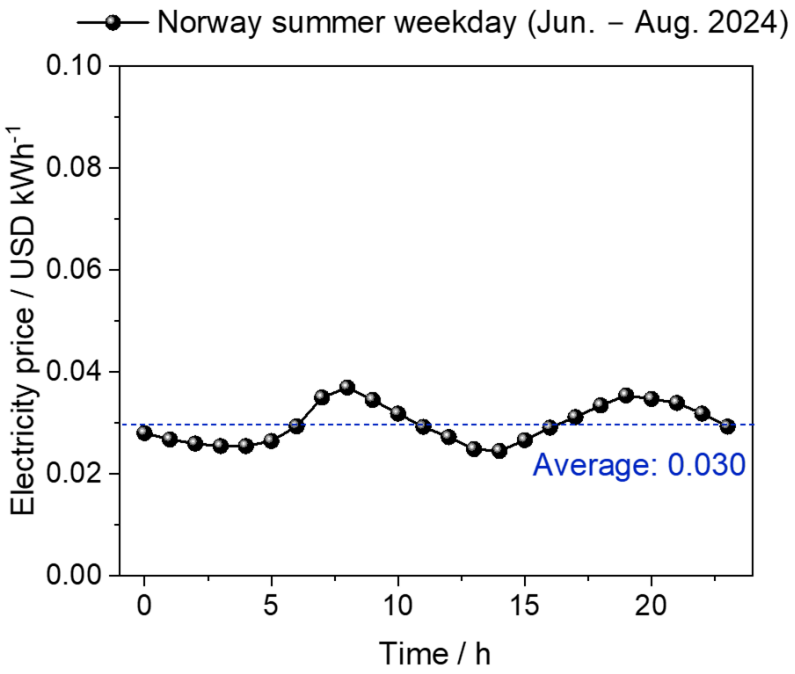

Supplementary Fig. 44 | Hourly averaged weekday electricity price in Norway from June to August 2024. The average electricity price is 0.030 USD kWh^{-1}, with a standard deviation of 0.004 USD kWh^{-1}.[12]

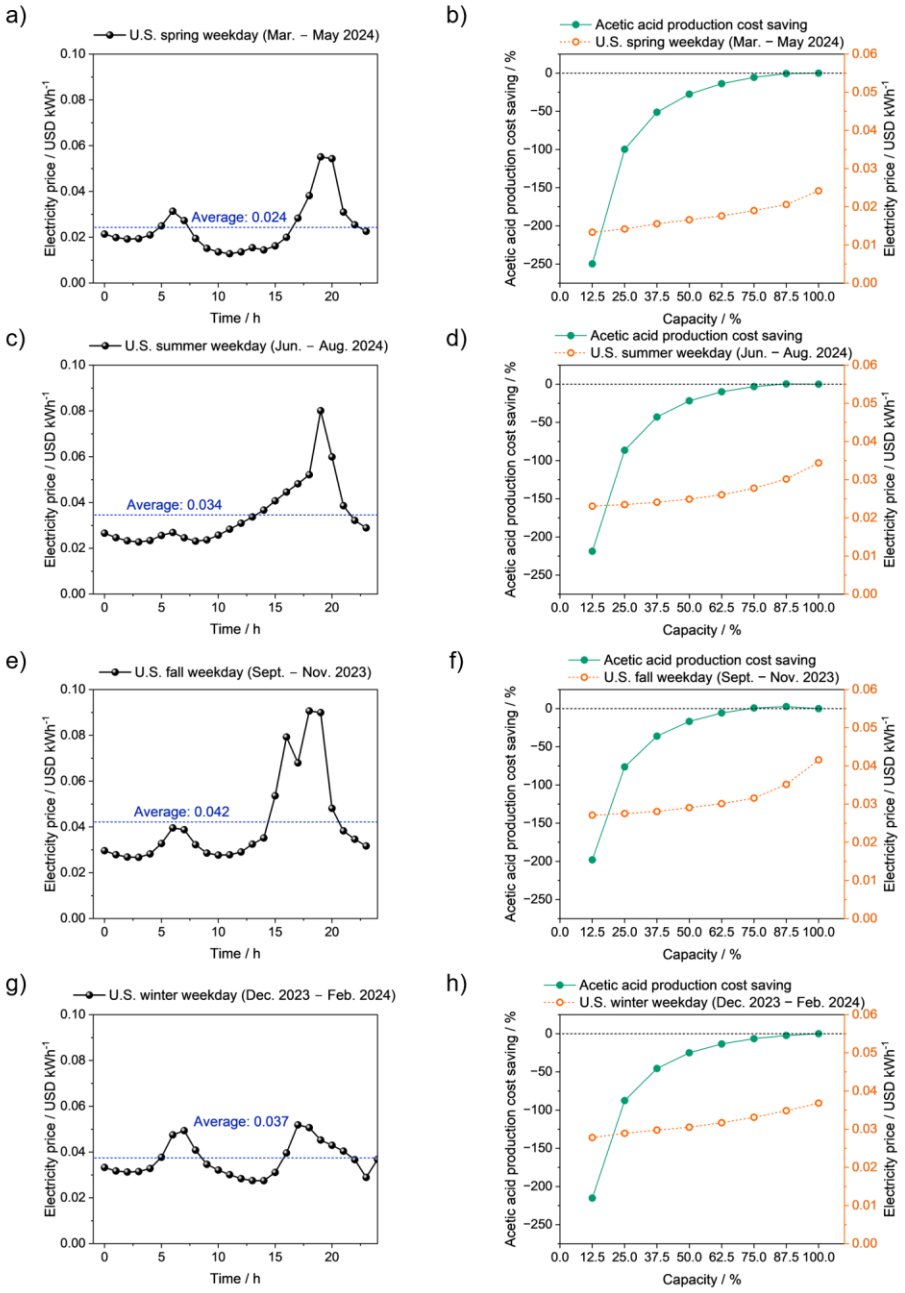

Supplementary Fig. 45 | Hourly averaged weekday electricity prices (a, c, e, g)13-16 and the corresponding techno-economic analysis of dynamic and steady state operation of CO electrolyzers for acetic acid production (b, d, f, h) in the United States from September 2023 to August 2024. Acetic acid production cost savings are plotted relative to operation at 100% capacity. Base-case capital expenses were used in this analysis.

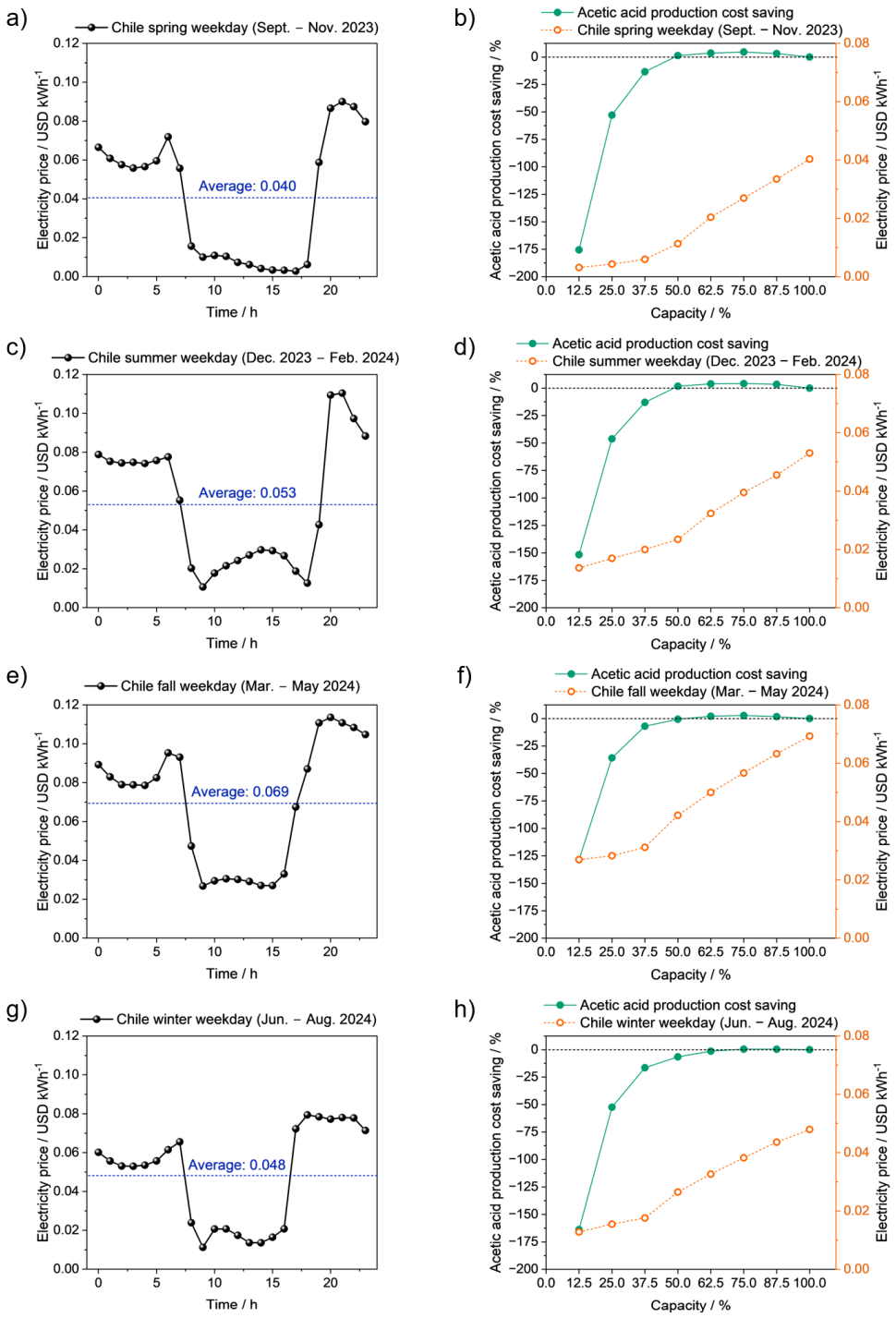

Supplementary Fig. 46 | Hourly averaged weekday electricity prices (a, c, e, g)17-20 and the corresponding techno-economic analysis of dynamic and steady state operation of CO electrolyzers for acetic acid production (b, d, f, h) in Chile from September 2023 to August 2024. Acetic acid production cost savings are plotted relative to operation at 100% capacity. Base-case capital expenses were used in this analysis.

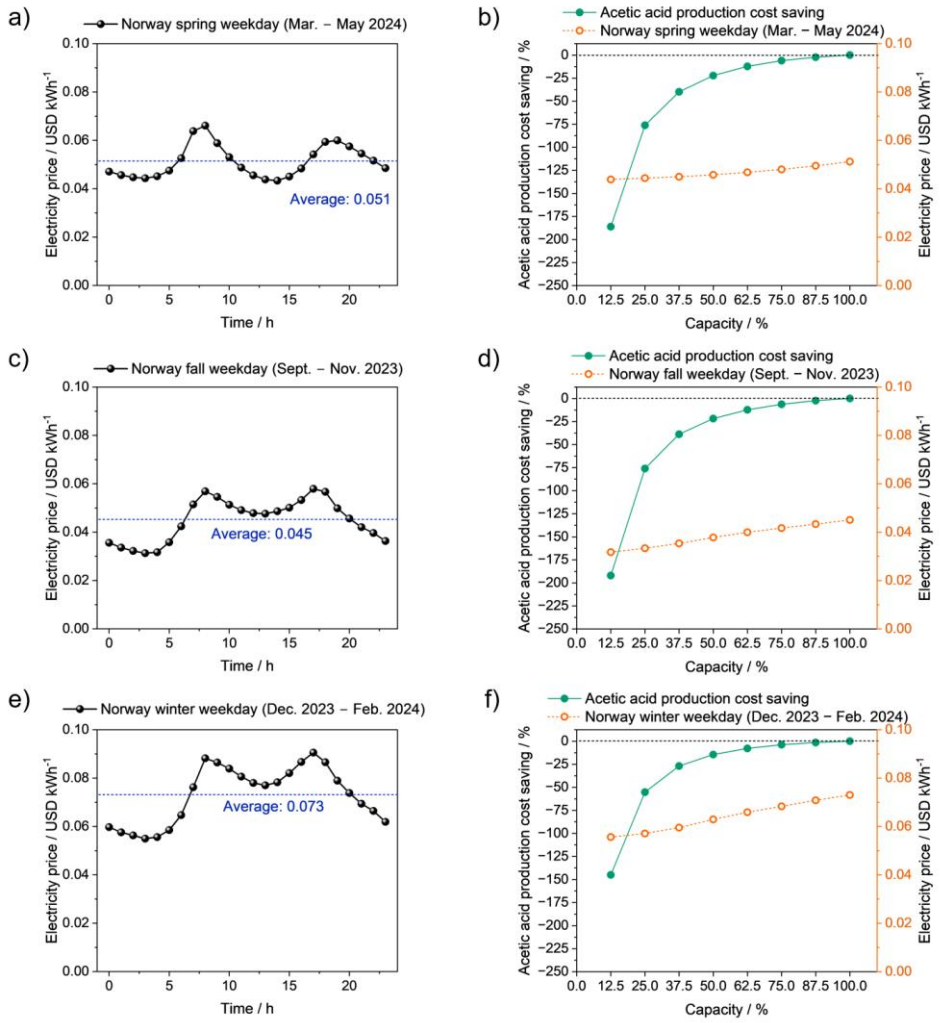

Supplementary Fig. 47 | Hourly averaged weekday electricity prices (a, c, e)21-23 and the corresponding techno-economic analysis of dynamic and steady state operation of CO electrolyzers for acetic acid production (b, d, f) in Norway from September 2023 to May 2024. Acetic acid production cost savings are plotted relative to operation at 100% capacity. For summer (June – August 2024), the hourly averaged weekday electricity price is shown in Supplementary Fig. 42, and the corresponding techno-economic analysis is shown in Fig. 5a. Base-case capital expenses were used in this analysis.

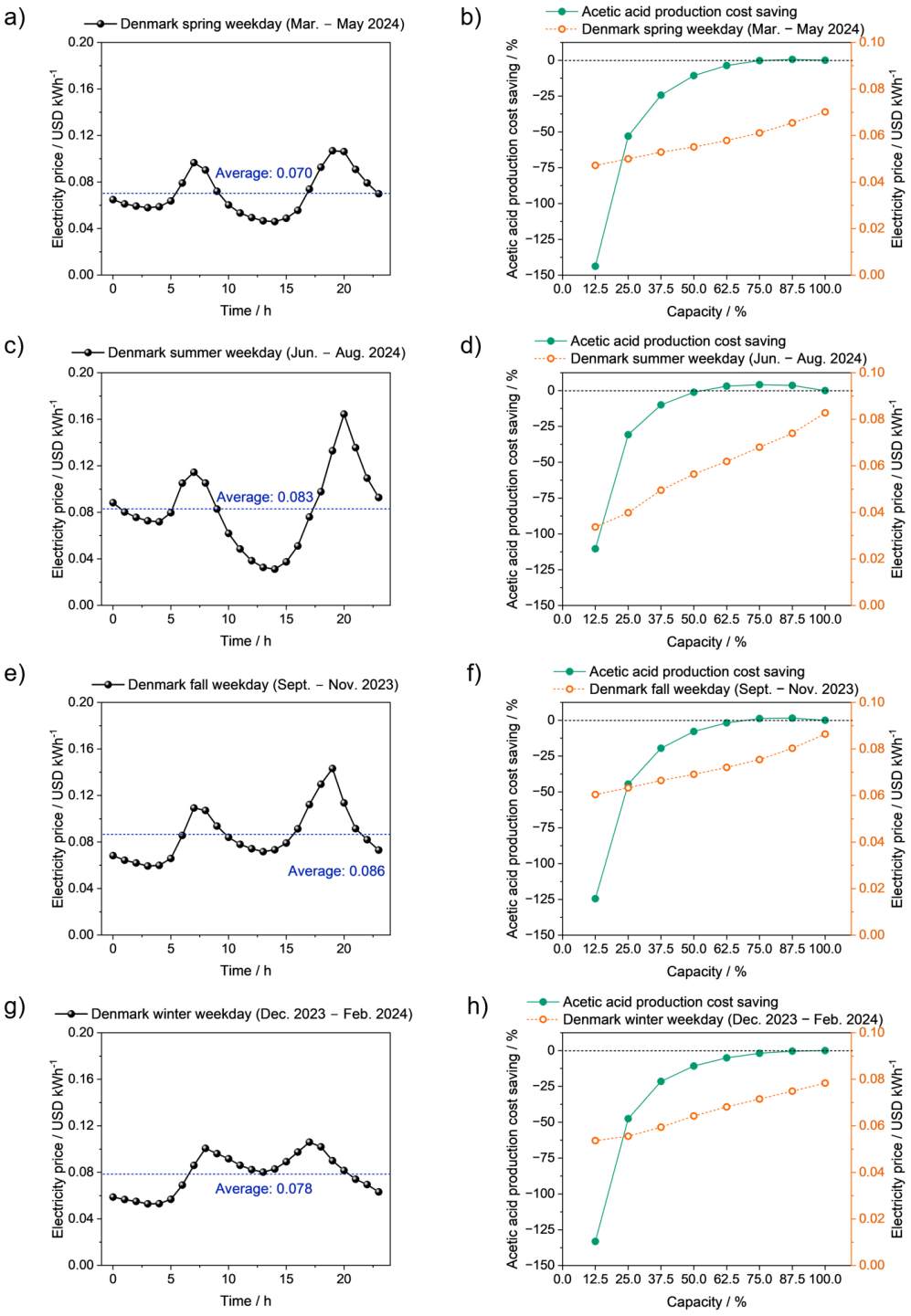

Supplementary Fig. 48 | Hourly averaged weekday electricity prices (a, c, e, g)24-27 and the corresponding techno-economic analysis of dynamic and steady state operation of CO electrolyzers for acetic acid production (b, d, f, h) in Denmark from September 2023 to August 2024. Acetic acid production cost savings are plotted relative to operation at 100% capacity. Base-case capital expenses were used in this analysis.

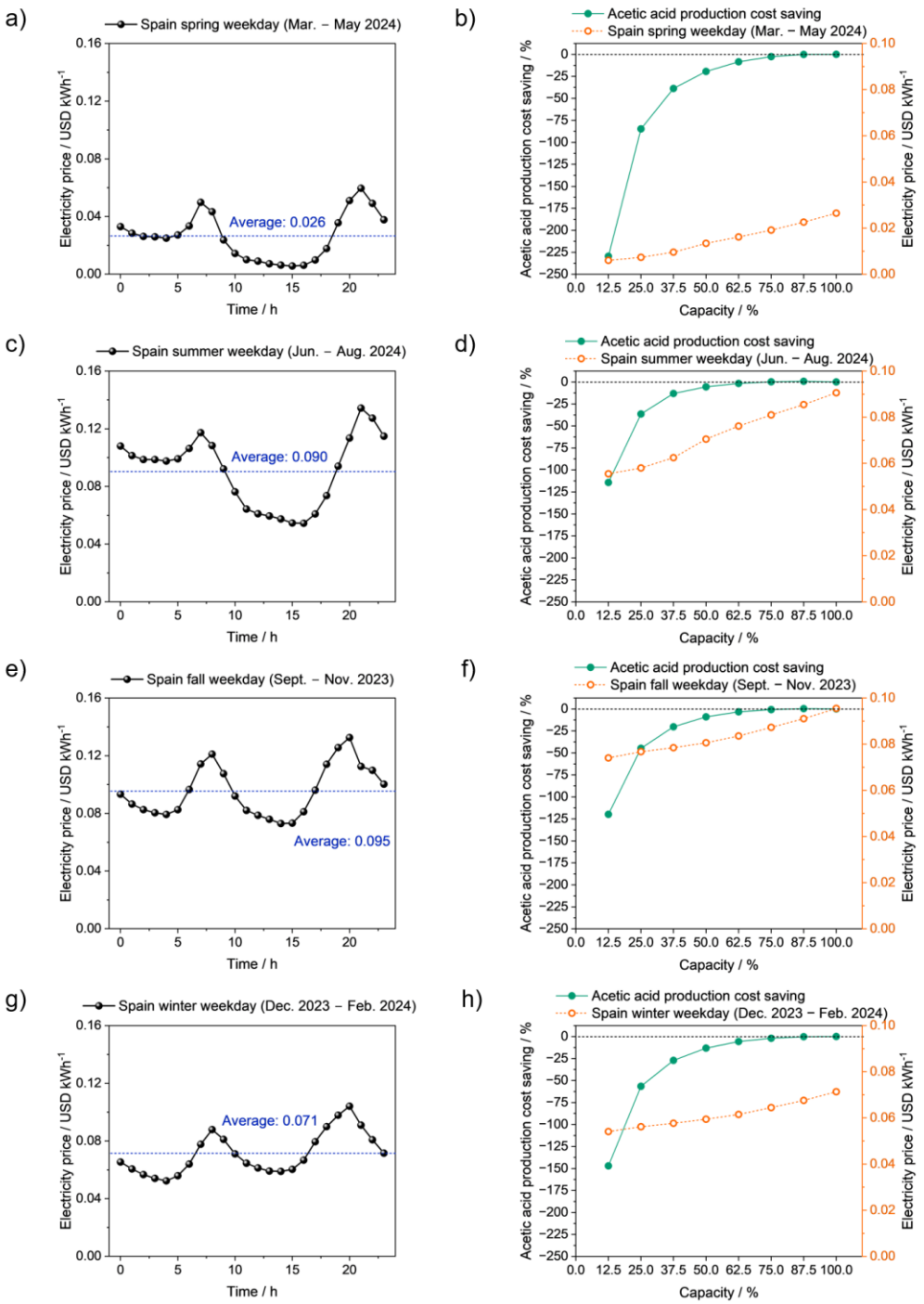

Supplementary Fig. 49 | Hourly averaged weekday electricity prices (a, c, e, g)28-31 and the corresponding techno-economic analysis of dynamic and steady state operation of CO electrolyzers for acetic acid production (b, d, f, h) in Spain from September 2023 to August 2024. Acetic acid production cost savings are plotted relative to operation at 100% capacity. Base-case capital expenses were used in this analysis.

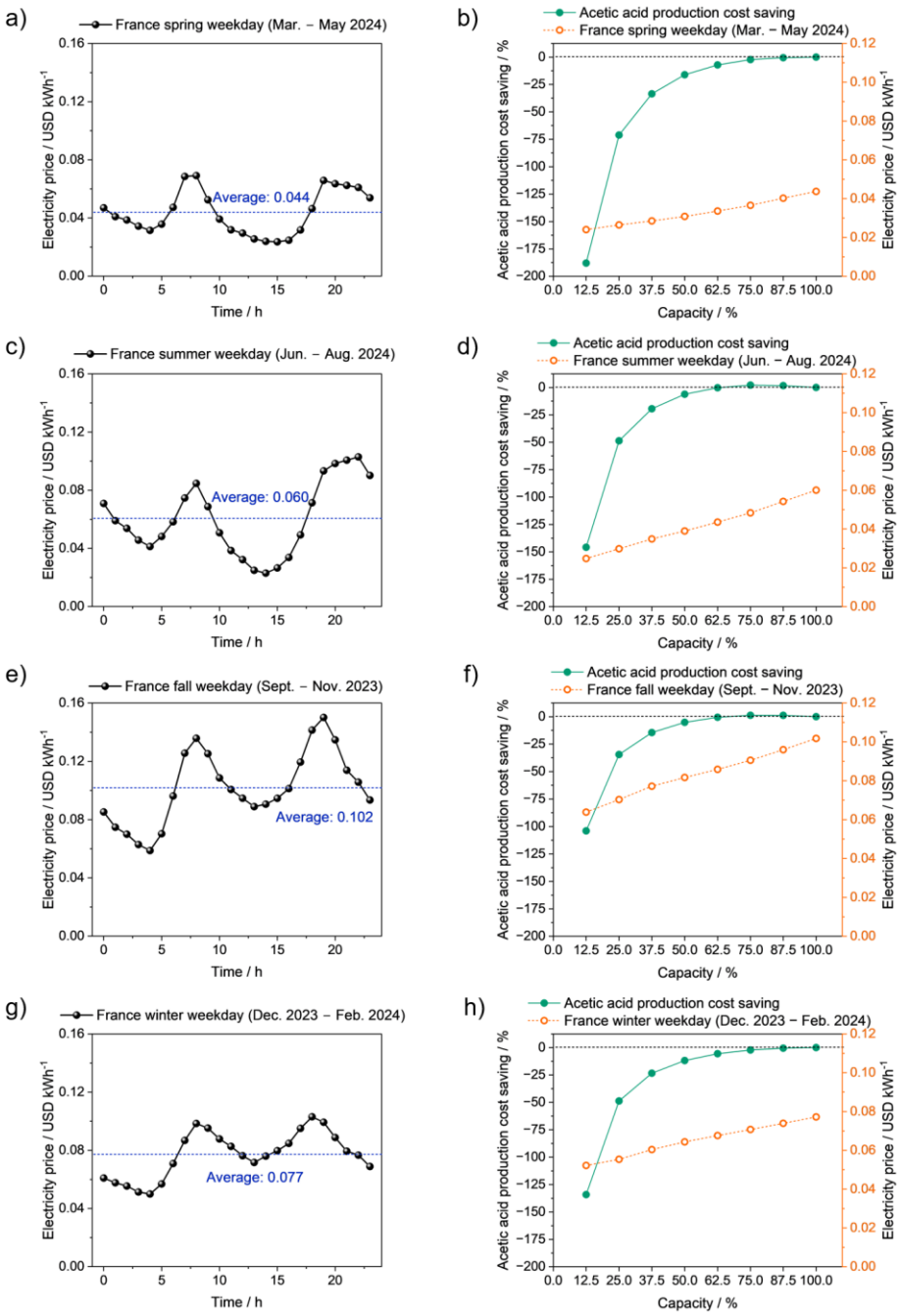

Supplementary Fig. 50 | Hourly averaged weekday electricity prices (a, c, e, g)32-35 and the corresponding techno-economic analysis of dynamic and steady state operation of CO electrolyzers for acetic acid production (b, d, f, h) in France from September 2023 to August 2024. Acetic acid production cost savings are plotted relative to operation at 100% capacity. Base-case capital expenses were used in this analysis.

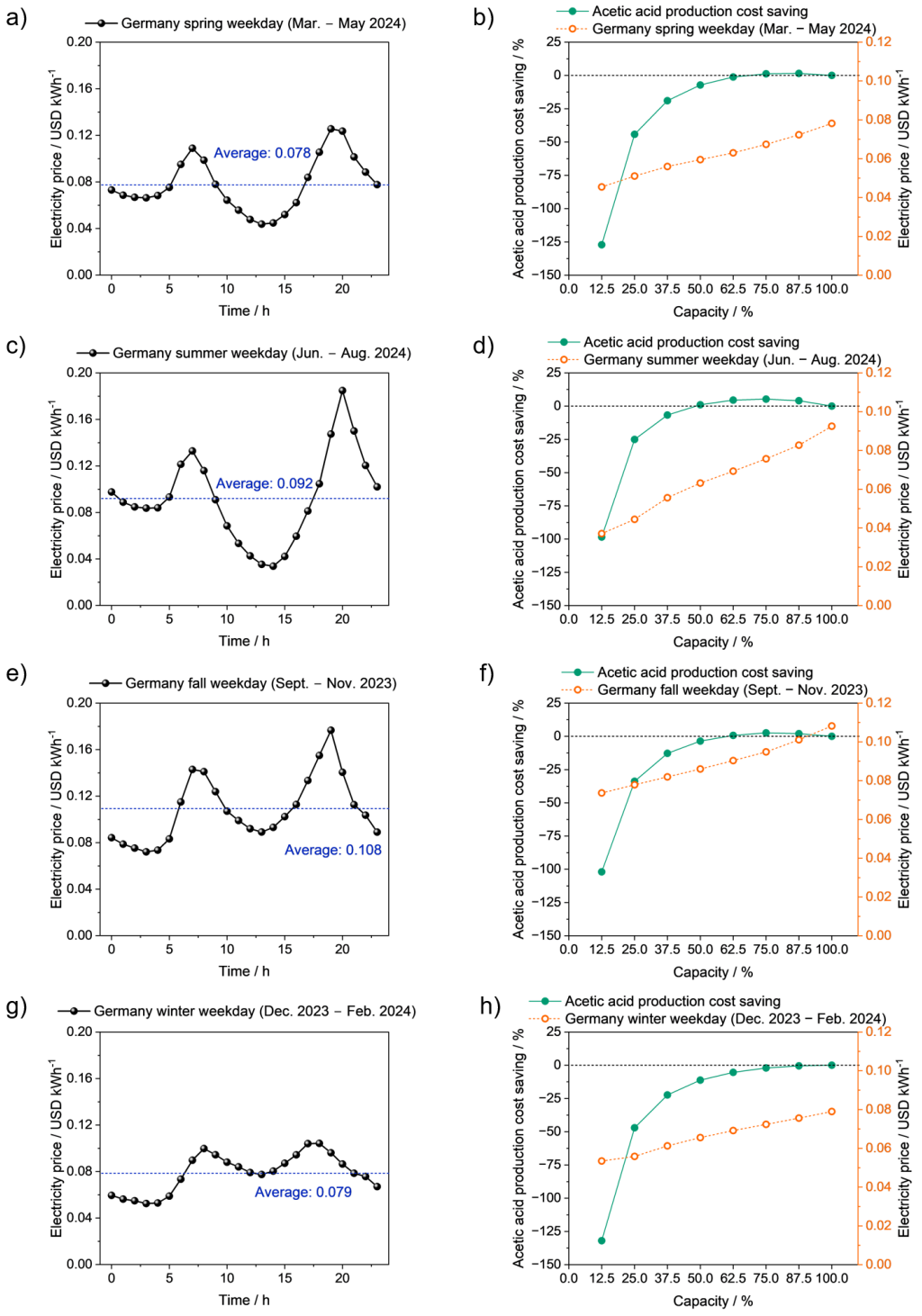

Supplementary Fig. 51 | Hourly averaged weekday electricity prices (a, c, e, g)36-39 and the corresponding techno-economic analysis of dynamic and steady state operation of CO electrolyzers for acetic acid production (b, d, f, h) in Germany from September 2023 to August 2024. Acetic acid production cost savings are plotted relative to operation at 100% capacity. Base-case capital expenses were used in this analysis.

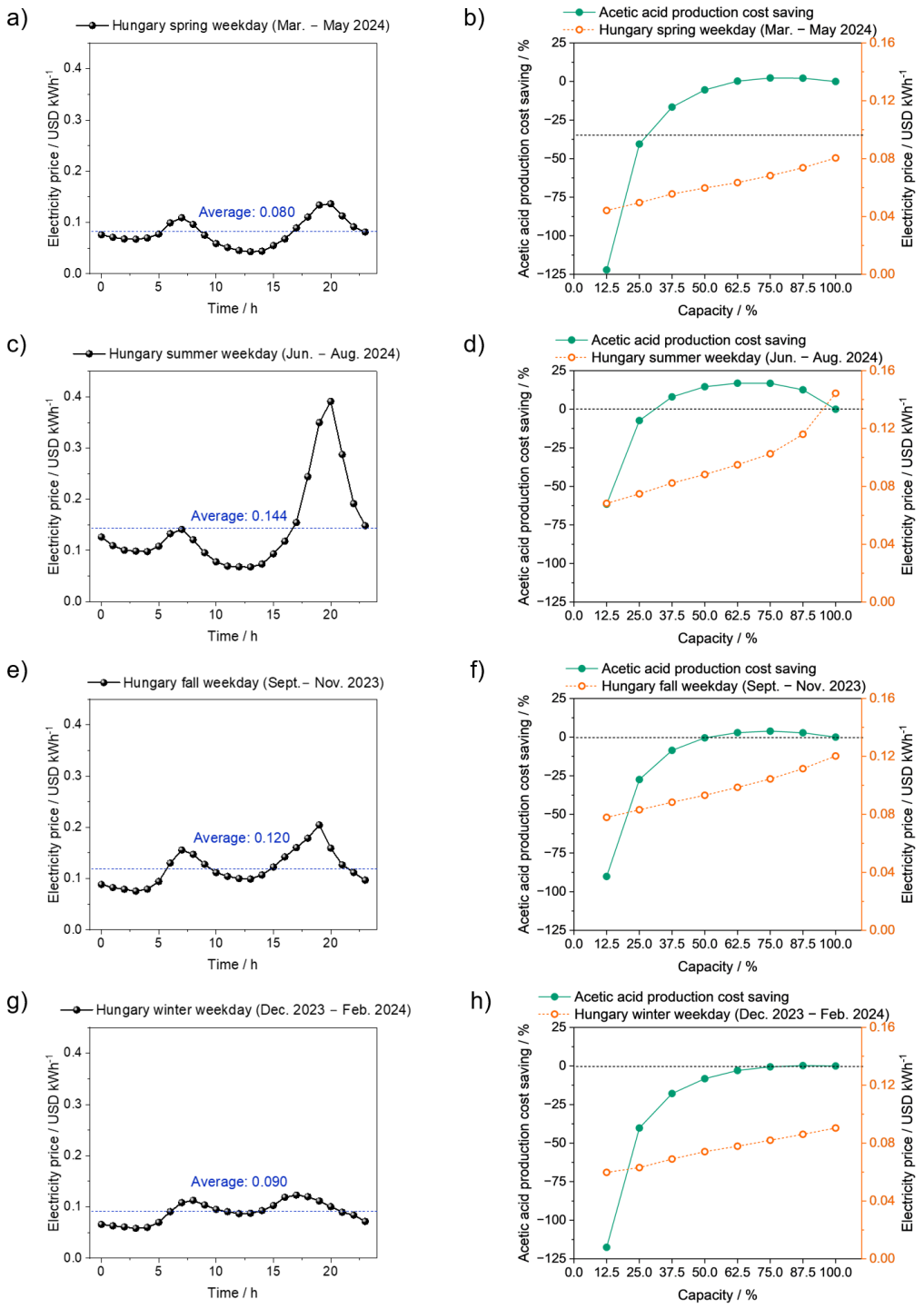

Supplementary Fig. 52 | Hourly averaged weekday electricity prices (a, c, e, g)40-43 and the corresponding techno-economic analysis of dynamic and steady state operation of CO electrolyzers for acetic acid production (b, d, f, h) in Hungary from September 2023 to August 2024. Acetic acid production cost savings are plotted relative to operation at 100% capacity. Base-case capital expenses were used in this analysis.

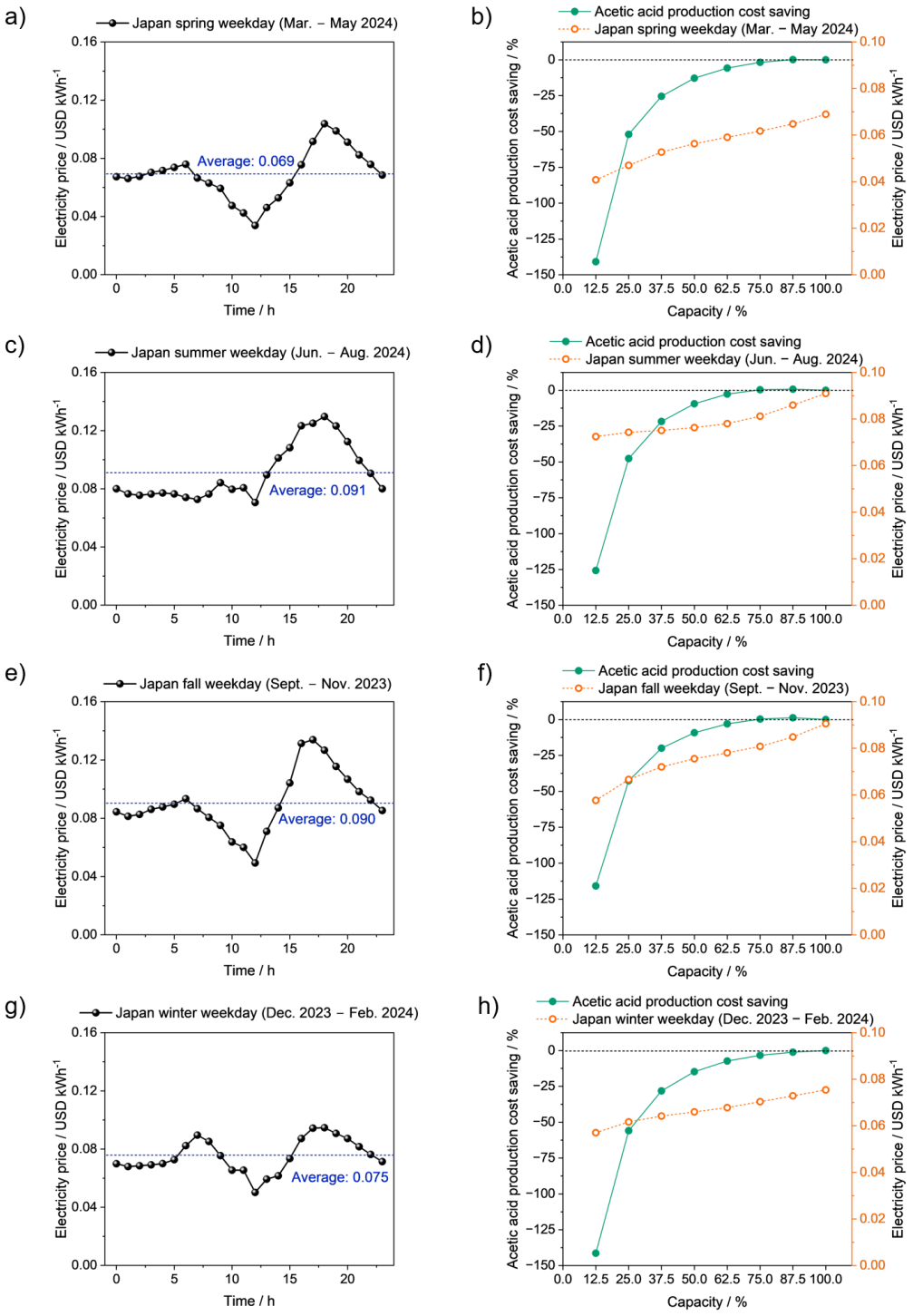

Supplementary Fig. 53 | Hourly averaged weekday electricity prices (a, c, e, g)44-47 and the corresponding techno-economic analysis of dynamic and steady state operation of CO electrolyzers for acetic acid production (b, d, f, h) in Japan from September 2023 to August 2024. Acetic acid production cost savings are plotted relative to operation at 100% capacity. Base-case capital expenses were used in this analysis.

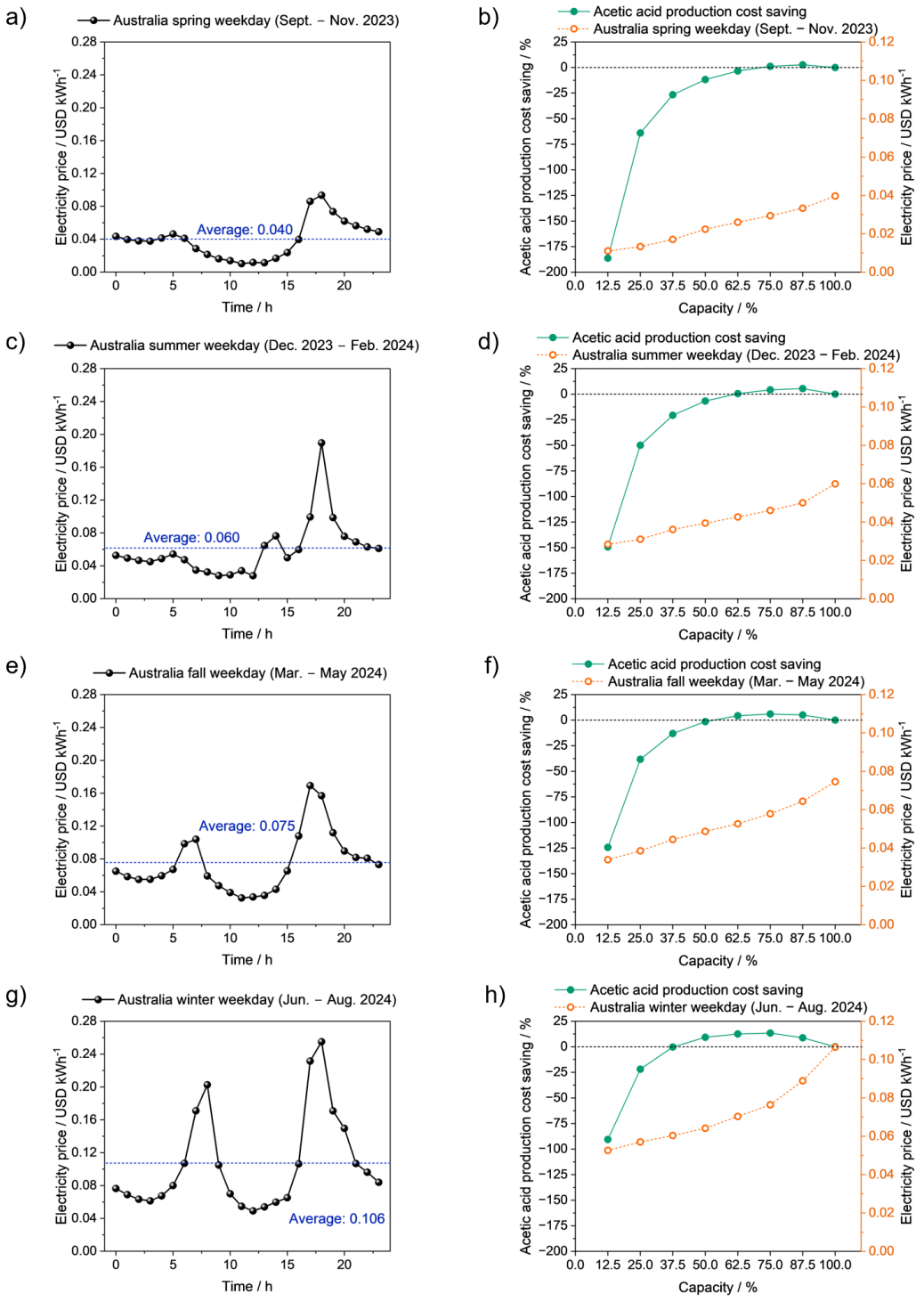

Supplementary Fig. 54 | Hourly averaged weekday electricity prices (a, c, e, g)48-51 and the corresponding techno-economic analysis of dynamic and steady state operation of CO electrolyzers for acetic acid production (b, d, f, h) in Australia from September 2023 to August 2024. Acetic acid production cost savings are plotted relative to operation at 100% capacity. Base-case capital expenses were used in this analysis.

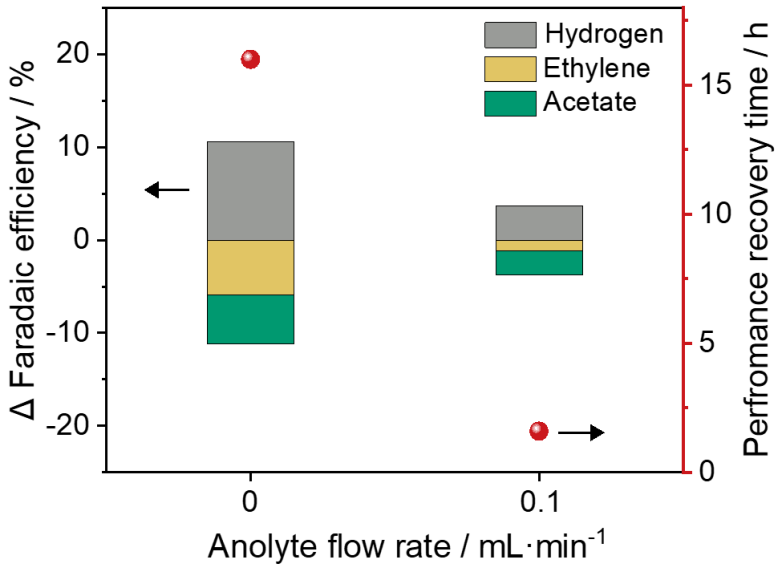

Supplementary Fig. 55 | Exploration of dynamic operation under stationary (0 mL min-1) and continuously flowing (0.1 mL min-1) anolyte conditions. The experiments were conducted over a 12-hour power-down dynamic operation at 1.8 V in CO. The left y-axis shows ΔFE, and the right y-axis shows the performance recovery time. Performance recovery was defined as Supplementary Fig. 33b.

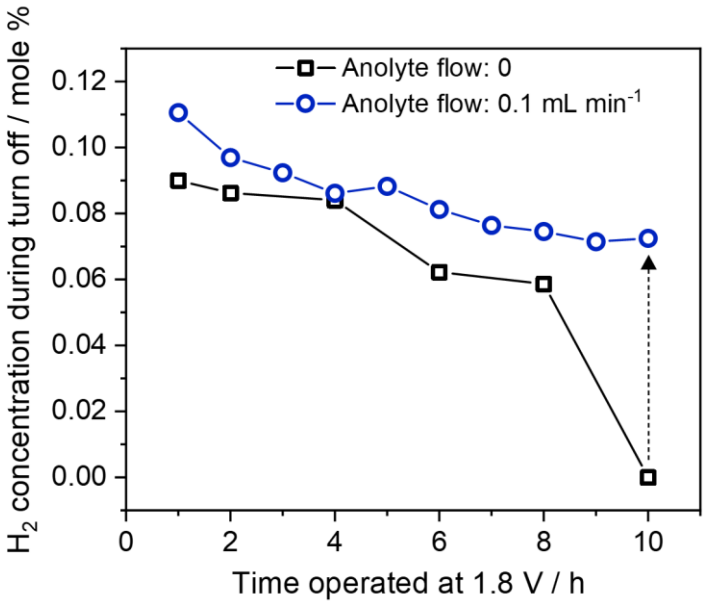

Supplementary Fig. 56 | Exploration of dynamic operation under stationary (0 mL min⁻1) and continuously flowing (0.1 mL min⁻1) anolyte conditions with different power-down durations at 1.8 V. Under stationary anolyte conditions, no hydrogen was detected after a 10-hour power-down period, indicating interface drying. In contrast, under continuously flowing anolyte conditions, hydrogen was still detected during the power-down period.

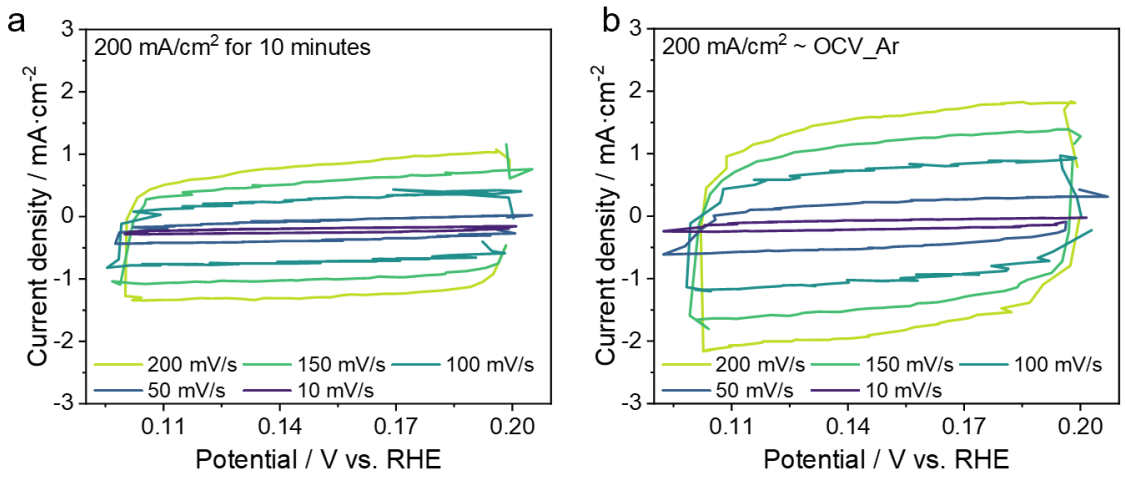

Supplementary Fig. 57 | CV curves at different scan rates for double-layer capacitance determination in electrochemically active surface area (ECSA) experiments. a | Steady state operation at 200 mA cm^{-2} for 10 minutes (measured at point C in Supplementary Fig. 26b). **b** | Power-off/power-on dynamic operation in Ar for 24 hours (measured at point D in Supplementary Fig. 26b).

Supplementary Table 1 | Comparison between pulse-controlled electrolysis and the power-down strategy for Cu-based catalysts.

Ref.	Reactor, Electrolyte & Gas	Catalyst	Dynamic Control (Pulse)	Degradation / Mitigation
Blaž Tomc et al. 2025 (J. CO2 Util.)[52]	H-cell (0.1 M $KHCO_3$, CO_2 bubbled)	Cu foil (bulk Cu)	Square-wave (–1.0 V + 2 s anodic pulses / 2 min)	Pulses cyclically oxidize/reduce Cu, keeping surface active.
Liviu C. Tănase et al. 2025 (Nat. Catal.)[53]	Custom quasi-in situ cell (0.1 M CO_2-sat. $KHCO_3$)	Cu(100) single crystal	1 s –1.0 V / +0.6–0.8 V alternating pulses	Short anodic pulses form Cu(I)–O species, suppressing bulk oxidation.
Antonia Herzog et al. 2024 (Nat. Commun.)[54]	H-cell (0.1 M CO_2-sat. $KHCO_3$)	Pre-reduced Cu_2O nanocubes (~30 nm)	Square-wave –1.0 V / +0.6 V (0.5–15 s)	Co-adsorbed OH raises pH, stabilizing Cu_2O; optimized pulses boost C_2.
Janis Timoshenko et al. 2022 (Nat. Catal.)[55]	H-cell (0.1 M $KHCO_3$, AEM-separated)	Cu_2O nanocubes (~30 nm)	Pulses –1.0 V / +0.6 V (0.5–10 s)	Mixed Cu^0/Cu^+ interface refreshed by short anodic steps, reducing H_2.
Takashi Ito et al. 2024 (EES Catal.)[56]	Flow cell (GDE, 1 M KOH (catholyte)	Cu nanoparticle / CuO nanowire	Anodic/cathodic (E_a/Ec) or dual-cathodic pulses	Redox cycling of CuO NWs forms GBs, sustaining C_2^+ activity.
Rileigh Casebolt DiDomenico et al. 2023 (ACS Catal.)[57]	H-cell (0.1 M $KHCO_3$)	Polycrystalline Cu	–0.9 V vs 0 V square pulses (varied freq.)	CO/H balance control reduces H-poisoning; mild oxidation refreshes Cu.
Jesse Kok et al. 2024 (J. Am. Chem. Soc.)[58]	zero-gap MEA (0.5–1 M $KHCO_3$, humidified CO_2)	Sputtered Cu	–200 mA cm^{-2} w/ OCP or O_2 pulses	Oxidative pulses re-oxidize Cu, suppressing Cu migration and C–oxide buildup.
Ke Ye et al. 2024 (Nat. Commun.)[59]	H-cell (0.1 M $KHCO_3$, CO_2-sat)	Polycrystalline Cu foil	–1.1 V / +0.6 V (10 s cycles)	Pulses generate Cu^0/Cu_2O mix, enhancing C–C coupling and C_2 formation.
Our work	Zero-gap cell (1 M KOH, CO)	Cu nanoparticle	1.8~1.9 V (cell voltage, 0-3days) / 200mA/cm^2	Avoids Cu oxidation and carbonate accumulation, enabling seamless coupling with intermittently available solar energy

Supplementary Table 2. Comparison of stability performance of CO electrolysis systems

Operation mode of dynamic operation	Stability (h)	Single cell reaction area (cm^2)	Current density (mA/cm^2)	Voltage (V)	Cathode catalyst	Anolyte	Ref
No	120	5	200	2.3	Cu	3 M KOH	Overa et al.[60]
No	125	100	300	2.25	Cu	2 M KOH	Crandall et al.[61]
No	18	1	100	2.5	Ag-Cu_2O	1 M NaOH	Dorakhan et al.[62]
No	500	5	500	3.5	Cu-Pd	1 M KOH	Ji et al.[63]
No	6	5	500	2.42	Cu	2 M KOH	Hasa et al.[64]
No	820	1	100	2.5	Cu-Ag	2.5 M KOH	Jin et al.[65]
No	150	2.25	400	5	silver-doped Cu_2O	H_2O	Wi et al.[66]
No	140	4	200	3	Cu	0.1 M CsOH	Xu et al.[67]
No	750	100	200	2.4	Cu 40-60nm	2M KOH	Deng et al. [68]
Yes	750	5	200	1.9 ~2.4	Cu 40-60nm	1 M KOH	**This Work**

Supplementary Table 3 | Acetic acid production cost savings at each capacity and the production cost at 100% capacity for 10 countries in spring. For Australia and Chile, hourly weekday electricity prices from September to November 2023 were used, while for other countries, hourly weekday electricity prices from March to May 2024 were used. The most cost-effective cases are shown in bold. Base-case capital expenses were used in this analysis.

Spring (September – November 2023 for Australia and Chile | March – May 2024 for other countries)										
Acetic acid production cost saving (%)										
	North America	South America	Europe						Asia	Oceania
Capacity (%)	United States	Chile	Norway	Denmark	Spain	France	Germany	Hungary	Japan	Australia
12.5	-249.6	-175.5	-186.1	-143.7	-229.5	-188.0	-127.1	-122.1	-140.8	-186.3
25	-99.7	-52.9	-76.1	-53.0	-84.7	-71.1	-44.2	-40.5	-52.0	-64.0
37.5	-51.2	-13.4	-39.8	-24.4	-38.8	-33.5	-19.0	-16.6	-25.5	-26.6
50	-27.5	1.3	-22.2	-10.7	-19.4	-16.1	-7.2	-5.5	-12.8	-11.8
62.5	-13.7	3.6	-12.2	-3.7	-8.4	-7.1	-1.2	0.3	-5.8	-3.4
75	-5.5	**4.6**	-6.0	-0.2	-2.6	-2.3	1.2	**2.3**	-1.7	1.1
87.5	-0.5	3.2	-2.2	**0.6**	-0.1	-0.6	**1.5**	2.1	**0.2**	**2.7**
100	**0.0**	0.0	**0.0**	0.0	**0.0**	**0.0**	0.0	0.0	0.0	0.0
Capacity (%)	Acetic acid production cost at 100% capacity (USD kg^{-1})									
100	0.866	1.056	1.185	1.407	0.893	1.096	1.502	1.529	1.393	1.049

Supplementary Table 4 | Acetic acid production cost savings at each capacity and the production cost at 100% capacity for 10 countries in summer. For Australia and Chile, hourly weekday electricity prices from December 2023 to February 2024 were used, while for other countries, hourly weekday electricity prices from June to August 2024 were used. The most cost-effective cases are shown in bold. Base-case capital expenses were used in this analysis.

Summer (December 2023 – February 2024 for Australia and Chile | June – August 2024 for other countries)										
Acetic acid production cost saving (%)										
	North America	South America	Europe						Asia	Oceania
Capacity (%)	United States	Chile	Norway	Denmark	Spain	France	Germany	Hungary	Japan	Australia
12.5	-218.7	-151.6	-239.2	-110.4	-114.3	-145.8	-98.4	-61.6	-125.7	-149.3
25	-86.5	-46.2	-99.6	-30.8	-36.4	-48.7	-25.1	-7.4	-47.7	-50.0
37.5	-43.0	-13.0	-53.4	-10.0	-13.1	-19.4	-6.7	8.0	-21.8	-20.7
50	-21.8	1.7	-31.0	-1.2	-5.6	-6.2	1.0	14.6	-9.4	-6.7
62.5	-10.0	3.9	-17.8	3.1	-1.6	-0.2	4.5	**16.9**	-2.7	0.5
75	-3.2	**4.2**	-9.5	**4.1**	0.2	**2.2**	**5.3**	16.8	0.4	4.2
87.5	**0.3**	3.5	-3.9	3.6	**0.8**	1.7	4.1	12.6	**0.7**	**5.4**
100	0.0	0.0	**0.0**	0.0	0.0	0.0	0.0	0.0	0.0	0.0
Capacity (%)	Acetic acid production cost at 100% capacity (USD kg^{-1})									
100	0.986	1.206	0.933	1.556	1.648	1.288	1.670	2.282	1.652	1.287

Supplementary Table 5 | Acetic acid production cost savings at each capacity and the production cost at 100% capacity for 10 countries in fall. For Australia and Chile, hourly weekday electricity prices from March to May 2024 were used, while for other countries, hourly weekday electricity prices from September to November 2023 were used. The most cost-effective cases are shown in bold. Base-case capital expenses were used in this analysis.

Fall (March – May 2024 for Australia and Chile | September – November 2023 for other countries)										
Acetic acid production cost saving (%)										
	North America	South America	Europe						Asia	Oceania
Capacity (%)	United States	Chile	Norway	Denmark	Spain	France	Germany	Hungary	Japan	Australia
12.5	-198.0	-128.5	-191.9	-124.5	-119.9	-104.0	-101.9	-90.1	-115.9	-124.4
25	-76.3	-35.8	-75.9	-44.6	-44.8	-34.5	-33.8	-27.5	-42.6	-38.3
37.5	-36.1	-7.0	-38.8	-19.5	-20.3	-14.5	-12.8	-8.6	-19.9	-13.1
50	-16.8	-0.6	-21.8	-7.8	-9.0	-5.1	-3.6	-0.5	-9.2	-1.5
62.5	-5.7	2.2	-12.3	-1.8	-3.3	-0.5	0.7	2.9	-3.0	4.2
75	0.8	**2.8**	-6.3	1.2	-0.8	**1.3**	**2.6**	**3.8**	0.3	**6.0**
87.5	**2.7**	1.8	-2.4	**1.5**	**0.3**	1.2	2.0	2.8	**1.2**	5.0
100	0.0	0.0	**0.0**	0.0	0.0	0.0	0.0	0.0	0.0	0.0
Capacity (%)	Acetic acid production cost at 100% capacity (USD kg^{-1})									
100	1.071	1.397	1.112	1.598	1.705	1.780	1.856	1.998	1.648	1.459

Supplementary Table 6 | Acetic acid production cost savings at each capacity and the production cost at 100% capacity for 10 countries in winter. For Australia and Chile, hourly weekday electricity prices from June to August 2024 were used, while for other countries, hourly weekday electricity prices from December 2023 to February 2024 were used. The most cost-effective cases are shown in bold. Base-case capital expenses were used in this analysis.

Winter (June – August 2024 for Australia and Chile | December 2023 – February 2024 for other countries)										
Acetic acid production cost saving (%)										
	North America	South America	Europe						Asia	Oceania
Capacity (%)	United States	Chile	Norway	Denmark	Spain	France	Germany	Hungary	Japan	Australia
12.5	-215.2	-163.9	-145.0	-133.2	-147.1	-134.2	-131.9	-117.5	-141.4	-90.6
25	-87.6	-52.4	-55.2	-47.5	-56.6	-48.7	-47.1	-40.2	-55.9	-21.9
37.5	-45.6	-16.4	-26.9	-21.5	-27.1	-23.4	-22.3	-17.9	-28.2	-0.3
50	-24.9	-6.5	-14.5	-10.7	-13.2	-11.8	-11.2	-8.2	-14.7	9.3
62.5	-13.4	-1.4	-7.8	-5.1	-5.7	-5.6	-5.4	-3.0	-7.3	12.5
75	-6.4	**0.5**	-3.8	-1.9	-2.0	-2.2	-2.1	-0.6	-3.4	**13.3**
87.5	-2.3	0.4	-1.4	-0.4	-0.2	-0.5	-0.5	**0.3**	-1.1	8.7
100	**0.0**	0.0	**0.0**	**0.0**	**0.0**	**0.0**	**0.0**	0.0	**0.0**	0.0
Capacity (%)	Acetic acid production cost at 100% capacity (USD kg^{-1})									
100	1.015	1.146	1.441	1.504	1.421	1.491	1.511	1.646	1.469	1.835

Supplementary Table 7 | Maximum acetic acid production cost saving at the corresponding capacity and the production cost at that capacity for 10 countries in spring. For Australia and Chile, hourly weekday electricity prices from September to November 2023 were used, while for other countries, hourly weekday electricity prices from March to May 2024 were used. The average electricity price and its standard deviation for this period are shown for each country. Base-case capital expenses were used in this analysis.

Spring (September – November 2023 for Australia and Chile | March – May 2024 for other countries)						
		Capacity (%)	Acetic acid production cost saving (%)	Corresponding acetic acid production cost (USD kg^{-1})	Average electricity price (USD kWh^{-1})	Standard deviation of electricity price (USD kWh^{-1})
North America	United States	100	0.0	0.866	0.024	0.011
South America	Chile	75	4.6	1.008	0.040	0.033
Europe	Norway	100	0.0	1.185	0.051	0.007
	Denmark	87.5	0.6	1.399	0.070	0.019
	Spain	100	0.0	0.893	0.026	0.016
	France	100	0.0	1.096	0.044	0.015
	Germany	87.5	1.5	1.480	0.078	0.024
	Hungary	75	2.3	1.494	0.080	0.027
Asia	Japan	87.5	0.2	1.391	0.069	0.017
Oceania	Australia	87.5	2.7	1.020	0.040	0.023

Supplementary Table 8 | Maximum acetic acid production cost saving at the corresponding capacity and the production cost at that capacity for 10 countries in summer. For Australia and Chile, hourly weekday electricity prices from December 2023 to February 2024 were used, while for other countries, hourly weekday electricity prices from June to August 2024 were used. The average electricity price and its standard deviation for this period are shown for each country. Base-case capital expenses were used in this analysis.

Summer (December 2023 – February 2024 for Australia and Chile | June – August 2024 for other countries)						
		Capacity (%)	Acetic acid production cost saving (%)	Corresponding acetic acid production cost (USD kg^{-1})	Average electricity price (USD kWh^{-1})	Standard deviation of electricity price (USD kWh^{-1})
North America	United States	87.5	0.3	0.983	0.034	0.014
South America	Chile	75	4.2	1.156	0.053	0.033
Europe	Norway	100	0.0	0.933	0.030	0.004
	Denmark	75	4.1	1.492	0.083	0.034
	Spain	87.5	0.8	1.634	0.091	0.025
	France	75	2.2	1.260	0.060	0.025
	Germany	75	5.3	1.582	0.092	0.039
	Hungary	62.5	16.9	1.897	0.144	0.088
Asia	Japan	87.5	0.7	1.640	0.091	0.019
Oceania	Australia	87.5	5.4	1.217	0.060	0.034

Supplementary Table 9 | Maximum acetic acid production cost saving at the corresponding capacity and the production cost at that capacity for 10 countries in fall. For Australia and Chile, hourly weekday electricity prices from March to May 2024 were used, while for other countries, hourly weekday electricity prices from September to November 2023 were used. The average electricity price and its standard deviation for this period are shown for each country. Base-case capital expenses were used in this analysis.

Fall (March – May 2024 for Australia and Chile | September – November 2023 for other countries)						
		Capacity (%)	Acetic acid production cost saving (%)	Corresponding acetic acid production cost (USD kg^{-1})	Average electricity price (USD kWh^{-1})	Standard deviation of electricity price (USD kWh^{-1})
North America	United States	87.5	2.7	1.042	0.042	0.020
South America	Chile	75	2.8	1.357	0.069	0.032
Europe	Norway	100	0.0	1.112	0.045	0.009
	Denmark	87.5	1.5	1.574	0.086	0.023
	Spain	87.5	0.3	1.700	0.095	0.018
	France	75	1.3	1.757	0.102	0.025
	Germany	75	2.6	1.808	0.108	0.028
	Hungary	75	3.8	1.921	0.120	0.034
Asia	Japan	87.5	1.2	1.627	0.091	0.021
Oceania	Australia	75	6.0	1.372	0.075	0.036

Supplementary Table 10 | Maximum acetic acid production cost saving at the corresponding capacity and the production cost at that capacity for 10 countries in winter. For Australia and Chile, hourly weekday electricity prices from June to August 2024 were used, while for other countries, hourly weekday electricity prices from December 2023 to February 2024 were used. The average electricity price and its standard deviation for this period are shown for each country. Base-case capital expenses were used in this analysis.

Winter (June – August 2024 for Australia and Chile | December 2023 – February 2024 for other countries)						
		Capacity (%)	Acetic acid production cost saving (%)	Corresponding acetic acid production cost (USD kg^{-1})	Average electricity price (USD kWh^{-1})	Standard deviation of electricity price (USD kWh^{-1})
North America	United States	100	0.0	1.015	0.037	0.008
South America	Chile	75	0.5	1.140	0.048	0.026
Europe	Norway	100	0.0	1.441	0.073	0.012
	Denmark	100	0.0	1.504	0.078	0.017
	Spain	100	0.0	1.421	0.071	0.015
	France	100	0.0	1.491	0.077	0.016
	Germany	100	0.0	1.511	0.079	0.016
	Hungary	87.5	0.3	1.642	0.090	0.020
Asia	Japan	100	0.0	1.469	0.075	0.012
Oceania	Australia	75	13.3	1.591	0.106	0.059

Supplementary Table 11 | Experimental conditions for dynamic operation studies in power-down mode. Deviations from the CO electroreduction conditions are highlighted in bold in the table.

Experiments	Holding Potential	Power-down duration	Power-down current density	Power-down anolyte	Power-down in Ar
Data	Fig. 4b	Supplementary Fig. 33	Supplementary Fig. 12	Supplementary Fig. 55	Supplementary Fig. 12
Gas	CO of 30 mL min^{-1}	CO of 30 mL min^{-1}	CO of 30 mL min^{-1}	CO of 30 mL min^{-1}	**Ar of 30 mL min^{-1}**
Anolyte	2.7 mL min^{-1}	2.7 mL min^{-1}	2.7 mL min^{-1}	**Stationary or 0.1 mL min^{-1}**	2.7 mL min^{-1}
Applying potential or current	**2.0, 1.9, 1.8, 1.7, 1.6 V, and OCV**	**1.9 V**	**0.2 – 20 mA cm^{-2}**	**1.8 V**	**OCV and 0.2 – 20 mA cm^{-2}**
Power-down time	10 mins	10 min -168 h	10 mins	12 h	10 mins
Showdown procedure	Applying potential	Applying potential	Applying current	1.8 V → Anolyte	Gas (CO to Ar) → Applying current
Turn-on procedure	200 mA cm^{-2}	200 mA cm^{-2}	200 mA cm^{-2}	Anolyte 2.7 mL min^{-1} → 200 mA cm^{-2}	200 mA cm^{-2} → Gas(Ar to CO)

Supplementary Table 12 | Experimental conditions for CV studies.

Experiments	Carbonate formation	Cu facet	Wide range CV scan
Data	Fig. 2d	Supplementary Fig. 5, 7, 15, 26, 36, and 37	Supplementary Fig. 16
Reaction before CV	CO reduction at 200 mA cm^{-2} for 24 hours	Follow the test procedure in Supplementary Fig. 5a, 7a, 7b, 15a, 26a, 26b, 36a, 37a or 37b	CO reduction at 200 mA cm^{-2} for 24 hours
Operation before CV	CV scan at 20mV s^{-1}	Switch gas from CO to Ar for 30s (for the CV in Ar) → CV scan at 20mV s^{-1}	Switch gas from CO to Ar for 30s (for the CV in Ar) → CV scan at 20mV s^{-1}
Gas during CV	30 mL min^{-1} CO	30 mL min^{-1} Ar	30 mL min^{-1} CO or Ar
CV range / V vs. RHE	–0.34 to 0.44	–0.05 to 0.55	–0.34 to 1.0
Operation after CV	Stop experiment	Perform CV for ECSA (if needed) → Apply 1 A→ Switch gas to CO (If continuing the experiment)	Stop experiment

Supplementary Table 13 | Techno-economic analysis assumptions and parameters for Capital Expenditure (CapEx) and Operating Expenses (OpEx). Detailed calculations for the electrolyzer installed cost and MEA replacement cost can be found in Shin et al.[69], while acetate protonation and electrolyte recovery cost calculations are detailed in Overa et al.[60]

Assumptions	Product production (at 100% capacity)	50,000 kg day^{-1} (Ref[69])
	Factory lifetime	20-year[69]
	Operating time	350 days $year^{-1}$(Ref[69])
	Income tax	0.389[69]
	Nominal interest rate	0.07
	Working capital	5% of TOC[69]
	Single pass conversion for acetic acid	50%[70]
CapEx – Bare Erected Cost (BEC): base case	Base electrolyzer cost	460 USD kW^{-1} (Ref[71])
	E4tech electrolyzer voltage	1.75 V[72]
	E4tech electrolyzer current density	400 mA cm^{-2} (Ref[72])
	Electrolyzer installation factor	1.12[72]
	Pressure swing adsorption (PSA) reference cost	1,979,043 USD[73]
	PSA reference capacity	1000 m^3 hr^{-1} (Ref[73])
	PSA capacity scaling factor	0.7[73]
	PSA installation factor	1
	Distillation reference cost – Acetic acid (0.5 M)	9,110,300 USD[60]
	Distillation reference cost – Acetic acid (3 M)	4,421,380 USD[60]
	Distillation capacity scaling factor	0.7[69]
	Distillation installation factor	1
	Balance of Plant	39% of total electrolyzer system cost[69]
CapEx – Engineering, Procurement and Construction Cost (EPCC): base case	Engineering, procurement and construction management (EPCM) contractor service	18% of BEC[74]
CapEx – Total Plant Cost (TPC): base case	Process contingency	25% of BEC[74]
	Project contingency	20% of the sum of BEC, EPC fees, and process contingency[74]
CapEx – Total Overnight Cost (TOC): base case	Owner's cost	20% of TPC[74]
CapEx – Total As-Spent Cost (TASC): base case	Interest during construction (IDC)	~3.44%

OpEx	CO cost	0.24 USD kg^{-1}(Ref[70])
	Water cost for OER	0.0054 USD gal^{-1}(Ref[69])
	Maintenance cost	2.5% of electrolyzer CapEx per year[69]
	Cell compartment replacement cost (every 7 year)	15% of electrolyzer CapEx per year[69]
	Cu cost	5.7E-3 USD g^{-1} (Ref[75])
	Cu loading	1 mg cm^{-2} (Ref[70])
	Ni cost	1.2E-2 USD g^{-1} (Ref[76])
	Ni loading	1 mg cm^{-2} (Ref[70])
	Fe cost	7E-5 USD g^{-1} (Ref[77])
	Fe loading	2 mg cm^{-2} (Ref[70])
	Membrane cost	5% of DOE H2A stack cost, 180 USD m^{-2} (Ref[69])
	MEA replacement interval	1 year[69]
	PSA operating cost	0.25 kWh m^{-3} (Ref[73])
	Distillation utility cost – Acetic acid (0.5 M)	17,267,900 USD $year^{-1}$ (Ref[60])
	Distillation utility cost – Acetic acid (3 M)	2,484,690 USD $year^{-1}$ (Ref[60])
	Electricity usage for acetate protonation and KOH regeneration	1.58 kWh kg^{-1} KOH[60]
	KOH : Liquid product acetate	2 :1 molar ratio[60]
	Operating labor – base labor rate	38.5 USD h^{-1} (Ref[78])
	Operating labor – Associated labor burden	30% of the base labor rate[78]
	Operating labor – Administration and overhead	25% of the burdened labor rate[78]
	Operating labor – Operators per day	5[78]

Supplementary Table 14 | Capital Expenditure (CapEx) parameters used for sensitivity analysis of the South Australia case (Supplementary Fig. 42). Additional details on the CapEx calculation are provided in Supplementary Note 3.

	Base case	Optimistic case	Pessimistic case	Most pessimistic case
Installation factor for PSA (f_{PSA})	1	1	1	1.17[79]
Installation factor for distillation ($f_{distillation}$)	1	1	1	2.47[80]
EPCM contractor service (f_{EPCM})[74]	18%	15%	20%	20%
EPCC[74]	1.18 BEC	1.15 BEC	1.20 BEC	1.20 BEC
[74]	25%	20%	35%	35%
Process contingency	0.25 BEC	0.20 BEC	0.35 BEC	0.35 BEC
Project contingency factor ($f_{project}$)[74]	20%	15%	30%	30%
Project contingency[74]	0.2 (BEC + 0.18 BEC + 0.25 BEC) = 0.286 BEC	0.15 (BEC + 0.15 BEC + 0.20 BEC) = 0.2025 BEC	0.3 (BEC + 0.2 BEC + 0.35 BEC) = 0.465 BEC	0.3 (BEC + 0.2 BEC + 0.35 BEC) = 0.465 BEC
TPC[74]	1.18 BEC + 0.25 BEC + 0.286 BEC = 1.716 BEC	1.15 BEC + 0.2 BEC + 0.2025 BEC = 1.5525 BEC	1.2 BEC + 0.35 BEC + 0.465 BEC = 2.015 BEC	1.2 BEC + 0.35 BEC + 0.465 BEC = 2.015 BEC
Owner's cost factor (f_{owner})[74]	20%	20%	20%	20%
Owner's cost[74]	0.2 TPC = 0.3432 BEC	0.2 TPC = 0.3105 BEC	0.2 TPC = 0.403 BEC	0.2 TPC = 0.403 BEC
TOC[74]	~ 2.06 BEC	~1.86 BEC	~2.42 BEC	~2.42 BEC
TASC	1.034 TOC = ~2.13 BEC	1.034 TOC = ~1.93 BEC	1.034 TOC = ~2.50 BEC	1.034 TOC = ~2.50 BEC

Supplementary Note 1 | Cu catalyst structure after different operation.

a. Power-off/power-on operation

To further investigate carbonate formation on the Cu catalyst, we conducted CV measurements to assess Cu surface reconstruction at OCV under CO atmosphere (Supplementary Fig. 5). The results show that all Cu facet-related features, including (100), (110), and (111),[4,5] exhibit a significant decrease after holding the electrolyzer at OCV in CO for 10 minutes, indicating substantial restructuring of the Cu catalyst. To rule out reconstruction caused by prolonged CO electroreduction, we conducted CV tests after 24 hours of CO electrolysis, a timeframe typically sufficient for Cu to reach a stable catalytic performance (Supplementary Fig. 9). The results revealed a further disappearance of the characteristic Cu surface facets (Supplementary Fig. 6), indicating that carbonate accumulation leads to the loss of accessible Cu active sites or a severe restructuring of the Cu surface. Electrochemical active surface area (ECSA) measurements further validate this conclusion. After a power-off/power-on dynamic operation in CO for 24 hours, the double-layer capacitance (C_{dl}) increased by 0.001 F cm^{-2}, substantially lower than the 0.003 F cm^{-2} increase observed under steady state operation (Supplementary Fig. 7a, b), suggesting that carbonate formation may interfere Cu surface site reconstruction. Additionally, scanning electron microscopy (SEM) revealed that the Cu catalyst subjected to steady state operation develop a rougher surface morphology, indicative of extensive surface reconstruction, whereas those exposed to power-off/power-on dynamic operation exhibit significantly less restructuring (Supplementary Fig. 8b, c). Notably, the carbonate accumulation process on Cu is only partially reversible—while some carbonate species can be removed at 200 mA cm^{-2}, prolonged exposure under CO-rich OCP conditions leads to irreversible surface passivation and incomplete activity recovery (Supplementary Fig. 10).

b. Power-down /power-on operation

To determine whether applying a slightly higher-than-OCV voltage would maintain the Cu catalyst's surface characteristics compared to steady state operation, we examined the catalyst surface structure by using CV (Supplementary Fig. 36 and 37), ECSA (Supplementary Fig. 7a, c) and SEM (Supplementary Fig. 8b, d). CV analysis showed that for dynamic operation at 1.8 V, the Cu facet-related features (100, 110, and 111) remained similar to those under steady state operation (Supplementary Fig. 36 and 37), with minor variations due to Cu surface reconstruction during CO electroreduction (Supplementary Fig. 37). This suggests that 1.8 V does not disrupt Cu reconstruction, allowing the catalyst to retain its surface characteristics. Additionally, the C_{dl} remained nearly unchanged between steady state operation (0.003 F cm^{-2}) and dynamic operation at 1.8 V (0.004 F cm^{-2}) (Supplementary Fig. 7a, c). SEM analysis further confirmed that the Cu surface morphology after dynamic operation at 1.8 V closely matched that of steady state operation (Supplementary Fig. 8b, d). These results demonstrate that applying a slightly

higher-than-OCV voltage (1.8–1.9 V) enables stable dynamic operation without significantly altering the catalyst surface structure. A holding voltage of 1.8 V was selected to investigate the Cu structure instead of 1.9 V (both within the suggested range from Fig. 4b), as 1.8 V represents a more stringent condition for assessing recoverability.

Supplementary Note 2 | CO removal strategies during power-off period

An alternative approach to preventing carbonate formation during OCV is to remove CO from the system. Experimental results show that under dynamic operation at OCV in Ar conditions, the hydrogen FE increased by ~10%, similar to that observed under OCV in CO conditions (Supplementary Fig. 12). However, we observed substantial performance variability after multiple OCV in Ar experiments, as indicated by the large error bars in the results (Supplementary Fig. 12). In some cases, performance even improved (Supplementary Fig. 13), unlike the consistent results under OCV in CO, confirming that this variation is not due to experimental error. To investigate the mechanism, Raman spectroscopy and CV measurements confirmed that Cu oxidizes to Cu_2O under OCV in Ar (Supplementary Fig. 14-16).[6-8,81]

Additionally, we characterized the Cu catalyst using *in-situ* X-ray absorption spectroscopy (XAS, Supplementary Fig. 17). To obtain a better surface signal, we used smaller Cu nanoparticles (8.0 ± 0.9 nm, denoted as CuO-Cu/C; Supplementary Fig. 18-20), which exhibited an increase in HER after exposure to OCV in CO, following the same trend as the 40–60 nm Cu nanoparticles used previously (Supplementary Fig. 21). The catalyst was fully reduced to Cu before switching to the OCV condition (Supplementary Fig. 22). *In-situ* X-ray absorption near edge structure (XANES) and extended X-ray absorption fine structure (EXAFS) analyses revealed that oxidation extended beyond the surface, with bulk Cu gradually oxidizing over time under OCV in Ar (Supplementary Fig. 23 and 24). The composition of Cu species was determined to be 63.1% Cu_2O, 32.2% Cu, and 4.7% $Cu(OH)_2$ (Supplementary Fig. 25, reduced $\chi^2 = 0.00010$).

While Cu_2O reduces back to Cu once the electrolyzer returns to CO electroreduction conditions (Supplementary Fig. 15 and 16), CV measurements revealed that after multiple OCV in Ar cycles, the Cu surface structure differed significantly from that observed under steady state operation (Supplementary Fig. 26), indicating a change in reconstruction behavior. This structural difference was further confirmed by double-layer capacitance measurements, where OCV in Ar resulted in a ΔC_{dl} of 0.007 F cm^{-2}, compared to 0.003 F cm^{-2} under steady state operation (Supplementary Fig. 7a, d). SEM analysis also showed that after OCV in Ar, the Cu surfaces became rougher, with larger particles (Supplementary Fig. 8b, e). These observations suggest that although Cu_2O can be reduced back to Cu, the reconstructed Cu surface does not return its original state after each cycle, leading to inconsistent performance. Consequently, these findings confirm that removing CO for power-off operation is not a viable strategy, as it negatively impacts Cu surface durability and reproducibility.

Supplementary Note 3 | Detailed calculations for techno-economic analysis.

The TEA model in this work is based on previously published models.[60,61,69,70,73,82] The spreadsheet used to compute production costs, provided in the Supplementary Information of Shin et al.[69] was modified for this work.

a. Capital expenditure (CapEx)

1. Bare Erected Cost (BEC)

Bare Erected Cost (BEC) includes the electrolyzer stack, balance of plant (BoP), distillation for liquid product separation, and pressure swing adsorption (PSA) for gas product separation. For the dynamic operation case, the electrolyzer area and BEC were assumed to be identical to those of continuous operation (100% capacity), corresponding to a production rate of 50,000 kg day^{-1}. The BEC was estimated as:

$$BEC = Installed\ electrolyer\ stack + Balance\ of\ plant + Installed\ distillation + Installed\ PSA \quad (1)$$

i. The electrolyzer stack BEC:

The electrolyzer stack equipment cost assessment followed the methods reported by Shin et al.[69], where the stack cost is obtained by multiplying the reference electrode cost per area by the electrolyzer area:

$$Electrolyzer\ stack\ equipment\ cost\ (USD) = Reference\ electrode\ cost\ per\ area\ \left(\frac{USD}{m^2}\right) \times electrolyzer\ area\ (m^2) \quad (2)$$

The reference electrode cost per area was calculated by adjusting the stack cost from the DOE Current Central H2A model (460 USD kW^{-1})[71]. According to the cost breakdown reported in the E4tech report[72], the cathode and anode originally comprise 25% each of the total stack cost. Thus, we accounted for 50% of the stack cost and added the cathode and anode catalyst costs using the reference electrode area (3125 cm^2). The reference electrolyzer operates at 1.75 V and 0.4 A cm^{-2} (2.19 kW). To estimate the BEC of the electrolyzer stack, an installation factor of 1.12 was applied to the stack equipment cost[72]. For this work, the cathode consisted of Cu (5.73E-6 USD mg^{-1})[75] with a loading of 1 mg cm^{-2},[70] and the anode consisted of Ni (1.21E-5 USD mg^{-1})[76] with a loading of 2 mg cm^{-2} [70] and Fe (7.00E-8 USD mg^{-1})[77] with a loading of 1 mg cm^{-2} [70].

Reference cathode cost:

$$Reference\ cathode\ cost = 5.73 \times 10^{-6}\ \left(\frac{USD}{mg}\right) \times 1\ \left(\frac{mg}{cm^2}\right) \times 3125\ cm^2 = 0.018\ USD \quad (3)$$

Reference anode cost:

$$Reference\ anode\ cost = \left(1.21 \times 10^{-5}\ \left(\frac{USD}{mg}\right) \times 2\ \left(\frac{mg}{cm^2}\right) + 7.0 \times 10^{-8} \left(\frac{USD}{mg}\right) \times 1 \left(\frac{mg}{cm^2}\right)\right) \times 3125\ cm^2 = 0.076\ USD \quad (4)$$

Reference electrolyzer cost:

$$Referecne\ electrolyzer\ cost\ \left(\frac{USD}{kW}\right) = \left(460\ \left(\frac{USD}{kW}\right) \times 0.5\right) + \frac{0.018\ USD}{2.19\ kW} + \frac{0.076\ USD}{2.19\ kW} \approx 230\ \left(\frac{USD}{kW}\right) \quad (5)$$

Reference electrode cost per area:

$$Reference\ electrolyzer\ ost\ per\ area\ \left(\frac{USD}{m^2}\right) = 230 \left(\frac{USD}{kW}\right) \times \frac{0.4\ A}{cm^2} \times 1.75\ V \times \frac{10^4 cm^2}{m^2} \times \frac{kW}{1000\ W} \times 1.12 \approx 1803\ \left(\frac{USD}{m^2}\right) \quad (6)$$

Electrolyzer area (m^2):

$$Electrolyzer\ area\ (m^2) = Total\ current\ needed\ (A) \times \frac{1}{Current\ density} \left(\frac{1}{\frac{A}{cm^2}}\right) \times \frac{1}{10^4} \left(\frac{m^2}{cm^2}\right) \quad (7)$$

where:

$$Total\ current\ needed\ (A) = Acetic\ acid\ production\ rate\ \left(\frac{kg}{day}\right) \times \frac{day}{24h} \times \frac{1}{Molecular\ weight\ \left(\frac{g}{mol}\right)} \times 4e^{-} \times F \times \frac{1}{\frac{selectivity}{100}} \quad (8)$$

where $F = 96{,}485\ C\ mol^{-1}$.

ii. Balance of plant BEC

Balance of plant cost was assumed to be 39% of the total electrolyzer system cost, with the electrolyzer stack representing the remaining 61%[69]:

$$Balance\ of\ Plant = Installed\ electrolyzer\ cost \times \frac{0.39}{0.61} \quad (9)$$

iii. Distillation BEC:

$$Distillation\ equipment\ cost\ (USD) = Distillation\ reference\ cost\ (USD) \times \left(\frac{electrolyte\ flow\ rate\ \left(\frac{L}{min}\right)}{Distillation\ reference\ capacity\ \left(\frac{L}{min}\right)}\right)^{0.7} \quad (10)$$

The distillation reference costs are $4,421,380 for a 3 M solution and $9,110,300 for a 0.5 M solution, and the reference capacity is 1000 L min^{-1}.[60]

Electrolyte flow rate:

$$Electrolyte\ flow\ rate\ \left(\frac{L}{min}\right) = Liquid\ product\ flow\ rate\ \left(\frac{L}{min}\right) \div 0.171 \quad (11)$$

Here, 0.171 represents the volume percentage corresponding to 3 M acetic acid. For the 0.5 M acetic acid case, the volume percentage was adjusted accordingly.

$$3\left(\frac{mol}{L}\right) \times 60.052\ \left(\frac{g}{mol}\right) \div 1052\left(\frac{kg}{m^3}\right) \times 1000\ \left(\frac{L}{m^3}\right) \times \frac{1}{1000}\left(\frac{kg}{g}\right) \quad (12)$$

Liquid product flow rate (L min^{-1}):

$$Liquid\ product\ flow\ rate\ \left(\frac{L}{min}\right) = Acetic\ acid\ production\ rate\ \left(\frac{kg}{day}\right) \times \frac{1}{density\left(\frac{kg}{m^3}\right)} \times \frac{1}{24}\left(\frac{day}{h}\right) \times 1000\left(\frac{L}{m^3}\right) \times 60\left(\frac{min}{h}\right) \quad (13)$$

Since the distillation CapEx was obtained from the literature[60] and it was unclear whether the reported value corresponded to the bare equipment cost or the installed cost (i.e., BEC in this work), an installation factor of 1.0 was assumed in the base case, treating the literature value as an installed (BEC-level) cost. A sensitivity analysis was conducted to evaluate the case in which the literature CapEx represented the bare equipment cost, and an installation factor of 2.47[80] was applied accordingly (Supplementary Fig. 42, Supplementary Table 14).

iv. PSA capital cost:

$$PSA\ CapEx\ (USD) = PSA\ reference\ cost\ (USD) \times \left(\frac{total\ flow\ rate\ \left(\frac{m^3}{h}\right)}{PSA\ reference\ capacity\ \left(\frac{m^3}{h}\right)}\right)^{0.7} \quad (14)$$

Here, the PSA reference cost is \$1,989,043, the reference capacity is 1000 $m^3\ h^{-1}$, and 0.7 is the PSA capacity scaling factor.[73]

Total gas flow rate:

$$Total\ gas\ flow\ \left(\frac{m^3}{h}\right) = CO\ outlet\ flow\ rate\ \left(\frac{m^3}{h}\right) + H_2\ flow\ rate\ \left(\frac{m^3}{h}\right) \quad (15)$$

CO inlet flow rate:

$$CO\ inlet\ flow\ rate\ \left(\frac{kg}{day}\right) = CO\ needed\ \left(\frac{kg}{day}\right) \times \frac{1}{\left(\frac{Conversion}{100}\right)} \quad (16)$$

CO needed:

$$CO\ needed\ \left(\frac{kg}{day}\right) = Acetic\ acid\ production\ rate\ \left(\frac{kg}{day}\right) \times 2 \times \left(\frac{MW_{CO}}{MW_{acetic\ acid}}\right) \quad (17)$$

The conversion was assumed to be 50%.[70]

CO outlet flow rate:

$$CO\ outlet\ flow\ rate\ \left(\frac{m^3}{h}\right) = CO\ inlet\ flow\ rate\ \left(\frac{kg}{day}\right) \times \left(1 - \frac{Conversion}{100}\right) \times \frac{1}{1.14\left(\frac{kg}{m^3}\right)} \times \frac{1}{24}\left(\frac{day}{h}\right) \quad (18)$$

Hydrogen flow rate:

$$H_2\ flow\ rate\ \left(\frac{m^3}{h}\right) = Total\ current\ (A) \times \left(1 - \frac{Selectivity}{100}\right) \times \frac{1}{2e^-} \times \frac{1}{F} \times 2.008\frac{g}{mol} \times \frac{1}{0.08988\ \left(\frac{kg}{m^3}\right)} \times \frac{1}{1000}\left(\frac{kg}{g}\right) \times 3600\left(\frac{s}{h}\right) \quad (19)$$

Similar to the distillation CapEx, the PSA CapEx was obtained from the literature[73], and the reported cost basis (bare equipment cost vs. installed cost) was not explicitly specified. In the base case, an installation factor of 1.0 was assumed, treating the literature value as an installed (BEC-level) cost. A sensitivity analysis was performed to evaluate the case in which the literature CapEx represented the bare equipment cost, and an installation factor of 1.17[79] was applied (Supplementary Fig. 42, Supplementary Table 14).

2. Engineering, Procurement, and Construction Cost (EPCC)

Engineering, procurement, and construction management (EPCM) contractor services (f_{EPCM}) were assumed to be 18% of the BEC in the base case. A sensitivity analysis was conducted by varying the EPCM contractor service factor from 15% to 20%, consistent with the NETL guidance[74].

$$EPCC = BEC\ \times\ (1 + f_{EPCM}) \quad (20)$$

3. Total Plant Cost (TPC).

The total plant cost (TPC) was calculated by incorporating both process and project contingencies. The process contingency factor ($f_{process}$) was assumed to be 25%, reflecting

a technology maturity level corresponding to small pilot-scale data[74], as a 10 kW electrolyzer system has been demonstrated[83]. A sensitivity analysis was conducted by varying $f_{process}$ from 20% to 35%.

The project contingency factor ($f_{project}$) was assumed to be 20%. Consistent with AACE/NETL guidance[74], the project contingency was calculated as 20% of the sum of BEC, EPCM cost, and process contingency. A sensitivity analysis was performed by varying $f_{project}$ from 15% to 30%.

The TPC was calculated as:

$$TPC = EPCC + f_{procss} \times BEC + f_{project} \times \left(BEC + f_{EPCM} \times BEC + f_{process} \times BEC\right) \quad (21)$$

4. Total Overnight Cost (TOC)

The owner's cost factor (f_{owner}) was assumed to be 20%[74], and owner's costs were calculated as:

$$Owner's\ costs = f_{owner} \times TPC \quad (22)$$

The total overnight cost (TOC) was then calculated as:

$$TOC = TPC + Owner's\ costs \quad (23)$$

5. Total As-Spent Cost (TASC)

The total as-spent cost (TASC) was estimated by accounting for interest during construction (IDC). A one-year construction period was assumed[73], with expenditures occurring on average at mid-year. A nominal interest rate of 7% was applied.

IDC was calculated as:

$$(1.07)^{0.5} - 1 = 0.0344 = 3.44\% \quad (24)$$

The TASC was then calculated as:

$$TASC = TOC + IDC \times TOC \approx 1.034 \times TOC \quad (25)$$

b. Operating expenses (OpEx)

Operating expenses (OpEx) include the electricity cost for electrolyzer operation, electricity cost for power-down, maintenance cost, cell compartment replacement cost, membrane electrode assembly (MEA) replacement cost, CO cost, water usage cost, distillation operation cost, PSA operating cost, acetate protonation and electrolyte regeneration cost, and operation labor cost.

1. Electricity cost for electrolyzer operation (100% capacity):

$$Electricity\ cost\ for\ electrolyzer\ operation\ \left(\frac{USD}{day}\right) = Power\ needed\ (MW) \times \frac{24h}{day} \times electricity\ price\ \left(\frac{USD}{kWh}\right) \quad (26)$$

where:

$$Power\ needed = Cell\ voltage\ \times\ Total\ current\ needed \quad (27)$$

Where total current needed is calculated using Supplementary Equation 8.

The cell voltage was 2.35 V, and the acetate selectivity was 50%, following the durability test result (Fig. 4a). For dynamic operation, the acetic acid production rate was adjusted according to the operating capacity, resulting in corresponding changes to the total current. The electricity price was also adjusted based on the operating capacity.

2. Electricity cost for power-down:

$$Electricity\ cost_{power\ down}\left(\frac{USD}{day}\right) = Power\ needed_{power\ down}\ (MW) \times Time_{power\ down}\frac{h}{day} \times Electricity\ price_{power\ down}\ \left(\frac{USD}{kWh}\right) \quad (28)$$

The electricity price used for power-down was the average electricity price during the power-down period, excluding the electricity price during power-on. The current density and voltage during power-down were 10 mA cm^{-2} and 1.9 V, respectively, based on our power-down experiments (Supplementary Fig. 35a). The electrolyzer area determined from the continuous operation at 50,000 kg day^{-1} (Supplementary Equation 7) was used to calculate the power needed during power-down.

Power-down time was calculated as:

$$Time_{power\ down} = 24h - Time_{power\ on} \quad (29)$$

For example, at 75% capacity, the power-on time is 18 h and the power-down time is 6 h.

3. Maintenance cost (350 days/year operation):

Maintenance cost was assumed to be 2.5% of the electrolyzer capital cost, with 350 operating days per year.[69]

$$Maintenance\ cost\ \left(\frac{USD}{day}\right) = Electrolyzer\ CapEx\ (USD) \times\ 0.025\ \div \frac{1\ year}{350\ days} \quad (30)$$

4. Cell compartment replacement cost (every 7 years)

Cell compartment replacement cost was assumed to be 15% of the electrolyzer capital cost and to occur every 7 years.[69]

$$Cell\ compartment\ replacement\ cost\ \left(\frac{USD}{day}\right) =$$
$$Electrolyzer\ CapEx\ (USD) \times\ 0.15\ \div \frac{1\ year}{365\ days} \times \frac{1}{7\ yr} \quad (31)$$

5. Membrane electrode assembly (MEA) replacement cost:

MEA replacement was assumed to occur annually[69].

$$MEA\ replacement\ cost\ \left(\frac{USD}{day}\right) =$$
$$MEA\ cost\ \left(\frac{USD}{m^2}\right) \times Electrolyzer\ area\ (m^2) \div \frac{1\ year}{365\ days} \quad (32)$$

Where MEA cost (USD m^{-2}) is:

$$MEA\ cost\ \left(\frac{USD}{m^2}\right) =$$
$$Membrane\ cost\ \left(\frac{USD}{m^2}\right) + Cathode\ cost\ \left(\frac{USD}{m^2}\right) + Anode\ cost\ \left(\frac{USD}{m^2}\right) =$$
$$180\ \left(\frac{USD}{m^2}\right) + 5.73 \times 10^{-6}\left(\frac{USD}{mg}\right) \times 1\left(\frac{mg}{cm^2}\right) \times 10^4\left(\frac{cm^2}{m^2}\right)$$
$$+\left(1.21 \times 10^{-5}\left(\frac{USD}{mg}\right) \times 2\left(\frac{mg}{cm^2}\right) + 7.0 \times 10^{-8}\left(\frac{USD}{mg}\right) \times 1\left(\frac{mg}{cm^2}\right)\right) \times 10^4\left(\frac{cm^2}{m^2}\right)$$
$$= 180.3\ \left(\frac{USD}{m^2}\right) \quad (33)$$

The electrolyzer area was calculated using Supplementary Equation 7.

6. **CO cost:**

$$CO\ cost\ \left(\frac{USD}{day}\right) = CO\ needed\ \left(\frac{kg}{day}\right) \times\ CO\ price\ \left(\frac{USD}{ton}\right) \times \frac{1\ ton}{1000\ kg} \quad (34)$$

CO needed is calculated using Supplementary Equation 17. The CO cost was estimated assuming CO generation from an SOEC at 241.4 USD ton^{-1}.[70]

7. **Water usage cost:**

Water usage was determined from the water consumption required for the oxygen evolution reaction at the anode[69].

$$Water\ usage\ cost\ \left(\frac{USD}{day}\right) =$$
$$Process\ water\ flow\ \left(\frac{gal}{day}\right) \times\ Process\ water\ cost\ \left(\frac{USD}{gal}\right) \quad (35)$$

where:

$$Process\ water\ flow\ \left(\frac{gal}{day}\right) = Total\ current\ (A) \times$$
$$\frac{1}{2e^-} \times \frac{1}{F} \times 0.018\left(\frac{kg}{mol}\right) \times 0.2642\left(\frac{gal}{kg}\right) \times 86400\left(\frac{s}{day}\right) \quad (36)$$

8. **Distillation operation cost:**

$$Distillation\ OpEx\ \left(\frac{USD}{day}\right) = Electrolyte\ flow\ rate\ \left(\frac{L}{min}\right) \div$$
$$Distillation\ reference\ capacity\ \left(\frac{L}{min}\right) \times Distillation\ OpEx_{reference\ capacity}\ \left(\frac{USD}{day}\right) (37)$$

The electrolyte flow rate was calculated using Supplementary Equation 11. The reference distillation capacity is 1000 L min^{-1}. The distillation utility costs are 2,484,690 USD $year^{-1}$ for 3 M acetate and 1,267,900 USD $year^{-1}$ for 0.5 M acetate, and the operating time is 350 days $year^{-1}$.[60]

Operating cost for reference capacity:

$$Distillation\ operating\ cost\ for\ reference\ capacity\ \left(\frac{USD}{day}\right) =$$
$$Distillation\ utility\ cost\ \left(\frac{USD}{year}\right) \times \frac{1\ year}{350\ day} \quad (38)$$

9. PSA operating cost:

$$PSA\ operating\ cost\ \left(\frac{USD}{day}\right) = Total\ gas\ flow\ \left(\frac{m^3}{h}\right) \times$$
$$PSA\ operating\ energy\ requirement\ \left(\frac{kWh}{m^3}\right) \times Electricity\ price\ \left(\frac{USD}{kWh}\right) \times 24\ h\ (39)$$

Total gas flow is calculated from Supplementary Equations 15 – 19. The PSA operating energy requirement is 0.25 kWh m^{-3}.[73]

10. Acetate protonation and electrolyte regeneration cost:

For the KOH electrolyte, the acetate:KOH molar ratio was assumed to be 1:2. Electricity usage for acetate protonation and electrolyte regeneration followed the methodology of Overa et al.,[60] assuming 1.58 kWh kg^{-1} KOH.

$$Acetate\ protonation\ and\ electrolyte\ regeneration\ cost\ \left(\frac{kWh}{kg_{acetate}}\right) = 1.58\left(\frac{kWh}{kg_{KOH}}\right) \times$$
$$KOH\ MW\left(\frac{kg_{KOH}}{kmol_{KOH}}\right) \times \left(\frac{2kmol_{KOH}}{1kmol_{acetate}}\right) \div Acetate\ MW\ \approx 3\frac{kWh}{kg_{acetate}} \quad (40)$$

$$Acetate\ protonation\ and\ electrolyte\ regeneration\ cost\ \left(\frac{USD}{day}\right) =$$
$$3\left(\frac{kWh}{kg}\right) \times Electricity\ price\ \left(\frac{USD}{kWh}\right) \times acetic\ acid\ production\ rate\ \left(\frac{kg}{day}\right) \quad (41)$$

11. Operating labor cost:

The average base labor rate was assumed to be 38.5 USD h^{-1}. The associated labor burden was estimated at 30% of the base labor rate, and administrative support was estimated at 25% of the burdened labor rate[78]. Five operators were assumed to be required, each working 8 hours per day.

$$Operation\ labor\ cost = 8\frac{h}{day} \times 38.5\frac{USD}{h} \times 1.3 \times 1.25 \times 5\ operators\ \approx 2502\frac{USD}{day} \quad (42)$$

c. Discounted cash flow analysis

The discounted cash flow analysis was applied with an income tax rate of 0.389[73], and a nominal interest rate of 0.07. It was assumed that construction of the facility is completed in the first year, with product production beginning in the second year. The total depreciable capital was taken as the TASC. Working capital was assumed to be 5% of the TOC, and a MACRS 10-year depreciation schedule was applied. At the end of the plant life, 20% of the total depreciable capital was assumed to be recovered as salvage value.[73] Finally, the production cost was determined by evaluating a selling price that resulted in a net present value of zero at the end of the process life.

Supplementary Note 4 | Choices of 10 countries globally for techno-economic analysis.

Ten countries were selected globally based on the availability of hourly electricity price data on the IEA website. For North America, the United States was selected from the two available countries (the United States and Mexico). For South America, Chile was selected due to its distinct binary-shaped hourly electricity price profile (Supplementary Fig. 46 a, c, e, g). Europe has the largest number of available countries on the IEA website. Norway was chosen because 89% of its electricity generation comes from non-intermittent renewable sources (hydropower) (Supplementary Fig. 43[84]), while Denmark was selected as another Northern European country where 92% of electricity generation is from renewables, with variable renewable energy accounting for 69%[85]. Spain, France, Germany, and Hungary were also selected as European countries for the analysis. For Asia, Japan was selected from the two available countries (Japan and Philippines). For Oceania, Australia was the only available country on the IEA website.

Supplementary References

1 Čejka, J. *et al.* A Raman spectroscopic study of the basic carbonate mineral callaghanite $Cu_2Mg_2(CO_3)(OH)_6{\cdot}2H_2O$. *Spectrochim. Acta A Mol. Biomol. Spectrosc.* **108**, 171-176 (2013).

2 Moradzaman, M. & Mul, G. In situ raman study of potential-dependent surface adsorbed carbonate, CO, OH, and C species on Cu electrodes during electrochemical reduction of CO_2. *ChemElectroChem* **8**, 1478-1485 (2021).

3 Xu, J. *et al.* High-pressure study of azurite $Cu_3(CO_3)_2(OH)_2$ by synchrotron radiation X-ray diffraction and Raman spectroscopy. *Phys. Chem. Miner.* **42**, 805-816 (2015).

4 Droog, J. M. M. & Schlenter, B. Oxygen electrosorption on copper single crystal electrodes in sodium hydroxide solution. *J. Electroanal. Chem.* **112**, 387-390 (1980).

5 Luc, W. *et al.* Two-dimensional copper nanosheets for electrochemical reduction of carbon monoxide to acetate. *Nat. Catal.* **2**, 423-430 (2019).

6 Arán-Ais, R. M., Scholten, F., Kunze, S., Rizo, R. & Roldan Cuenya, B. The role of in situ generated morphological motifs and Cu(i) species in C2+ product selectivity during CO2 pulsed electroreduction. *Nat. Energy* **5**, 317-325 (2020).

7 Chen, X. *et al.* Controlling speciation during CO_2 reduction on Cu-alloy electrodes. *ACS Catal.* **10**, 672-682 (2020).

8 Auer, A. *et al.* Self-activation of copper electrodes during CO electro-oxidation in alkaline electrolyte. *Nat. Catal.* **3**, 797-803 (2020).

9 Australian Government Department of Climate Change, Energy, the Environment and Water. Australian Energy Update 2025. Australian Government https://www.energy.gov.au/publications/australian-energy-update-2025 (2025).

10 International Energy Agency. Real-Time Electricity Tracker. IEA https://www.iea.org/data-and-statistics/data-tools/real-time-electricity-tracker?from=2024-6-1&to=2024-8-31&category=price&country=AUS&subregion=South+Australia&subregionalView=true (accessed August 2024).

11 International Energy Agency. Norway. https://www.iea.org/countries/norway/energy-mix (accessed August 2024).

12 International Energy Agency. Real-Time Electricity Tracker. IEA https://www.iea.org/data-and-statistics/data-tools/real-time-electricity-tracker?from=2024-6-1&to=2024-8-31&category=price&country=NOR (accessed August 2024).

13 International Energy Agency. Real-Time Electricity Tracker. IEA https://www.iea.org/data-and-statistics/data-tools/real-time-electricity-tracker?from=2024-6-1&to=2024-8-31&category=demand&country=USA (accessed August 2024).

14 International Energy Agency. Real-Time Electricity Tracker. IEA https://www.iea.org/data-and-statistics/data-tools/real-time-electricity-tracker?from=2024-3-1&to=2024-5-31&category=demand&country=USA (accessed August 2024).

15 International Energy Agency. Real-Time Electricity Tracker. IEA https://www.iea.org/data-and-statistics/data-tools/real-time-electricity-tracker?from=2023-12-1&to=2024-2-29&category=demand&country=USA (accessed August 2024).
16 International Energy Agency. Real-Time Electricity Tracker. IEA https://www.iea.org/data-and-statistics/data-tools/real-time-electricity-tracker?from=2023-9-1&to=2023-11-30&category=demand&country=USA (accessed August 2024).
17 International Energy Agency. Real-Time Electricity Tracker. IEA https://www.iea.org/data-and-statistics/data-tools/real-time-electricity-tracker?from=2024-6-1&to=2024-8-31&category=demand&country=CHL (accessed August 2024).
18 International Energy Agency. Real-Time Electricity Tracker. IEA https://www.iea.org/data-and-statistics/data-tools/real-time-electricity-tracker?from=2024-3-1&to=2024-5-31&category=demand&country=CHL (accessed August 2024).
19 International Energy Agency. Real-Time Electricity Tracker. IEA https://www.iea.org/data-and-statistics/data-tools/real-time-electricity-tracker?from=2023-12-1&to=2024-2-29&category=demand&country=CHL (accessed August 2024).
20 International Energy Agency. Real-Time Electricity Tracker. IEA https://www.iea.org/data-and-statistics/data-tools/real-time-electricity-tracker?from=2023-9-1&to=2023-11-30&category=demand&country=CHL (accessed August 2024).
21 International Energy Agency. Real-Time Electricity Tracker. IEA https://www.iea.org/data-and-statistics/data-tools/real-time-electricity-tracker?from=2024-3-1&to=2024-5-31&category=demand&country=NOR (accessed August 2024).
22 International Energy Agency. Real-Time Electricity Tracker. IEA https://www.iea.org/data-and-statistics/data-tools/real-time-electricity-tracker?from=2023-9-1&to=2023-11-30&category=demand&country=NOR (accessed August 2024).
23 International Energy Agency. Real-Time Electricity Tracker. IEA https://www.iea.org/data-and-statistics/data-tools/real-time-electricity-tracker?from=2023-12-1&to=2024-2-29&category=demand&country=NOR (accessed August 2024).
24 International Energy Agency. Real-Time Electricity Tracker. IEA https://www.iea.org/data-and-statistics/data-tools/real-time-electricity-tracker?from=2024-6-1&to=2024-8-31&category=demand&country=DNK (accessed August 2024).
25 International Energy Agency. Real-Time Electricity Tracker. IEA https://www.iea.org/data-and-statistics/data-tools/real-time-electricity-tracker?from=2024-3-1&to=2024-5-31&category=demand&country=DNK (accessed August 2024).

26 International Energy Agency. Real-Time Electricity Tracker. IEA https://www.iea.org/data-and-statistics/data-tools/real-time-electricity-tracker?from=2023-12-1&to=2024-2-29&category=demand&country=DNK (accessed August 2024).
27 International Energy Agency. Real-Time Electricity Tracker. IEA https://www.iea.org/data-and-statistics/data-tools/real-time-electricity-tracker?from=2023-9-1&to=2023-11-30&category=demand&country=DNK (accessed August 2024).
28 International Energy Agency. Real-Time Electricity Tracker. IEA https://www.iea.org/data-and-statistics/data-tools/real-time-electricity-tracker?from=2024-6-1&to=2024-8-31&category=demand&country=ESP (accessed August 2024).
29 International Energy Agency. Real-Time Electricity Tracker. IEA https://www.iea.org/data-and-statistics/data-tools/real-time-electricity-tracker?from=2024-3-1&to=2024-5-31&category=demand&country=ESP (accessed August 2024).
30 International Energy Agency. Real-Time Electricity Tracker. IEA https://www.iea.org/data-and-statistics/data-tools/real-time-electricity-tracker?from=2023-12-1&to=2024-2-29&category=demand&country=ESP (accessed August 2024).
31 International Energy Agency. Real-Time Electricity Tracker. IEA https://www.iea.org/data-and-statistics/data-tools/real-time-electricity-tracker?from=2023-9-1&to=2023-11-30&category=demand&country=ESP (accessed August 2024).
32 International Energy Agency. Real-Time Electricity Tracker. IEA https://www.iea.org/data-and-statistics/data-tools/real-time-electricity-tracker?from=2024-6-1&to=2024-8-31&category=demand&country=FRA (accessed August 2024).
33 International Energy Agency. Real-Time Electricity Tracker. IEA https://www.iea.org/data-and-statistics/data-tools/real-time-electricity-tracker?from=2024-3-1&to=2024-5-31&category=demand&country=FRA (accessed August 2024).
34 International Energy Agency. Real-Time Electricity Tracker. IEA https://www.iea.org/data-and-statistics/data-tools/real-time-electricity-tracker?from=2023-12-1&to=2024-2-29&category=demand&country=FRA (accessed August 2024).
35 International Energy Agency. Real-Time Electricity Tracker. IEA https://www.iea.org/data-and-statistics/data-tools/real-time-electricity-tracker?from=2023-9-1&to=2023-11-30&category=demand&country=FRA (accessed August 2024).
36 International Energy Agency. Real-Time Electricity Tracker. IEA https://www.iea.org/data-and-statistics/data-tools/real-time-electricity-tracker?from=2024-6-1&to=2024-8-31&category=demand&country=DEU (accessed August 2024).

37 International Energy Agency. Real-Time Electricity Tracker. IEA https://www.iea.org/data-and-statistics/data-tools/real-time-electricity-tracker?from=2024-3-1&to=2024-5-31&category=demand&country=DEU (accessed August 2024).
38 International Energy Agency. Real-Time Electricity Tracker. IEA https://www.iea.org/data-and-statistics/data-tools/real-time-electricity-tracker?from=2023-12-1&to=2024-2-29&category=demand&country=DEU (accessed August 2024).
39 International Energy Agency. Real-Time Electricity Tracker. IEA https://www.iea.org/data-and-statistics/data-tools/real-time-electricity-tracker?from=2023-9-1&to=2023-11-30&category=demand&country=DEU (accessed August 2024).
40 International Energy Agency. Real-Time Electricity Tracker. IEA https://www.iea.org/data-and-statistics/data-tools/real-time-electricity-tracker?from=2024-6-1&to=2024-8-31&category=demand&country=HUN (accessed August 2024).
41 International Energy Agency. Real-Time Electricity Tracker. IEA https://www.iea.org/data-and-statistics/data-tools/real-time-electricity-tracker?from=2024-3-1&to=2024-5-31&category=demand&country=HUN (accessed August 2024).
42 International Energy Agency. Real-Time Electricity Tracker. IEA https://www.iea.org/data-and-statistics/data-tools/real-time-electricity-tracker?from=2023-12-1&to=2024-2-29&category=demand&country=HUN (accessed August 2024).
43 International Energy Agency. Real-Time Electricity Tracker. IEA https://www.iea.org/data-and-statistics/data-tools/real-time-electricity-tracker?from=2023-9-1&to=2023-11-30&category=demand&country=HUN (accessed August 2024).
44 International Energy Agency. Real-Time Electricity Tracker. IEA https://www.iea.org/data-and-statistics/data-tools/real-time-electricity-tracker?from=2024-6-1&to=2024-8-31&category=demand&country=JPN (accessed August 2024).
45 International Energy Agency. Real-Time Electricity Tracker. IEA https://www.iea.org/data-and-statistics/data-tools/real-time-electricity-tracker?from=2024-3-1&to=2024-5-31&category=demand&country=JPN (accessed August 2024).
46 International Energy Agency. Real-Time Electricity Tracker. IEA https://www.iea.org/data-and-statistics/data-tools/real-time-electricity-tracker?from=2023-12-1&to=2024-2-29&category=demand&country=JPN (accessed August 2024).
47 International Energy Agency. Real-Time Electricity Tracker. IEA https://www.iea.org/data-and-statistics/data-tools/real-time-electricity-tracker?from=2023-9-1&to=2023-11-30&category=demand&country=JPN (accessed August 2024).

48 International Energy Agency. Real-Time Electricity Tracker. IEA https://www.iea.org/data-and-statistics/data-tools/real-time-electricity-tracker?from=2024-6-1&to=2024-8-31&category=demand&country=AUS (accessed August 2024).
49 International Energy Agency. Real-Time Electricity Tracker. IEA https://www.iea.org/data-and-statistics/data-tools/real-time-electricity-tracker?from=2024-3-1&to=2024-5-31&category=demand&country=AUS (accessed August 2024).
50 International Energy Agency. Real-Time Electricity Tracker. IEA https://www.iea.org/data-and-statistics/data-tools/real-time-electricity-tracker?from=2023-12-1&to=2024-2-29&category=demand&country=AUS (accessed August 2024).
51 International Energy Agency. Real-Time Electricity Tracker. IEA https://www.iea.org/data-and-statistics/data-tools/real-time-electricity-tracker?from=2023-9-1&to=2023-11-30&category=demand&country=AUS (accessed August 2024).
52 Tomc, B. *et al.* Pulsed electrolysis controls copper restructuring via dissolution–redeposition to prolong selective CO_2 reduction to ethylene. *J. CO2 Util.* **105**, 103358 (2026).
53 Tănase, L. C. *et al.* Morphological and chemical state effects in pulsed CO_2 electroreduction on Cu(100) unveiled by correlated spectro-microscopy. *Nat. Catal.* **8**, 881-890 (2025).
54 Herzog, A. *et al.* Operando Raman spectroscopy uncovers hydroxide and CO species enhance ethanol selectivity during pulsed CO_2 electroreduction. *Nat. Commun.* **15**, 3986 (2024).
55 Timoshenko, J. *et al.* Steering the structure and selectivity of CO_2 electroreduction catalysts by potential pulses. *Nat. Catal.* **5**, 259-267 (2022).
56 Ito, T., Raj, J., Zhang, T., Roy, S. & Wu, J. Operational strategies of pulsed electrolysis to enhance multi-carbon product formation in electrocatalytic CO_2 reduction. *EES Catal.* **2**, 997-1005 (2024).
57 Casebolt DiDomenico, R. *et al.* Pulsing the applied potential in electrochemical CO_2 reduction enhances the C_2 activity by modulating the dynamic competitive binding of *CO and *H. *ACS Catal.* **14**, 785-796 (2024).
58 Kok, J., de Ruiter, J., van der Stam, W. & Burdyny, T. Interrogation of oxidative pulsed methods for the stabilization of copper electrodes for CO_2 electrolysis. *J. Am. Chem. Soc.* **146**, 19509-19520 (2024).
59 Ye, K. *et al.* Molecular level insights on the pulsed electrochemical CO_2 reduction. *Nat. Commun.* **15**, 9781 (2024).
60 Overa, S. *et al.* Enhancing acetate selectivity by coupling anodic oxidation to carbon monoxide electroreduction. *Nat. Catal.* **5**, 738-745 (2022).
61 Crandall, B. S. *et al.* Kilowatt-scale tandem CO_2 electrolysis for enhanced acetate and ethylene production. *Nat. Chem. Eng.* **1**, 421-429 (2024).
62 Dorakhan, R. *et al.* A silver–copper oxide catalyst for acetate electrosynthesis from carbon monoxide. *Nat. Synth.* **2**, 448-457 (2023).

63 Ji, Y. *et al.* Selective CO-to-acetate electroreduction via intermediate adsorption tuning on ordered Cu–Pd sites. *Nat. Catal.* **5**, 251-258 (2022).
64 Hasa, B. *et al.* Benchmarking anion-exchange membranes for electrocatalytic carbon monoxide reduction. *Chem Catal.* **3** (2023).
65 Jin, J. *et al.* Constrained C2 adsorbate orientation enables CO-to-acetate electroreduction. *Nature* **617**, 724-729 (2023).
66 Wi, T.-U. *et al.* Upgrading carbon monoxide to bioplastics via integrated electrochemical reduction and biosynthesis. *Nature Synthesis* **3**, 1392-1403 (2024).
67 Xu, Q. *et al.* Identifying and alleviating the durability challenges in membrane-electrode-assembly devices for high-rate CO electrolysis. *Nat. Catal.* **6**, 1042-1051 (2023).
68 Deng, W. *et al.* Diaphragm-based carbon monoxide electrolyzers for multicarbon production under alkaline conditions. *Nat. Commun.* **16**, 8444 (2025).
69 Shin, H., Hansen, K. U. & Jiao, F. Techno-economic assessment of low-temperature carbon dioxide electrolysis. *Nat. Sustain.* **4**, 911-919 (2021).
70 Deng, W. *et al.* Techno-economics of polymer-membrane-based CO_2 electrolysers. *Nat. Rev. Clean Technol.* **1**, 255–268 (2025).
71 U.S. Department of Energy. DOE Hydrogen and Fuel Cells Program Record: Hydrogen Production Cost from Electrolysis 2019. DOE Hydrogen and Fuel Cells Program https://www.hydrogen.energy.gov/docs/hydrogenprogramlibraries/pdfs/19009_h2_production_cost_pem_electrolysis_2019.pdf?Status=Master (2019). (2019).
72 Austin Power Engineering. PEM & Alkaline Electrolyzers Bottom-Up Manufacturing Cost Analysis. Austin Power Engineering https://austinpowereng.com/Fuel%20cell/AustinPower-E4tech%20FCS2014%20Final.pdf (2014).
73 Jouny, M., Luc, W. & Jiao, F. General techno-economic analysis of CO_2 electrolysis systems. *Ind. Eng. Chem. Res.* **57**, 2165-2177 (2018).
74 Gerdes, K., Summers, W. & Wimer, J. Quality Guidelines for Energy System Studies: Cost Estimation Methodology for NETL Assessments of Power Plant Performance, https://www.osti.gov/servlets/purl/1567736/. Report No. DOE/NETL-2011/1455, 1513278, DOE/NETL-2011/1455, 1513278 (2011).
75 Statista. Average Prices for Copper Worldwide from 2014 to 2026. Statista https://www.statista.com/statistics/675854/average-prices-copper-worldwide/ (2024). *Statista*.
76 Statista. Monthly Prices for Nickel Worldwide from January 2014 to January 2025. Statista https://www.statista.com/statistics/673504/monthly-prices-for-nickel-worldwide/ (2025).
77 Statista. Iron Ore Price 2000–2023. https://www.statista.com/statistics/282830/iron-ore-prices-since-2003/ (2024). *Statista*.
78 Hughes, S. *et al.* Sensitivity Analysis Tool for Electrochemical Conversion of CO₂ To CO: User Guide, https://doi.org/10.2172/2234013. Report No. DOE/NETL--2024/4405, 2234013, DOE/NETL-2024/4405, 2234013 (2023).

79 Contacts, N. T., Deutsch, T., Topolski, K. & Kee, J. NX Fuels H2 Shot Incubator Phase I: Cooperative Research and Development Final Report, CRADA Number CRD-22-23256, https://docs.nrel.gov/docs/fy24osti/88983.pdf. *Renewable Energy* (2024).

80 Dutta, A. *et al.* Process Design and Economics for Conversion of Lignocellulosic Biomass to Ethanol: Thermochemical Pathway by Indirect Gasification and Mixed Alcohol Synthesis, https://docs.nrel.gov/docs/fy11osti/51400.pdf. Report No. NREL/TP-5100-51400, 1015885, NREL/TP-5100-51400, 1015885 (2011).

81 Mayer, S. T. & Muller, R. H. An in situ raman spectroscopy study of the anodic oxidation of copper in alkaline media. *J. Electrochem. Soc.* **139**, 426 (1992).

82 Xia, R. *et al.* Electrochemical oxidation of nitric oxide to concentrated nitric acid with carbon-based catalysts at near-ambient conditions. *Nat. Catal.* **8**, 328-337 (2025).

83 Livewire, L. Lectrolyst Unveils Record 10 kW CO2-to-Acetate System, https://livewire.lectrolyst.com/p/lectrolyst-unveils-record-10-kw-co2-to-acetate-system. *Lectrolyst Livewire* (2025).

84 International Energy Agency. Norway. https://www.iea.org/countries/norway/energy-mix (accessed August 2024).

85 International Energy Agency. Real-Time Electricity Tracker. IEA https://www.iea.org/data-and-statistics/data-tools/renewable-energy-progress-tracker (accessed August 2024).